

GlucFM: A Dual-Stream Foundation Model for Continuous Glucose Monitoring

Zechen Li^{1,2,*}, Keerthana Natarajan¹, Weizhi Zhang¹, Menglian Zhou¹, Simon A. Lee¹, Yuwei Zhang¹, Maxwell A. Xu¹, Zeinab Esmailpour¹, Flora D. Salim², Mark Malhotra¹, Lindsey Sunden¹, Shwetak Patel¹, Yuzhe Yang^{1,†}, Ahmed A. Metwally^{1,†}

¹Google Research, ²University of New South Wales, Sydney, [†]Co-last authors, ^{*}Work done during an internship at Google

Continuous glucose monitoring (CGM) provides a dense view of daily metabolic physiology, yet existing generic time-series and CGM-specific foundation models often encode glucose traces as entangled single-stream sequences, leaving the distinct temporal structure of glycemic dynamics only implicitly modeled. We present GlucFM, a lightweight CGM foundation model that aligns irregular recordings to a 24-hour chronological grid, preserves observation masks, and decomposes glucose dynamics into slow physiological state and transient event streams, capturing low-frequency glycemic baselines and short-term deviations that may reflect acute physiological responses or sensor artifacts. GlucFM is pretrained on 109,066 hours of unlabeled CGM recordings from 477 subjects with two complementary objectives: masked contextual latent prediction over fused daily representations and temporal dynamics prediction over state and event streams. Across four diverse cohorts and seven clinical prediction tasks, GlucFM achieves the strongest subject-disjoint linear-probing performance among evaluated baselines, improving average PR-AUC by 4.1 points over the best CGM-specific foundation model. Its gains are most pronounced on core metabolic outcomes, leading PR-AUC on all diabetes-risk and β -cell dysfunction tasks and on 3 of 4 insulin-resistance tasks. GlucFM also achieves the best overall cross-dataset transfer performance and strong few-shot adaptation among evaluated methods, and consistent gains when aggregating multiple days for subject-level prediction, highlighting physiology-aware decomposition as an effective inductive bias for transferable CGM representation learning.

1. Introduction

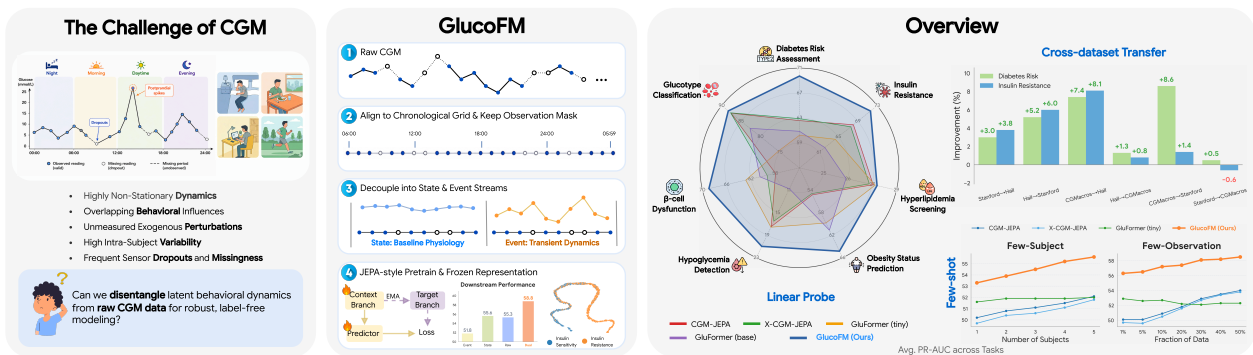


Figure 1 | Overview of GlucFM, a lightweight foundation model for continuous glucose monitoring.

Continuous glucose monitoring (CGM) provides a dense window into daily metabolic physiology, reflecting fasting baselines, nocturnal patterns, postprandial excursions, and fluctuations influenced by behavior, physiology, and sensor conditions. Its use has expanded from type 1 diabetes management, including hypoglycemia prevention, time-in-range monitoring, and closed-loop insulin delivery, to type

Table 1 | Conceptual comparison between GlucoFM and representative TS/CGM foundation models. Checkmarks indicate components explicitly designed in the original model. *Decomp.* denotes decomposition, and *Aug.* denotes augmentation.

Model	Pretraining Objective	CGM-Specific	Daily Modeling	Signal Decomp.	CGM-aware Aug.
Chronos [3]	Quantized autoregressive forecasting	✗	✗	✗	✗
MOMENT [18]	Masked time-series modeling	✗	✗	✗	✗
Mantis [15]	Contrastive representation learning	✗	✗	✗	✗
GluFormer [32]	Next-token prediction	✓	✗	✗	✗
CGM-LSM [31]	Next-token prediction	✓	✗	✗	✗
CGMformer [30]	Masked token prediction	✓	✓	✗	✗
CGM-JEPA [38]	Masked latent prediction	✓	✓	✗	✗
GlucoFM (ours)	Contextual JEPA + Dynamics	✓	✓	✓	✓

2 diabetes, prediabetes, and normoglycemic cohorts, where it helps characterize glycemic variability, treatment response, early metabolic dysfunction, and heterogeneous glucose phenotypes [23, 36, 37, 40, 53]. These signals are increasingly used for metabolic phenotyping, including diabetes risk, insulin resistance, β -cell dysfunction, hypoglycemia, obesity, hyperlipidemia, and glucotypes [19].

Despite this promise, high-quality clinical labels remain expensive, laborious to obtain, sparse, and cohort-specific, limiting fully supervised modeling [37]. This motivates self-supervised CGM foundation models that learn reusable representations from unlabeled recordings and transfer them to downstream metabolic prediction tasks. Recent time-series and CGM-specific foundation models have advanced representation learning through forecasting, autoregressive generation, masked modeling, and latent prediction [30–32, 38]. However, many existing approaches still encode CGM as a single sequence representation, leaving physiological and sensing structure only implicitly modeled. CGM dynamics are inherently multi-scale: slow glycemic trends coexist with short-term deviations potentially influenced by meals, activity, stress, or sensor artifacts. Meanwhile, heterogeneous sampling densities and missingness patterns from device protocols motivate sensing-aware modeling beyond naive interpolation and raw-value reconstruction. These challenges call for a CGM foundation model that explicitly incorporates physiology-motivated decomposition and sensing-aware design.

Motivated by the multi-scale dynamics of CGM, we propose **GlucoFM**, a lightweight self-supervised foundation model for CGM representation learning. GlucoFM is a research prototype designed solely for retrospective physiological representation learning. GlucoFM aligns irregular recordings to a 24-hour chronological grid while preserving observation masks, and uses a dual-stream state–event encoder to separately model slow glycemic trends and transient deviations before fusion. Rather than reconstructing raw glucose values, GlucoFM is pretrained with JEPA-style latent objectives [4] that combine masked contextual representation learning and temporal dynamics modeling. It further incorporates CGM-aware augmentations that simulate value perturbations, heterogeneous sampling rates, and sensor dropouts, encouraging robust daily representations that capture both global glycemic context and local temporal changes. As summarized in Table 1, GlucoFM differs from prior TS/CGM foundation models through explicit state–event decomposition and CGM-aware augmentation.

We pretrain GlucoFM on 109,066 hours of unlabeled CGM recordings from 477 subjects and evaluate frozen representations across four downstream cohorts covering seven unique clinical prediction tasks. As shown in Figure 1, all CGM-specific baselines included in this figure are re-pretrained on the same unlabeled CGM corpus, enabling a controlled comparison of architectural and objective-level differences. GlucoFM achieves the strongest average subject-disjoint linear probing performance across the seven tasks, and further demonstrates strong cross-dataset transfer and few-shot adaptation. Ablations support the contributions of the dual-stream encoder, CGM-aware augmentation, and temporal dynamics objective.

Our contributions are threefold:

- **Lightweight daily CGM foundation model.** GlucoFM learns daily glucose representations from unlabeled CGM while preserving observation masks and absolute time-of-day structure.
- **Physiology- and sensing-aware representation learning.** GlucoFM combines state–event dual-stream modeling, CGM-aware augmentation, masked contextual latent prediction, and temporal dynamics modeling to encode complementary glycemic dynamics.
- **Comprehensive frozen-representation evaluation.** Across four CGM cohorts and seven clinical prediction tasks, GlucoFM shows strong subject-disjoint linear probing, cross-dataset transfer, few-shot adaptation, and multiday subject-level prediction.

2. Related Work

Self-Supervised and Foundation Models for Time Series. Self-supervised time-series learning commonly uses contrastive learning, masked modeling, forecasting, or latent prediction [22,49,56,57]. Recent time-series foundation models scale these ideas to heterogeneous corpora, including masked encoders such as MOMENT [18], tokenized or decoder-only forecasters such as Chronos-2 [2,3] and TimesFM [13], probabilistic forecasters such as Lag-Llama [42], and multi-task models such as Moirai [52] and UniTS [17]. While these models provide strong general-purpose backbones, they typically treat time series as generic numerical sequences and are optimized for forecasting, reconstruction, or broad task transfer. GlucoFM instead targets CGM-specific daily representation learning, where temporal alignment, sensing irregularity, and glycemic structure are central.

Clinical and Physiological Representation Learning. Clinical representation learning has produced pretrained models for longitudinal EHRs [20,24,27,41,44], sleep physiology [45,55], wearable sensing [25,28,29,39,54,59,61], and broader physiological signals [1,10,26,47]. These works demonstrate the value of domain-specific pretraining under label scarcity, patient heterogeneity, and noisy real-world measurement. However, CGM has distinct temporal structure: glucose traces combine slow basal regulation, circadian variation, and short-term excursions potentially influenced by meals, insulin, stress, activity, or sensor artifacts over hours to days [50]. GlucoFM focuses on this glucose-specific structure by learning daily representations directly from CGM rather than relying on generic EHR, sleep, cardiovascular, or wearable encoders.

CGM Representation Learning for Metabolic Phenotyping. CGM has been used to study metabolic heterogeneity through postprandial response prediction, glucotype discovery, cohort profiling, and prediction of insulin resistance, β -cell dysfunction, and metabolic risk [7,19,21,23,33,35,37,48,58]. Much of this work relies on handcrafted metrics, clustering, supervised predictors, or study-specific protocols, limiting reusable representation learning across cohorts and tasks. Recent CGM foundation models, such as CGMformer [30], CGM-LSM [31], CGM-JEPA [38], and GluFormer [32], advance masked modeling, autoregressive forecasting, finetuning, or cohort-level prediction. In contrast, GlucoFM learns a compact frozen CGM encoder for subject-disjoint clinical prediction, cross-dataset transfer, and low-label adaptation.

Missingness-Aware CGM Modeling. Missingness is central in clinical time-series modeling and is commonly addressed through imputation, mask-aware architectures, or continuous-time methods [8,9,43,46]. In CGM, gaps can arise from sensor warm-up, removal, dropout, calibration issues, or nonwear, and naive imputation may obscure meaningful glucose dynamics. GlucoFM therefore uses a mask-aware daily grid that preserves chronological structure while distinguishing observed measurements from missing positions, supporting representation learning under real-world CGM irregularity.

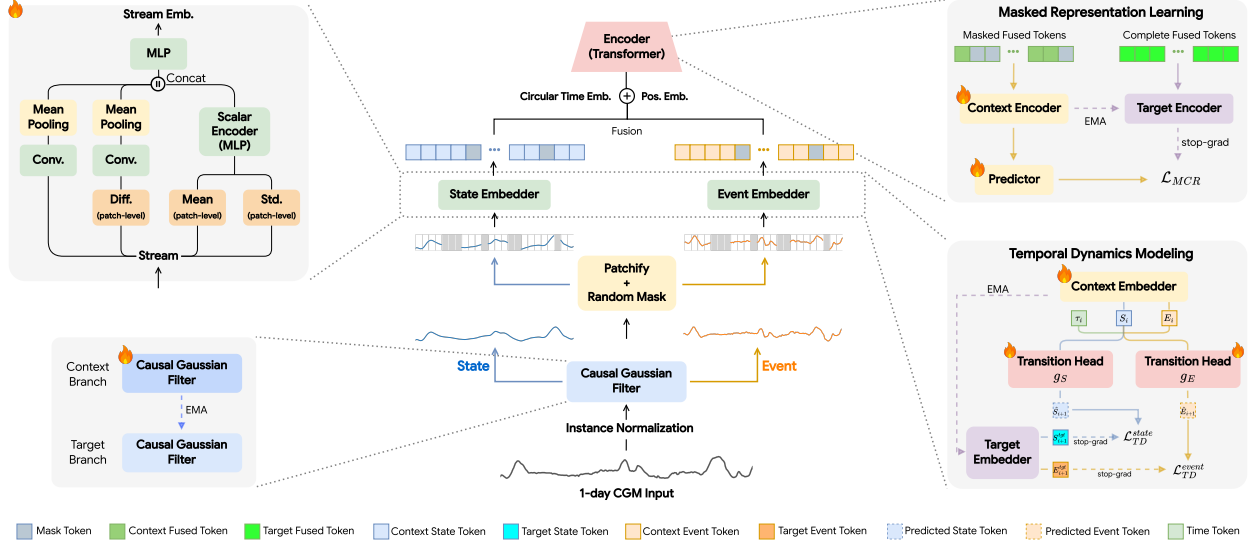


Figure 2 | Model framework and pretraining objectives of GlucoFM.

3. Methodology

3.1. Modeling Input CGM Data Streams

Chronological Grid Alignment. Given CGM readings $X = \{x_i\}_{i=1}^N$ with timestamps $T = \{t_i\}_{i=1}^N$, our goal is to learn representations that preserve both glucose dynamics and absolute time-of-day structure. Since CGM recordings can be irregular due to heterogeneous sampling rates and sensor dropouts, we align each recording segment to a fixed 24-hour chronological grid with $\Delta t = 5$ minutes and $L = 288$ positions. The first timestamp defines the absolute circadian start index, $s = \lfloor (60 \cdot \text{hour}(t_1) + \text{minute}(t_1)) / \Delta t \rfloor$. The aligned input consists of a glucose sequence $\hat{X} \in \mathbb{R}^L$ and an observation mask $M \in \{0, 1\}^L$, where $M_j = 1$ only for physically observed measurements. Missing positions are filled only for tensor construction, while M is preserved throughout representation learning. This separates chronological alignment from interpolation and allows GlucoFM to handle different sampling rates and sensor dropouts on a common daily grid.

CGM-aware Data Augmentation. We use two families of on-the-fly augmentations during pretraining. *Value perturbations* simulate realistic CGM signal variation, including low-frequency baseline wander and short compression-like drops, while preserving the observation mask. *Structural sparsification* alters the observation pattern itself by randomly decimating dense 5-minute recordings into 15-minute-like sampling and masking short contiguous disconnection blocks. These augmentations expose GlucoFM to sensor drift, compression artifacts, heterogeneous sampling rates, and physical dropouts, while randomized ordering and decayed co-occurrence probabilities prevent over-corrupting individual sequences.

3.2. State–Event Dual-Stream Encoder

Mask-aware Signal Decomposition. CGM signals naturally contain both low-frequency metabolic states and high-frequency transient events. Low-frequency components reflect stable glycemic baselines and slower regulatory patterns, while high-frequency components represent short-term deviations from the local trend, which may arise from transient physiology and behavior. To avoid encoding these heterogeneous dynamics as a single entangled sequence, GlucoFM decouples the aligned signal into state and event components before masked representation learning, as shown in Figure 2.

Given the aligned sequence \hat{X} and observation mask M , we first apply mask-aware normalization and compute patch-level statistics, including glucose summaries and rate-of-change features. We then estimate the low-frequency state using a learnable causal Gaussian filter. The filter bandwidth σ is initialized at $\sigma = 6.0$ and constrained within $[2.0, 12.0]$ grid steps, corresponding to approximately 10–60 minutes on the 5-minute grid. This range allows the filter to separate short-term fluctuations from slower glycemic trends while adapting its smoothing scale during pretraining. Causality is enforced by using only current and past observations when estimating the local trend, preventing future glucose values from leaking into the representation. The filter is also mask-aware, normalizing only over valid observations to avoid dropout-induced boundary artifacts.

The filtered trend defines the state component, while the residual captures high-frequency event-level deviations:

$$\hat{X}_{\text{state}} = \text{Filter}(\hat{X}, M), \quad \hat{X}_{\text{event}} = (\hat{X} - \hat{X}_{\text{state}}) \odot M. \quad (1)$$

State and event signals are encoded by two parallel streams and fused into unified patch tokens.

Patch Tokenization and Circadian Encoding. After state–event decomposition, GlucoFM tokenizes each sequence into 24 non-overlapping temporal patches, each covering 12 grid steps, corresponding to one hour. The state stream encodes the filtered trend together with mask-aware state statistics, while the event stream encodes residual deviations together with rate-of-change statistics. The two stream outputs are then fused into unified physiological patch tokens. To preserve absolute time-of-day information, each token is augmented with circular time features, $\tau(i) = [\sin(2\pi i/L), \cos(2\pi i/L)]$, where i is the absolute grid index and $L = 288$. This encoding allows the context encoder to model glucose dynamics with awareness of circadian phase.

3.3. Latent Predictive Pretraining

GlucFM uses two complementary JEPA-style objectives to predict latent representations rather than reconstruct potentially interpolated or noisy glucose values.

Masked Contextual Representation Learning. In our first pretraining objective, we randomly mask temporal patches in the online branch, with the masking ratio sampled from $[0.5, 0.6]$. In the online branch, each selected patch is replaced by a learnable mask token, and the resulting full patch grid is encoded by a context encoder $f_{\theta_{\text{ctx}}}$. In parallel, the full physically observed sequence is encoded by an EMA target encoder $f_{\theta_{\text{tgt}}}$ to provide stable latent targets. The target encoder is updated with EMA momentum coefficient m , initialized to 0.997, as $\theta_{\text{tgt}} \leftarrow m\theta_{\text{tgt}} + (1 - m)\theta_{\text{ctx}}$. A lightweight predictor maps the context-branch tokens to the target latent space and predicts the representations of masked patches. Let Z_i^{pred} and Z_i^{tgt} denote the predicted and target latent tokens at patch i . The masked contextual representation loss is:

$$\mathcal{L}_{\text{MCR}} = \frac{\sum_{i=1}^P w_i m_i^{\text{mask}} \text{SmoothL1}(Z_i^{\text{pred}}, Z_i^{\text{tgt}})}{\sum_{i=1}^P w_i m_i^{\text{mask}} + \epsilon}, \quad (2)$$

where P is the number of temporal patches, m_i^{mask} indicates whether patch i is masked, and w_i is the fraction of physically observed measurements within the patch.

Temporal Dynamics Modeling. Masked contextual prediction learns daily contextual representations, but CGM phenotypes also depend on how glucose dynamics evolve over time. We therefore introduce a second JEPA-style objective that predicts next-patch state and event representations. Given context-branch state and event tokens (S_i, E_i) at patch i , two lightweight transition heads g_S and g_E predict the next-patch state and event targets:

$$\hat{S}_{i+1} = S_i + g_S([S_i, E_i, \tau_i]), \quad \hat{E}_{i+1} = E_i + g_E([E_i, S_i, \tau_i]), \quad (3)$$

where τ_i is the circular time embedding. The residual update form encourages the heads to model temporal changes rather than directly copying the current representation. The targets $(S_{i+1}^{\text{tgt}}, E_{i+1}^{\text{tgt}})$ are taken from the EMA target branch before global Transformer self-attention, so the next-patch targets do not already encode information from later patches. The temporal dynamics loss is:

$$\mathcal{L}_{\text{TD}} = \frac{1}{2} \left(\frac{\sum_{i=1}^{P-1} q_i \text{SmoothL1}(\hat{S}_{i+1}, S_{i+1}^{\text{tgt}})}{\sum_{i=1}^{P-1} q_i + \epsilon} + \frac{\sum_{i=1}^{P-1} q_i \text{SmoothL1}(\hat{E}_{i+1}, E_{i+1}^{\text{tgt}})}{\sum_{i=1}^{P-1} q_i + \epsilon} \right), \quad (4)$$

where q_i weights each transition by the observed support of adjacent patches and excludes patches hidden from the context branch. This objective encourages the state stream to encode gradual baseline shifts and the event stream to encode transient deviations, providing an explicit temporal constraint on the decoupled representations.

Overall Objective. The final pretraining loss is:

$$\mathcal{L} = \lambda_{\text{MCR}} \mathcal{L}_{\text{MCR}} + \lambda_{\text{TD}} \mathcal{L}_{\text{TD}}. \quad (5)$$

We set $\lambda_{\text{MCR}} = \lambda_{\text{TD}} = 1.0$. GlucoFM uses compact 3-layer Transformer context and EMA target encoders with hidden dimension 128, 4 attention heads, and feed-forward dimension 256, together with a lightweight 1-layer Transformer predictor. During downstream evaluation, we discard the EMA target branch and retain only the frozen online encoder. GlucoFM has 0.72M trainable parameters and 1.18M total parameters during pretraining, with the difference mainly due to the EMA target branch. Additional implementation details are provided in Appendix C.

4. Experiments

4.1. Experimental Setup

Datasets. Table 2 summarizes the datasets used in this study. We enforce strict subject separation between pretraining and downstream evaluation, ensuring no overlap between pretraining subjects and downstream test groups. For self-supervised pretraining, we aggregate five CGM cohorts spanning 5-minute and 15-minute sampling rates, totaling 477 subjects and 109,066 hours of recordings. This mixture exposes GlucoFM to diverse glucose dynamics, sensor densities, and population characteristics. For downstream evaluation, we use four CGM

Table 2 | Composition of GlucoFM datasets.

Dataset	Sample Rate	# Subjects	Duration (h)
<i>Pre-train Datasets</i>			
Wear-CGM	5	192	75,330
ShanghaiT2DM [60]	15	44	12,414
Stanford [37]	5	19	8,761
BIG IDEAs [11]	5	16	3,017
Colas [12]	5	206	9,544
<i>Downstream Datasets</i>			
CGMacros [14]	5 15	45	10,376 10,998
ShanghaiT2DM [60]	15	65	15,634
Stanford [37]	5	37	27,571
Hall [19]	5	56	7,090

cohorts with 203 participants and 71,669 hours of CGM data, covering seven diagnosis-level prediction tasks: diabetes risk assessment, insulin resistance, β -cell dysfunction, glucotype, hyperlipidemia, hypoglycemia, and obesity classification. All downstream evaluations use subject-disjoint splits to prevent overlap between training and test subjects, enabling robust assessment across heterogeneous CGM cohorts. Additional dataset details are provided in Appendix A.

Baselines. We compare GlucoFM with *three groups of baselines*: general-purpose time-series foundation models, a CGM-specific open-weight model pretrained on a separate cohort, and CGM-specific models retrained on our pretraining corpus. Implementation details are provided in Appendix B. General-purpose baselines include Chronos-2 [2], MOMENT [18], Mantis [15], and MantisV2 [16].

Table 3 | Linear-probe performance. The best result is shown in **bold**, and the second-best result is underlined. All values report mean performance over 10 iterations of 5-fold subject-grouped cross-validation. **Core** denotes key CGM-based metabolic phenotyping tasks.

Method	Params	Metrics	CGMacros				ShanghaiT2DM			Stanford			Hall				Avg
			Diabetes	IR	Hyperlip.	Obesity	IR	Hyperlip.	Hypogly.	Diabetes	β -cell Dys.	IR	Diabetes	IR	Hyperlip.	Glucose	
<i>General Time-series Foundation Models with Large-scale Pretraining</i>																	
Chronos-2 (small)	28M	PR	51.6	82.7	30.5	56.0	65.0	34.8	16.0	69.2	58.6	62.5	51.7	44.9	24.2	54.2	50.1
		AUC	68.0	67.5	52.1	53.7	55.0	50.6	49.1	65.4	57.3	64.2	64.9	57.7	61.3	62.6	59.2
		F1	49.4	61.7	50.1	52.7	52.6	51.5	50.5	61.3	54.8	59.6	60.9	55.0	52.5	58.6	55.1
Chronos-2	120M	PR	54.3	84.1	34.0	58.1	59.8	34.7	18.9	68.5	58.5	59.2	48.6	51.3	20.6	54.4	50.4
		AUC	69.7	69.9	55.8	56.6	49.5	49.7	53.0	65.6	57.8	60.2	60.4	62.7	50.3	63.0	58.9
		F1	50.2	63.3	53.7	54.2	49.0	50.4	52.8	61.9	55.5	56.6	58.4	58.2	50.9	56.2	55.1
MOMENT (small)	40M	PR	54.0	83.8	30.3	60.9	58.3	38.3	16.3	70.4	57.2	63.0	59.2	53.1	19.4	55.6	51.4
		AUC	69.1	70.6	51.5	58.7	49.0	55.9	52.9	67.6	55.5	65.1	69.7	62.1	48.7	61.7	59.9
		F1	49.8	63.6	50.9	55.7	49.3	52.9	51.4	62.5	53.8	60.1	64.5	59.0	50.4	59.3	55.9
MOMENT (large)	385M	PR	50.3	87.4	32.0	61.8	59.6	42.4	14.3	71.9	61.8	58.1	52.1	44.9	18.4	55.8	50.8
		AUC	66.1	75.2	53.2	59.9	47.8	60.8	49.6	69.1	58.9	59.4	65.0	56.6	51.4	63.2	59.7
		F1	46.8	67.2	<u>52.5</u>	56.3	48.6	57.2	49.7	63.7	55.7	56.1	60.5	53.3	47.7	57.8	55.2
Mantis	8M	PR	61.8	90.9	30.1	63.4	59.2	30.6	22.9	75.1	63.5	<u>67.1</u>	54.2	55.7	<u>24.8</u>	77.5	55.5
		AUC	75.5	80.3	49.8	60.8	48.2	46.0	58.6	71.4	61.5	<u>68.2</u>	67.1	66.2	57.9	82.6	63.9
		F1	56.0	71.6	49.8	57.2	48.4	47.5	53.8	<u>65.9</u>	58.5	<u>62.3</u>	59.6	59.8	53.7	73.3	58.4
MantisV2	4.2M	PR	<u>63.6</u>	<u>91.2</u>	30.3	62.8	64.1	33.3	<u>22.0</u>	75.2	<u>65.7</u>	64.6	57.7	59.3	25.0	81.5	<u>56.9</u>
		AUC	76.7	<u>80.3</u>	49.1	60.3	52.7	48.5	59.6	71.2	<u>64.4</u>	65.5	67.5	66.7	<u>58.8</u>	84.7	<u>64.7</u>
		F1	56.2	<u>68.9</u>	49.2	55.9	51.2	48.1	<u>53.3</u>	65.7	<u>58.6</u>	60.4	61.1	<u>60.8</u>	<u>52.6</u>	76.7	<u>58.5</u>
<i>Externally Pretrained CGM Foundation Model</i>																	
CGMformer	0.85M	PR	63.3	89.9	31.8	68.1	54.8	40.6	11.9	<u>75.9</u>	62.2	61.8	51.1	48.0	18.0	79.6	54.1
		AUC	<u>77.1</u>	78.0	54.2	66.0	43.6	<u>58.4</u>	42.1	<u>71.4</u>	59.2	63.2	66.6	58.2	46.5	84.3	62.1
		F1	<u>57.2</u>	67.6	52.1	60.5	45.5	<u>55.1</u>	45.3	66.2	55.7	59.0	59.3	56.3	48.4	77.1	57.5
<i>CGM Foundation Models Retrained on Our Pretraining Corpus</i>																	
CGM-JEPA	0.52M	PR	63.0	86.2	28.7	55.5	69.1	37.4	17.8	66.4	58.7	61.5	<u>59.9</u>	56.8	17.3	87.6	54.7
		AUC	75.9	73.8	47.6	53.8	60.8	53.6	56.8	61.2	55.4	61.6	<u>73.5</u>	<u>68.1</u>	40.5	90.7	62.4
		F1	55.4	66.3	48.2	53.2	57.2	51.3	50.4	58.7	53.9	58.1	65.0	<u>59.4</u>	42.8	<u>82.2</u>	57.3
X-CGM-JEPA	0.52M	PR	<u>63.6</u>	86.6	29.8	55.3	66.9	35.5	16.9	67.4	60.0	61.9	59.3	56.2	17.5	<u>87.7</u>	54.6
		AUC	76.6	73.6	48.0	53.2	<u>58.4</u>	52.1	55.7	61.8	56.4	62.0	73.0	67.7	40.0	<u>90.6</u>	62.1
		F1	<u>56.5</u>	65.1	48.2	52.5	<u>55.4</u>	49.9	49.0	59.1	54.4	58.1	<u>64.8</u>	59.2	42.8	82.1	56.9
GluFormer (tiny)	0.65M	PR	59.4	86.1	28.2	60.2	58.1	33.9	17.9	74.3	63.3	64.5	48.9	50.9	21.6	75.4	53.0
		AUC	73.9	72.5	47.9	57.9	47.6	51.1	53.3	68.9	61.9	65.4	63.3	63.6	58.0	81.7	61.9
		F1	51.7	65.4	48.0	55.4	47.8	50.3	49.1	63.0	58.5	61.7	57.9	59.4	<u>53.1</u>	72.7	56.7
GluFormer (base)	135M	PR	62.9	87.2	31.4	61.4	56.5	31.5	11.5	69.8	61.1	56.1	51.9	51.6	16.4	82.7	52.3
		AUC	76.7	74.8	53.1	60.5	44.9	46.7	43.9	63.1	58.0	56.3	66.0	61.6	46.9	87.9	60.0
		F1	55.7	67.8	<u>52.5</u>	57.2	46.3	48.1	44.8	59.2	55.4	54.8	58.7	58.3	47.7	80.7	56.2
GlucoFM	0.72M	PR	65.9	91.9	36.1	<u>64.9</u>	<u>67.0</u>	33.5	21.1	77.3	69.0	67.6	66.2	60.2	14.4	88.3	58.8
		AUC	78.7	81.2	<u>54.7</u>	<u>62.6</u>	57.8	50.5	<u>59.2</u>	72.8	68.7	69.1	75.9	70.7	41.6	90.7	66.7
		F1	58.3	<u>69.6</u>	50.2	<u>59.4</u>	<u>55.4</u>	49.1	50.7	66.2	63.3	64.0	64.5	62.0	43.1	82.4	59.9

Controlled CGM-specific baselines include CGM-JEPA and X-CGM-JEPA [38], and GluFormer [32], all retrained on the same corpus as GlucoFM. We use GluFormer as the representative autoregressive CGM baseline because CGM-LSM [31] has a closely related architecture and next-token objective. We also evaluate CGMformer [30], an open-weight CGM-specific model pretrained on an external 964-participant cohort with non-public raw data.

Setup. We report ROC-AUC, PR-AUC, and Macro-F1. ROC-AUC measures global discriminative ability, PR-AUC emphasizes performance under class imbalance, and Macro-F1 evaluates class-balanced decision quality across diagnostic categories. GlucoFM is pretrained for 120 epochs on a single NVIDIA H100 GPU with batch size 128, learning rate 10^{-4} , weight decay 10^{-2} , and a separate learning rate of

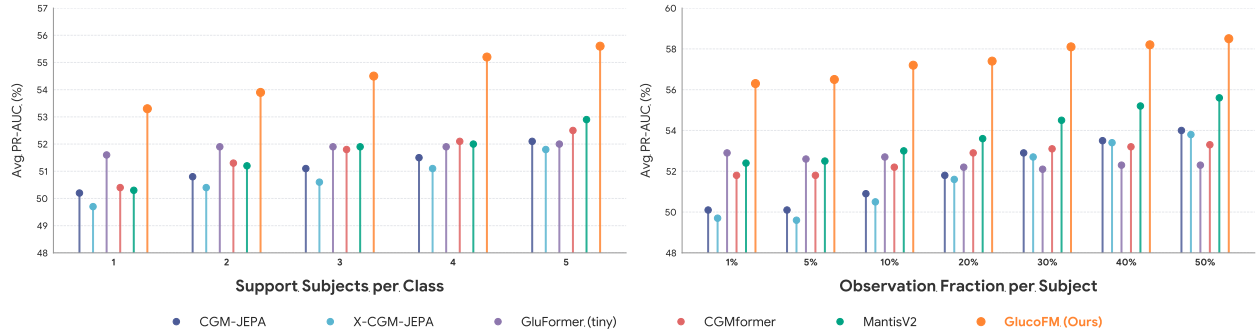


Figure 3 | Few-shot adaptation under limited labeled subjects (left) and limited per-subject observations (right), reported as task-averaged PR-AUC.

10^{-3} for the learnable Gaussian bandwidth. Detailed model training setup is provided in Appendix C.

4.2. Experimental Results

We evaluate GlucoFM along three complementary axes that reflect different clinically relevant utility scenarios: subject-disjoint linear probing, few-shot adaptation, and cross-dataset transferability. Additional setup details and full results with fold-level variance are provided in Appendix D.

Subject-Disjoint Linear Probing. We first evaluate whether GlucoFM learns task-relevant representations that remain linearly separable under subject-disjoint generalization. For each method, we freeze the encoder, extract embeddings from non-overlapping 24-hour windows, and train the same logistic regression classifier on the extracted representations. We use subject-grouped cross-validation, ensuring that all windows from the same subject appear only in either the training or test fold. Each held-out window is predicted independently, with evaluation performed over all held-out test windows. As shown in Table 3, GlucoFM achieves the strongest overall performance, obtaining the best task-averaged PR-AUC, ROC-AUC, and Macro-F1, while ranking within the top two on 11/14, 11/14, and 9/14 task-dataset evaluations, respectively.

The gains are most evident on core metabolic phenotyping outcomes. In PR-AUC, GlucoFM leads all diabetes-risk and β -cell dysfunction evaluations, and 3/4 insulin-resistance evaluations, suggesting that its frozen representations capture clinically relevant glycemic structure rather than only generic temporal patterns. GlucoFM also outperforms CGMformer in PR-AUC on 11/14 evaluations despite CGMformer being pretrained on a larger external 964-participant cohort, and exceeds CGM-specific baselines re-pretrained on the same corpus on 11/14 evaluations. This suggests that the improvements are not solely explained by pretraining scale, but are consistent with the benefit of CGM-aware pretraining objectives and temporal inductive biases. The main exception is ShanghaiT2DM, which may reflect a device- and sampling-rate shift: it is Libre-derived with 15-minute sampling, while our pretraining corpus contains relatively fewer real Libre/15-minute recordings. Overall, GlucoFM provides the strongest frozen representation across the benchmark, with particularly clear advantages on clinically central metabolic tasks.

Few-Shot Adaptation. We evaluate GlucoFM under two low-label adaptation settings. In *limited-subject adaptation*, we restrict the number of labeled support subjects per class within the training fold. In *limited-observation adaptation*, we retain all training subjects but use only a fraction of each subject’s 24-hour windows for classifier training. We compare against strong baselines, including CGM-JEPA, X-CGM-JEPA, GluFormer (tiny), CGMformer, and MantisV2. We use 5-fold subject-grouped cross-validation with 10 repeated iterations and 5 random support samplings per split.

Table 4 | Cross-dataset transfer results. “+” denotes GlucoFM’s gain over the second-best method; “-” denotes its gap to the best baseline.

Metrics	Stanford → Hall				Hall → Stanford			
	<i>Diabetes Risk Assessment</i>		<i>Insulin Resistance</i>		<i>Diabetes Risk Assessment</i>		<i>Insulin Resistance</i>	
	PR-AUC [†]	ROC-AUC [†]	PR-AUC [†]	ROC-AUC [†]	PR-AUC [†]	ROC-AUC [†]	PR-AUC [†]	ROC-AUC [†]
CGM-JEPA	53.0	73.4	55.0	67.9	68.1	64.3	61.3	61.8
X-CGM-JEPA	55.4	73.7	57.8	68.2	68.2	64.7	61.7	62.4
GluFormer (tiny)	58.6	70.4	50.8	62.2	67.6	65.6	59.7	58.3
GlucoFM	61.6 (+3.0)	74.7 (+1.0)	61.6 (+3.8)	72.1 (+3.9)	73.4 (+5.2)	69.7 (+4.1)	67.7 (+6.0)	69.2 (+6.8)

Metrics	CGMacros → Hall				Hall → CGMacros			
	<i>Diabetes Risk Assessment</i>		<i>Insulin Resistance</i>		<i>Diabetes Risk Assessment</i>		<i>Insulin Resistance</i>	
	PR-AUC [†]	ROC-AUC [†]	PR-AUC [†]	ROC-AUC [†]	PR-AUC [†]	ROC-AUC [†]	PR-AUC [†]	ROC-AUC [†]
CGM-JEPA	50.6	69.6	53.4	67.1	87.5	78.1	89.1	77.0
X-CGM-JEPA	49.5	69.1	53.6	67.2	87.3	77.8	89.2	77.1
GluFormer (tiny)	55.9	70.2	50.0	65.1	83.9	74.1	84.8	71.0
GlucoFM	63.3 (+7.4)	78.2 (+8.0)	61.7 (+8.1)	72.5 (+5.3)	88.8 (+1.3)	81.3 (+3.2)	90.0 (+0.8)	78.8 (+1.7)

Metrics	CGMacros → Stanford				Stanford → CGMacros			
	<i>Diabetes Risk Assessment</i>		<i>Insulin Resistance</i>		<i>Diabetes Risk Assessment</i>		<i>Insulin Resistance</i>	
	PR-AUC [†]	ROC-AUC [†]	PR-AUC [†]	ROC-AUC [†]	PR-AUC [†]	ROC-AUC [†]	PR-AUC [†]	ROC-AUC [†]
CGM-JEPA	64.1	60.9	59.8	60.3	87.8	78.4	85.9	74.0
X-CGM-JEPA	65.4	62.3	59.7	60.2	88.3	78.5	83.6	70.7
GluFormer (tiny)	68.5	64.0	64.0	65.2	85.2	76.2	87.9	76.3
GlucoFM	77.1 (+8.6)	73.6 (+9.6)	65.4 (+1.4)	64.8 (-0.4)	88.3 (+0.5)	79.9 (+1.4)	87.3 (-0.6)	73.3 (-3.0)

Figure 3 shows that GlucoFM achieves the highest average PR-AUC across both support-subject and observation-fraction settings. The gains are especially clear in the most label-scarce regime, where only one or two subjects per class are available, suggesting that GlucoFM provides more useful class structure for low-label adaptation. As more support subjects are added, performance generally improves, but GlucoFM maintains a consistent advantage over both CGM-specific and general time-series baselines. In contrast, performance changes more smoothly when varying the fraction of observations per subject, suggesting that subject diversity is more limiting than dense recordings from a small number of individuals. Overall, these results indicate that GlucoFM learns label-efficient representations that remain effective even when per-subject observations are sparse.

Cross-Dataset Generalization. We further evaluate cohort transfer by training a linear probe on one source dataset and testing it directly on another using frozen representations. We focus on diabetes risk assessment and insulin resistance, which are shared across CGMacros, Stanford, and Hall. To isolate representation transferability, we compare with CGM-specific baselines pretrained on the same CGM corpus and use the target dataset only for final evaluation.

As shown in Table 4, GlucoFM achieves the best overall transfer performance, ranking first on 21 of 24 PR-AUC and ROC-AUC evaluations. The gains are strongest for transfers involving Hall and for CGMacros → Stanford diabetes-risk assessment, indicating that GlucoFM captures metabolic structure that transfers across cohorts and devices. The few non-leading cases mainly occur for Stanford → CGMacros insulin resistance, where GlucoFM remains close to the best baseline.

Multiday Representation Observation. We further evaluate whether longer CGM observation improves subject-level prediction using frozen GlucoFM representations. For each subject, we select one fixed eligible K_{\max} -day CGM anchor episode and enumerate adjacent K -day subwindows within the same anchor for $K = 1, \dots, K_{\max}$. Each day is independently encoded by the frozen GlucoFM encoder,

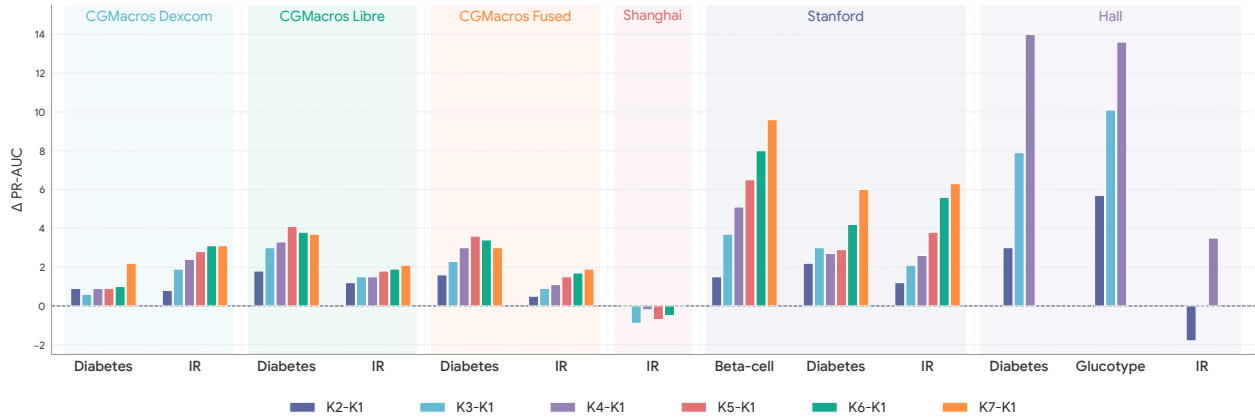


Figure 4 | **Effect of multiday CGM observation.** Paired PR-AUC change from the one-day subject representation to K -day representations, $\Delta_K = \text{PR-AUC}(K) - \text{PR-AUC}(1)$. Positive values indicate improvement over $K = 1$. Hall uses $K \leq 4$; other cohorts use $K \leq 7$.

and embeddings within each subwindow are mean-pooled into one subject-level representation. For each K and start position, every subject contributes one representation and each test subject receives one prediction, so subwindows from the same subject are not treated as independent test samples. Metrics are computed by start position and averaged within each repeated evaluation. We train linear probes with 10 iterations of 5-fold subject-level cross-validation and report the paired PR-AUC change.

Figure 4 shows that longer CGM observation often improves subject-level prediction. The gains are strongest on Stanford and Hall, suggesting that multiple daily CGM profiles provide a more stable estimate of subject-level metabolic phenotypes. CGMacros further provides a paired-sensor setting, where Dexcom and Libre are recorded from the same subjects over the same period. We evaluate each sensor separately and include a matched fused setting, where same-subject same-day Dexcom and Libre embeddings are averaged before multiday aggregation. The mostly positive gains across these settings suggest that frozen GlucoFM embeddings capture subject-level signals that are reproducible across sensor views. ShanghaiT2DM IR is an exception under simple mean pooling, but $\text{concat}(\text{mean}, \text{max})$ pooling (Figure 5) yields clear gains at longer horizons, especially at $K = 6$ and 7. Overall, these results show that GlucoFM can support multiday subject-level prediction, while the best aggregation strategy may depend on the cohort, sensor type, and clinical label.

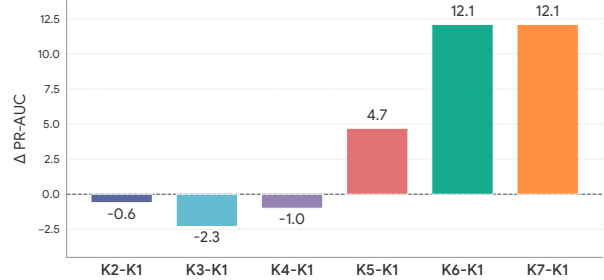


Figure 5 | 7-day ShanghaiT2DM IR under $\text{concat}(\text{mean}, \text{max})$ aggregation.

Same-window GMI Comparison. We further compare GlucoFM with a same-window 7-day threshold baseline based on a glucose management indicator (GMI)-equivalent value [6] for diabetes classification. The GMI-equivalent value is computed from the mean glucose over the same selected seven CGM days used by GlucoFM: $\text{GMI} = 3.31 + 0.02392 \times \text{mean glucose}_{\text{mg/dL}}$. For Stanford, diabetes is treated as a binary task, where subjects with $\text{GMI} \geq 5.7$ are assigned to the risk-positive class and those with $\text{GMI} < 5.7$ to the negative class. For CGMacros, diabetes is treated as a three-class task using thresholds at 5.7 and 6.4: $\text{GMI} < 5.7$, $5.7 \leq \text{GMI} < 6.4$, and $\text{GMI} \geq 6.4$. In the fused CGMacros setting, GMI is computed from combined Dexcom and Libre readings within the matched seven-day window. Since this baseline is deterministic, we use macro-F1 as the primary metric.

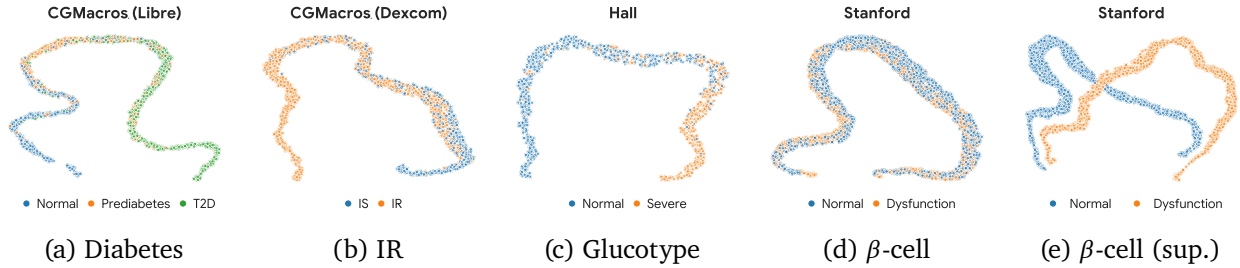


Figure 6 | UMAP visualizations of frozen GlucoFM embeddings. Panels (a)–(d) show unsupervised UMAP projections; panel (e) shows a supervised UMAP for β -cell dysfunction.

As shown in Table 5, GlucoFM consistently outperforms the same-window 7-day GMI-equivalent threshold baseline across Stanford and CGMacros sensor settings. The gains are largest on CGMacros-Dexcom and the fused setting, indicating stronger diabetes category classification than a rule based only on seven-day mean glucose. Since the GMI baseline reduces each seven-day window to a single average-glucose-derived value, these results suggest that GlucoFM retains additional CGM information, including variability, excursions, and temporal structure. The smaller but positive gain on CGMacros-Libre further shows that the benefit of representation learning depends on the sensor setting and baseline strength.

Table 5 | GMI-equivalent comparison on Macro-F1.

Dataset	GMI Rule	GlucoFM	Δ
Stanford	59.6	67.0	+07.4
CGMacros-Dexcom	36.3	53.7	+17.4
CGMacros-Libre	63.7	65.6	+01.9
CGMacros-Fused	56.9	65.9	+09.0

Frozen Representation Visualization. We use UMAP [34] to qualitatively inspect task-related structure in frozen GlucoFM embeddings before downstream adaptation. As shown in Figure 6(a–d), embeddings form continuous manifolds rather than clearly separated clusters, consistent with the gradual nature of glucose regulation and metabolic dysfunction [5, 51]. Even without label supervision, several labels are enriched in different regions, especially for diabetes risk, insulin resistance, and glucotype patterns, suggesting that GlucoFM captures physiologically relevant variation. More subtle outcomes such as β -cell dysfunction remain more entangled in the unsupervised view, while the supervised UMAP in Figure 6(e) shows that label-guided projections can reveal more separable structure from the same frozen embeddings. These visualizations provide qualitative support for task-related organization in GlucoFM representations.

Pretraining Scalability Analysis. We evaluate how GlucoFM scales with unlabeled data by sampling 20–100% of subjects from each pretraining cohort using five random seeds, while keeping the model architecture and downstream protocol fixed. As shown in Figure 7, average PR-AUC increases steadily as more pretraining data are used. Notably, GlucoFM trained with only 20% of the corpus already matches CGM-specific foundation model baselines trained on the full corpus, suggesting strong data efficiency, consistent with the inductive biases introduced by state–event modeling and JEPA-style pretraining. Performance continues to improve with additional unlabeled data, indicating that GlucoFM is not saturated at the current scale. The narrow shaded region shows that the trend is stable across subject subsampling seeds, suggesting that the improvements are not driven by a particular subset of pretraining subjects.

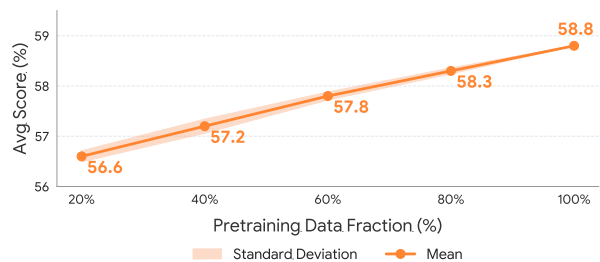


Figure 7 | Pretraining data scaling analysis.

Performance continues to improve with additional unlabeled data, indicating that GlucoFM is not saturated at the current scale. The narrow shaded region shows that the trend is stable across subject subsampling seeds, suggesting that the improvements are not driven by a particular subset of pretraining subjects.

5. Ablation

We ablate the key design choices of GlucoFM under the same pretraining and downstream evaluation protocols. The main text reports task-averaged results, with full task-wise results in Appendix E.

Dual Stream vs. Single Stream. We compare a raw-input tokenizer, state-only and event-only single-stream encoders, and the proposed dual-stream state–event encoder. For fairness, all variants receive the corresponding patch-level statistics and temporal-difference features; they differ only in how glucose signals and auxiliary features are organized. As shown in Figure 8, the dual-stream encoder performs best across all metrics, showing that slow glyceic trends and transient deviations provide complementary information.

The event-only variant is weakest, suggesting that residual fluctuations alone are too unstable for robust metabolic representation learning. The raw-input and state-only variants remain competitive, indicating that generic glucose patterns and low-frequency trends both contain useful clinical signal. However, both are improved by the full dual-stream model, supporting our design choice of separately encoding slow and fast dynamics before fusion.

Temporal Dynamics Weight. Figure 9 evaluates the weight of the temporal dynamics objective. Removing this objective ($\lambda_{TD} = 0$) reduces task-averaged performance across all metrics, indicating that masked contextual latent prediction alone does not fully capture clinically useful glucose evolution. Performance improves as λ_{TD} increases and reaches a broad optimum around 0.6–1.0, then gradually declines when the dynamics term becomes too dominant. This supports a balanced pretraining objective: contextual prediction captures global daily structure, while temporal dynamics modeling provides complementary constraints on local state–event transitions.

Training-time Data Augmentation. We evaluate whether GlucoFM benefits from the proposed CGM-aware augmentation pipeline. As shown in Figure 10, augmentation improves task-averaged downstream performance across all metrics. Value-level perturbations provide modest gains by exposing the model to amplitude shifts and transient artifacts, while structural sparsification contributes more by simulating realistic missingness and heterogeneous sampling rates. This suggests that robustness to observation-pattern variation is particularly important for CGM representation learning. Overall, augmentation improves robustness but acts as a complement to the representation design rather than replacing it.

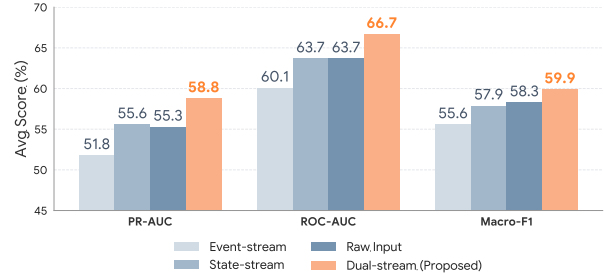


Figure 8 | Encoder design ablation.

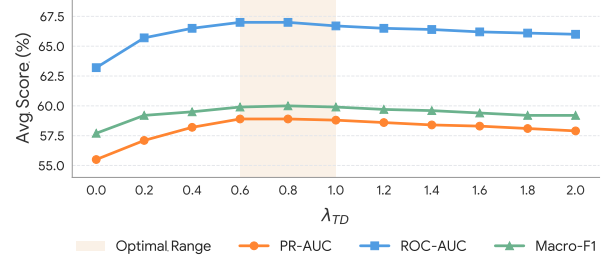


Figure 9 | Temporal dynamics weight ablation.

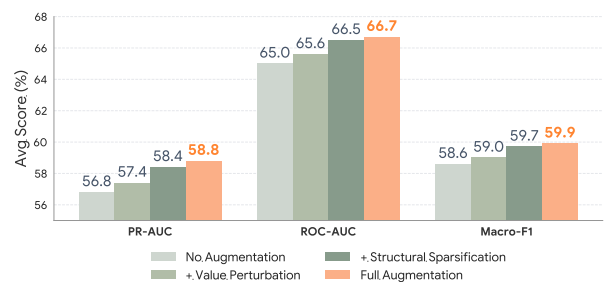


Figure 10 | Data augmentation ablation.

Dense Interpolation. We test whether GlucoFM requires the dense interpolation preprocessing commonly used by CGM-specific baselines. We compare dense interpolation alone with dense interpolation plus structural sparsification. As shown in Figure 11, both interpolated variants underperform the default mask-aware setting, although they remain competitive with CGM-specific foundation model baselines on average. Adding structural sparsification narrows the gap, suggesting that exposure to structured missingness can partially reduce interpolation-induced shortcuts. Overall, preserving the observation mask is more effective for GlucoFM than treating imputed values as fully observed measurements, especially when CGM recordings contain heterogeneous sampling rates and sensor dropouts.

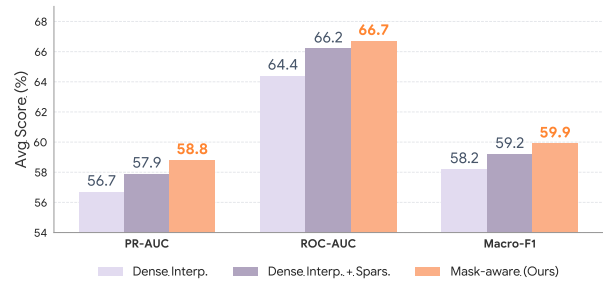


Figure 11 | Dense interpolation ablation.

6. Discussion

Limitations. Despite these findings, GlucoFM is limited by the scale and diversity of available CGM data. Large-scale CGM pretraining remains challenging because data collection requires physical sensors, multi-day participant compliance, and often additional laboratory or clinical assessments for downstream labels. Although we use subject-grouped splits, identical downstream protocols, and re-pretrain available CGM-specific baselines on the same corpus when code permits, the pretraining population remains modest and may not fully capture demographic, device, lifestyle, and disease heterogeneity. Our evaluation is restricted to retrospective diagnosis-level prediction tasks and does not assess longitudinal outcomes, treatment response, or prospective clinical deployment. Moreover, although multiday embedding aggregation improves subject-level prediction, the encoder itself still models 24-hour windows independently, leaving longer-range temporal modeling to simple downstream aggregation. GlucoFM is a research prototype, has not been cleared or approved by any regulatory authority, and is not intended to diagnose, treat, cure, or prevent any disease, nor should it be used as a substitute for professional medical advice.

Future Work. Future work should scale pretraining to larger and more diverse CGM cohorts, including broader device coverage and more real 15-minute recordings. Extending GlucoFM from post-hoc multiday aggregation to native multi-day context modeling may better capture longitudinal metabolic state, treatment response, and slower changes over weeks or months. Another important direction is real-time CGM modeling under evolving missingness, device changes, and behavioral context. We do not target short-term glucose forecasting in this work, which often requires external context such as meal composition, activity, stress, and sleep; integrating such context may enable future models to bridge daily metabolic phenotyping and short-horizon prediction.

Conclusion. We introduced GlucoFM, a lightweight CGM foundation model that aligns irregular glucose recordings to a chronological daily grid, preserves observation masks, and decomposes glucose dynamics into slow state and transient event streams. Across multiple cohorts and seven diagnosis-level prediction tasks, GlucoFM achieves strong frozen linear probing, low-label adaptation, cross-dataset transfer, and multiday subject-level prediction. These results suggest that CGM foundation models benefit from preserving sensing structure and explicitly modeling the multi-scale nature of glucose dynamics, rather than treating CGM as a generic one-dimensional time series. By learning transferable representations from unlabeled CGM, GlucoFM may reduce reliance on large labeled clinical cohorts for metabolic phenotyping; however, it should be validated within the intended population and clinical workflow before real-world use. We will release the code and reproducibility scripts to support

transparent evaluation and future CGM foundation-model research.

References

- [1] Salar Abbaspourazad, Oussama Elachqar, Andrew Miller, Saba Emrani, Udhyakumar Nallasamy, and Ian Shapiro. Large-scale training of foundation models for wearable biosignals. In *The Twelfth International Conference on Learning Representations*, 2024.
- [2] Abdul Fatir Ansari, Oleksandr Shchur, Jaris Küken, Andreas Auer, Boran Han, Pedro Mercado, Syama Sundar Rangapuram, Huibin Shen, Lorenzo Stella, Xiyuan Zhang, Mononito Goswami, Shubham Kapoor, Danielle C. Maddix, Pablo Guerron, Tony Hu, Junming Yin, Nick Erickson, Prateek Mutalik Desai, Hao Wang, Huzefa Rangwala, George Karypis, Yuyang Wang, and Michael Bohlke-Schneider. Chronos-2: From univariate to universal forecasting. *arXiv preprint arXiv:2510.15821*, 2025.
- [3] Abdul Fatir Ansari, Lorenzo Stella, Caner Turkmen, Xiyuan Zhang, Pedro Mercado, Huibin Shen, Oleksandr Shchur, Syama Sundar Rangapuram, Sebastian Pineda Arango, Shubham Kapoor, Jasper Zschiegner, Danielle C. Maddix, Hao Wang, Michael W. Mahoney, Kari Torkkola, Andrew Gordon Wilson, Michael Bohlke-Schneider, and Yuyang Wang. Chronos: Learning the language of time series. *Transactions on Machine Learning Research*, 2024.
- [4] Mahmoud Assran, Quentin Duval, Ishan Misra, Piotr Bojanowski, Pascal Vincent, Michael Rabbat, Yann LeCun, and Nicolas Ballas. Self-supervised learning from images with a joint-embedding predictive architecture. In *Proceedings of the IEEE/CVF Conference on Computer Vision and Pattern Recognition*, pages 15619–15629, 2023.
- [5] Etienne Becht, Leland McInnes, John Healy, Charles-Antoine Dutertre, Immanuel W. H. Kwok, Lai Guan Ng, Florent Ginhoux, and Evan W. Newell. Dimensionality reduction for visualizing single-cell data using umap. *Nature Biotechnology*, 2019.
- [6] Richard M Bergenstal, Roy W Beck, Kelly L Close, George Grunberger, David B Sacks, Aaron Kowalski, Adam S Brown, Lutz Heinemann, Grazia Aleppo, Donna B Ryan, Tonya D Riddlesworth, and William T Cefalu. Glucose management indicator (GMI): A new term for estimating A1C from continuous glucose monitoring. *Diabetes Care*, 41(11):2275–2280, Nov 2018.
- [7] Sarah E. Berry, Ana M. Valdes, David A. Drew, Francesco Asnicar, Mohsen Mazidi, Jonathan Wolf, Joan Capdevila, George Hadjigeorgiou, Richard Davies, Haya Al Khatib, Christopher Bonnett, Sajaysurya Ganesh, Elco Bakker, Deborah Hart, Massimo Mangino, Jordi Merino, Inbar Linenberg, Patrick Wyatt, Jose M. Ordovas, Christopher D. Gardner, Linda M. Delahanty, Andrew T. Chan, Nicola Segata, Paul W. Franks, and Tim D. Spector. Human postprandial responses to food and potential for precision nutrition. *Nature Medicine*, 26(6):964–973, 2020.
- [8] Wei Cao, Dong Wang, Jian Li, Hao Zhou, Lei Li, and Yitan Li. Brits: Bidirectional recurrent imputation for time series. *Advances in neural information processing systems*, 31, 2018.
- [9] Zhengping Che, Sanjay Purushotham, Kyunghyun Cho, David Sontag, and Yan Liu. Recurrent neural networks for multivariate time series with missing values. *Scientific reports*, 8(1):6085, 2018.
- [10] Baiyu Chen, Wilson Wongso, Zechen Li, Yonchanok Khaokaew, Hao Xue, and Flora Salim. Co-modo: Cross-modal video-to-imu distillation for efficient egocentric human activity recognition. *Proc. ACM Interact. Mob. Wearable Ubiquitous Technol.*, 2026.

- [11] Peter Cho, Juseong Kim, Brinnae Bent, and Jessilyn Dunn. BIG IDEAs Lab Glycemic Variability and Wearable Device Data. *PhysioNet*, September 2023. Version 1.1.2.
- [12] Ana Colás, Luis Vigil, Borja Vargas, David Cuesta-Frau, and Manuel Varela. Detrended fluctuation analysis in the prediction of type 2 diabetes mellitus in patients at risk: Model optimization and comparison with other metrics. *PLOS ONE*, 14(12):e0225817, 2019.
- [13] Abhimanyu Das, Weihao Kong, Rajat Sen, and Yichen Zhou. A decoder-only foundation model for time-series forecasting. In *Proceedings of the 41st International Conference on Machine Learning*, ICML'24. JMLR.org, 2024.
- [14] Anurag Das, David Kerr, Namino Glantz, Wendy Bevier, Rony Santiago, Ricardo Gutierrez-Osuna, and Bobak J. Mortazavi. Cgmacros: a pilot scientific dataset for personalized nutrition and diet monitoring. *Scientific Data*, 12:1557, 2025.
- [15] Vasilii Feofanov, Marius Alonso, Songkang Wen, Romain Ilbert, Hongbo Guo, Malik Tiomoko, Lujia Pan, Jianfeng Zhang, and Ievgen Redko. Mantis: Lightweight calibrated foundation model for user-friendly time series classification. In *1st ICML Workshop on Foundation Models for Structured Data*, 2025.
- [16] Vasilii Feofanov, Songkang Wen, Jianfeng Zhang, Lujia Pan, and Ievgen Redko. Mantisv2: Closing the zero-shot gap in time series classification with synthetic data and test-time strategies. *arXiv preprint arXiv:2602.17868*, 2026.
- [17] Shanghua Gao, Teddy Koker, Owen Queen, Thomas Hartvigsen, Theodoros Tsiligkaridis, and Marinka Zitnik. UniTS: A unified multi-task time series model. In *The Thirty-eighth Annual Conference on Neural Information Processing Systems*, 2024.
- [18] Mononito Goswami, Konrad Szafer, Arjun Choudhry, Yifu Cai, Shuo Li, and Artur Dubrawski. Moment: A family of open time-series foundation models. In *International Conference on Machine Learning*, 2024.
- [19] Heather Hall, Dalia Perelman, Alessandra Breschi, Patricia Limcaoco, Ryan Kellogg, Tracey McLaughlin, and Michael Snyder. Glucotypes reveal new patterns of glucose dysregulation. *PLoS biology*, 16(7):e2005143, 2018.
- [20] Zilin Jing, Vincent Jeanselme, Yuta Kobayashi, Simon A Lee, Chao Pang, Aparajita Kashyap, Yanwei Li, Xinzhuo Jiang, and Shalmali Joshi. One loss to rule them all: Marked time-to-event for structured ehr foundation models. *arXiv preprint arXiv:2602.00541*, 2026.
- [21] Ayya Keshet, Smadar Shilo, Anastasia Godneva, Yeela Talmor-Barkan, Yaron Aviv, Eran Segal, and Hagai Rossman. Cgmap: characterizing continuous glucose monitor data in thousands of non-diabetic individuals. *Cell metabolism*, 35(5):758–769, 2023.
- [22] Dani Kiyasseh, Tingting Zhu, and David A Clifton. Clocs: Contrastive learning of cardiac signals across space, time, and patients. In *International Conference on Machine Learning*, pages 5606–5615. PMLR, 2021.
- [23] David C Klonoff, Richard M Bergenstal, Eda Cengiz, Mark A Clements, Daniel Espes, Juan Espinoza, David Kerr, Boris Kovatchev, David M Maahs, Julia K Mader, Nestoras Mathioudakis, Ahmed A Metwally, Shahid N Shah, Bin Sheng, Michael P Snyder, Guillermo Umpierrez, Mandy M Shao, Agatha F Scheideman, Alessandra T Ayers, Cindy N Ho, and Elizabeth Healey. Continuous glucose monitoring data analysis 2.0: functional data pattern recognition and artificial intelligence applications. *Journal of Diabetes Science and Technology*, 19(6):1515–1527, 2025.

- [24] Ilaria Landi, Benjamin S. Glicksberg, Hsien-Chin Lee, Sarah Cherng, Giulia Landi, Matteo Danieleto, Joel T. Dudley, Cesare Furlanello, and Riccardo Miotto. Deep representation learning of electronic health records to unlock patient stratification at scale. *npj Digital Medicine*, 3(96), 2020.
- [25] Simon A. Lee, Cyrus Tanade, Hao Zhou, Juhyeon Lee, Megha Thukral, Md Sazzad Hissain Khan, Keum San Chun, Baiying Lu, Migyeong Gwak, Mehrab Bin Morshed, Viswam Nathan, Md Mahbubur Rahman, Li Zhu, Subramaniam Venkatraman, and Sharanya Arcot Desai. HiMAE: Hierarchical masked autoencoders discover resolution-specific structure in wearable time series. In *The Fourteenth International Conference on Learning Representations*, 2026.
- [26] Sirui Li, Shuhan Xiao, Mihir Joshi, Ahmed Metwally, Daniel McDuff, Wei Wang, and Yuzhe Yang. HEARTS: Benchmarking llm reasoning on health time series. *arXiv preprint arXiv:2603.06638*, 2026.
- [27] Yikuan Li, Shishir Rao, José Roberto Ayala Solares, Abdelaali Hassaine, Rema Ramakrishnan, Dexter Canoy, Yajie Zhu, Kazem Rahimi, and Gholamreza Salimi-Khorshidi. Behrt: Transformer for electronic health records. *Scientific Reports*, 10(1):7155, 2020.
- [28] Zechen Li, Baiyu Chen, Hao Xue, and Flora D. Salim. Zara: Training-free motion time-series reasoning via evidence-grounded llm agents. *arXiv preprint arXiv:2508.04038*, 2026.
- [29] Zechen Li, Shohreh Deldari, Linyao Chen, Hao Xue, and Flora D. Salim. SensorLLM: Aligning large language models with motion sensors for human activity recognition. In *Proceedings of the 2025 Conference on Empirical Methods in Natural Language Processing*, pages 354–379, 2025.
- [30] Yurun Lu, Dan Liu, Zhongming Liang, Rui Liu, Pei Chen, Yitong Liu, Jiachen Li, Zhanying Feng, Lei M. Li, Bin Sheng, Weiping Jia, Luonan Chen, Huating Li, and Yong Wang. A pretrained transformer model for decoding individual glucose dynamics from continuous glucose monitoring data. *National Science Review*, 12(5):nwaf039, May 2025.
- [31] Junjie Luo, Abhimanyu Kumbara, Mansur Shomali, Rui Han, Anand Iyer, Grazia Aleppo, Ritu Agarwal, and Gordon Gao. A large sensor foundation model pretrained on continuous glucose monitor data for diabetes management. *npj Health Systems*, 2025.
- [32] Guy Lutsker, Gal Sapir, Smadar Shilo, Jordi Merino, Anastasia Godneva, Jerry R. Greenfield, Dorit Samocha-Bonet, Raja Dhir, Francisco Gude, Shie Mannor, Eli Meirum, Eric P. Xing, Gal Chechik, Hagai Rossman, and Eran Segal. A foundation model for continuous glucose monitoring data. *Nature*, pages 1–9, 2026.
- [33] Marcos Matabuena, Rahul Ghosal, Javier Enrique Aguilar, Ayya Keshet, Robert Wagner, Carmen Fernández Merino, Juan Sánchez Castro, Vadim Zipunnikov, Jukka-Pekka Onnela, and Francisco Gude. Glucodensity functional profiles outperform traditional continuous glucose monitoring metrics. *Scientific Reports*, 2025.
- [34] Leland McInnes, John Healy, and James Melville. Umap: Uniform manifold approximation and projection for dimension reduction. *arXiv preprint arXiv:1802.03426*, 2020.
- [35] Ahmed A. Metwally, A. Ali Heydari, Daniel McDuff, Alexandru Solot, Zeinab Esmaeilpour, Anthony Z. Faranesh, Menglian Zhou, Girish Narayanswamy, Maxwell A. Xu, Xin Liu, Yuzhe Yang, David B. Savage, Mark Malhotra, Conor Heneghan, Shwetak Patel, Cathy Speed, and Javier L. Prieto. Insulin resistance prediction from wearables and routine blood biomarkers. *Nature*, pages 1–11, 2026.

- [36] Ahmed A. Metwally, Heyjun Park, Yue Wu, Tracey McLaughlin, and Michael P. Snyder. Use of continuous glucose monitoring with machine learning to identify metabolic subphenotypes and inform precision lifestyle changes. *Journal of Diabetes Science and Technology*, 20(3), 2026.
- [37] Ahmed A. Metwally, Dalia Perelman, Heyjun Park, Yue Wu, Alok Kumar Jha, Seth Sharp, Alessandra Celli, Ekrem Ayhan, Fahim Abbasi, Anna L. Gloyn, Tracey McLaughlin, and Michael P. Snyder. Prediction of metabolic subphenotypes of type 2 diabetes via continuous glucose monitoring and machine learning. *Nature Biomedical Engineering*, 9(8):1222–1239, Aug 2025.
- [38] Hada Melino Muhammad, Zechen Li, Flora Salim, and Ahmed A. Metwally. Cgm-jepa: Learning consistent continuous glucose monitor representations via predictive self-supervised pretraining. *arXiv preprint arXiv:2605.00933*, 2026.
- [39] Girish Narayanswamy, Xin Liu, Kumar Ayush, Yuzhe Yang, Xuhai Xu, Shun Liao, Jake Garrison, Shyam A. Taylor, Jacob Sunshine, Yun Liu, Tim Althoff, Shrikanth Narayanan, Pushmeet Kohli, Jiening Zhan, Mark Malhotra, Shwetak Patel, Samy Abdel-Ghaffar, and Daniel McDuff. Scaling wearable foundation models. In *The Thirteenth International Conference on Learning Representations*, 2025.
- [40] Heyjun Park, Ahmed A. Metwally, Alireza Delfarah, Yue Wu, Dalia Perelman, Caleb Mayer, Curtis McGinity, Majid Rodgar, Alessandra Celli, Tracey McLaughlin, Emmanuel Mignot, and Michael Snyder. High-resolution lifestyle profiling and metabolic subphenotypes of type 2 diabetes. *npj Digital Medicine*, 8(352), 2025.
- [41] Laila Rasmy, Yang Xiang, Ziqian Xie, Cui Tao, and Degui Zhi. Med-bert: pretrained contextualized embeddings on large-scale structured electronic health records for disease prediction. *npj Digital Medicine*, 4(86), 2021.
- [42] Kashif Rasul, Arjun Ashok, Andrew Robert Williams, Hena Ghonia, Rishika Bhagwatkar, Arian Khorasani, Mohammad Javad Darvishi Bayazi, George Adamopoulos, Roland Riachi, Nadhir Hassen, Marin Biloš, Sahil Garg, Anderson Schneider, Nicolas Chapados, Alexandre Drouin, Valentina Zantedeschi, Yuriy Nevmyvaka, and Irina Rish. Lag-llama: Towards foundation models for probabilistic time series forecasting. *arXiv preprint arXiv:2310.08278*, 2024.
- [43] Yulia Rubanova, Ricky TQ Chen, and David K Duvenaud. Latent ordinary differential equations for irregularly-sampled time series. *Advances in neural information processing systems*, 32, 2019.
- [44] Artem Shmatko, Alexander Wolfgang Jung, Kumar Gaurav, Søren Brunak, Laust Hvas Mortensen, Ewan Birney, Tom Fitzgerald, and Moritz Gerstung. Learning the natural history of human disease with generative transformers. *Nature*, 647(8088):248–256, 2025.
- [45] Zitao Shuai, Zongzhe Xu, David Yang, Wei Wang, and Yuzhe Yang. OSF: On pre-training and scaling of sleep foundation models. *arXiv preprint arXiv:2603.00190*, 2026.
- [46] Satya Narayan Shukla and Benjamin M Marlin. Interpolation-prediction networks for irregularly sampled time series. *arXiv preprint arXiv:1909.07782*, 2019.
- [47] Dimitris Spathis, Ignacio Perez-Pozuelo, Soren Brage, Nicholas J. Wareham, and Cecilia Mascolo. Self-supervised transfer learning of physiological representations from free-living wearable data. In *Proceedings of the Conference on Health, Inference, and Learning*, CHIL '21, page 69–78, New York, NY, USA, 2021. Association for Computing Machinery.
- [48] Hikaru Sugimoto, Gal Sapir, Ayya Keshet, and Shinya Kuroda. Use of continuous glucose monitoring to stratify individuals without diabetes. *Communications Medicine*, 2026.

- [49] Sana Tonekaboni, Danny Eytan, and Anna Goldenberg. Unsupervised representation learning for time series with temporal neighborhood coding. In *International Conference on Learning Representations*, 2021.
- [50] Julie Wagner, Howard Tennen, and Howard Wolpert. Continuous glucose monitoring: a review for behavioral researchers. *Psychosomatic Medicine*, 74(4):356–365, 2012.
- [51] F. Alexander Wolf, Fiona K. Hamey, Mireya Plass, Jordi Solana, Joakim S. Dahlin, Berthold Göttgens, Nikolaus Rajewsky, Lukas Simon, and Fabian J. Theis. Paga: graph abstraction reconciles clustering with trajectory inference through a topology preserving map of single cells. *Genome Biology*, 2019.
- [52] Gerald Woo, Chenghao Liu, Akshat Kumar, Caiming Xiong, Silvio Savarese, and Doyen Sahoo. Unified training of universal time series forecasting transformers. In *Forty-first International Conference on Machine Learning*, 2024.
- [53] Yue Wu, Ben Ehlert, Ahmed A. Metwally, Dalia Perelman, Heyjun Park, Andrew Wallace Brooks, Fahim Abbasi, Basil Michael, Alessandra Celli, Caroline Bejikian, Ekrem Ayhan, Yingzhou Lu, Samuel M. Lancaster, Daniel Hornburg, Lucia Ramirez, David Bogumil, Sarah Pollock, Frank Wong, Denver Bradley, Georg Gutjahr, Ekanath Srihari Rangan, Tao Wang, Lettie McGuire, P. Venkat Rangan, and Michael P. Snyder. Individual variations in glycemic responses to carbohydrates and underlying metabolic physiology. *Nature Medicine*, 31(7):2232–2243, 2025.
- [54] Maxwell A. Xu, Girish Narayanswamy, Kumar Ayush, Dimitris Spathis, Shun Liao, Shyam A. Tailor, Ahmed Metwally, A. Ali Heydari, Yuwei Zhang, Jake Garrison, Samy Abdel-Ghaffar, Xuhai Xu, Ken Gu, Jacob Sunshine, Ming-Zher Poh, Yun Liu, Tim Althoff, Shrikanth Narayanan, Pushmeet Kohli, Mark Malhotra, Shwetak Patel, Yuzhe Yang, James M. Rehg, Xin Liu, and Daniel McDuff. Lsm-2: Learning from incomplete wearable sensor data. *arXiv preprint arXiv:2506.05321*, 2025.
- [55] Zongzhe Xu, Zitao Shuai, Eideen Mozaffari, Ravi S Aysola, Rajesh Kumar, and Yuzhe Yang. SleepLM: Natural-language intelligence for human sleep. *arXiv preprint arXiv:2602.23605*, 2026.
- [56] Yuzhe Yang, Xin Liu, Jiang Wu, Silviu Borac, Dina Katabi, Ming-Zher Poh, and Daniel McDuff. Simper: Simple self-supervised learning of periodic targets. In *International Conference on Learning Representations (ICLR)*, 2023.
- [57] Zhihao Yu, Xu Chu, Yujie Jin, Yasha Wang, and Junfeng Zhao. Smart: Towards pre-trained missing-aware model for patient health status prediction. In *NeurIPS 2024*, 2024.
- [58] David Zeevi, Tal Korem, Niv Zmora, David Israeli, Daphna Rothschild, Adina Weinberger, Orly Ben-Yacov, Dar Lador, Tali Avnit-Sagi, Maya Lotan-Pompan, Jotham Suez, Jemal Ali Mahdi, Elad Matot, Gal Malka, Noa Kosower, Michal Rein, Gili Zilberman-Schapira, Lenka Dohnalová, Meirav Pevsner-Fischer, Rony Bikovsky, Zamir Halpern, Eran Elinav, and Eran Segal. Personalized nutrition by prediction of glycemic responses. *Cell*, 163(5):1079–1094, 2015.
- [59] Yuwei Zhang, Kumar Ayush, Siyuan Qiao, A. Ali Heydari, Girish Narayanswamy, Maxwell A Xu, Ahmed Metwally, Jinhua Xu, Jake Garrison, Xuhai Xu, Tim Althoff, Yun Liu, Pushmeet Kohli, Jiening Zhan, Mark Malhotra, Shwetak Patel, Cecilia Mascolo, Xin Liu, Daniel McDuff, and Yuzhe Yang. SensorLM: Learning the language of wearable sensors. In *The Thirty-ninth Annual Conference on Neural Information Processing Systems*, 2026.

- [60] Qinpei Zhao, Jinhao Zhu, Xuan Shen, Chuwen Lin, Yinjia Zhang, Yuxiang Liang, Baige Cao, Jiangfeng Li, Xiang Liu, Weixiong Rao, and Congrong Wang. Chinese diabetes datasets for data-driven machine learning. *Scientific Data*, 10, 2023.
- [61] Hao Zhou, Simon A. Lee, Cyrus Tanade, Keum San Chun, Juhyeon Lee, Migyeong Gwak, Megha Thukral, Justin Sung, Eugene Hwang, Mehrab Bin Morshed, Li Zhu, Viswam Nathan, Md Mahbubur Rahman, Subramaniam Venkatraman, and Sharanya Arcot Desai. Physiology-aware masked cross-modal reconstruction for biosignal representation learning. *arXiv preprint arXiv:2605.00973*, 2026.

A. Datasets

A.1. CGM Segmentation and Missingness Handling

Before extracting 24-hour windows, we split each subject’s raw CGM trace into continuous recording segments based on timestamp gaps. Gaps of at most 1 hour are treated as short interruptions within the same segment. After aligning the trace to the target 5-minute grid, these missing positions are retained as unobserved entries with NaN glucose values and mask value 0, rather than being treated as real measurements. In contrast, gaps longer than 1 hour are treated as segment boundaries, and the trace is split into separate segments.

As a result, each 24-hour training window is extracted from a continuous recording segment and does not contain any single real-data gap longer than 1 hour. This preserves realistic short missingness while avoiding windows that span long non-wear or sensor-disconnection periods. For fair comparison, all applicable baselines use the same pretraining inputs and identical downstream fold splits as GlucoFM.

A.2. Pretraining Datasets

To increase the diversity of unlabeled pretraining data, we extract 24-hour windows from each continuous CGM segment using a fixed-seed random overlapping strategy. For each segment, we randomly sample overlapping 24-hour windows with a coverage ratio between 20% and 80%, rather than using only fixed non-overlapping windows. This exposes the model to diverse daily start times and temporal contexts while keeping sampling reproducible. Since pretraining is self-supervised and label-free, overlapping windows improve temporal coverage without introducing label leakage; downstream evaluation instead uses non-overlapping windows with subject-grouped splits.

Wear-CGM. The Wear-CGM dataset is a non-public multimodal CGM dataset collected as part of Google/Fitbit research studies across two sequential research phases with non-overlapping participants. The protocols for the Wear-CGM datasets were approved by Advarra (Institutional Review Board (IRB) no. Pro00059582 and Pro00069880). All participants provided written informed consent prior to data collection, which included permission for the use of de-identified data in secondary research and algorithm development. It contains CGM recordings from healthy, non-diabetic adults in the United States, collected using Dexcom G6 Pro sensors at 5-minute intervals. Phase 1 included 105 participants in an observational protocol lasting approximately 4 weeks, with 2–3 sensors used per participant. Phase 2 included 87 participants over up to 15 days and incorporated standardized meal challenges designed to elicit metabolic responses. Phase 2 also collected clinical measurements, including fasting glucose and insulin, comprehensive metabolic panels, lipid panels, HbA1c, C-reactive protein, and up to two 2-hour oral glucose tolerance tests after overnight fasting. Together, the two phases provide 75,330 hours of CGM recordings. Although the dataset also contains wearable, nutrition, and blood-pressure measurements, only CGM data are used in this work.

BIG IDEAs. The BIG IDEAs dataset [11] contains CGM recordings from 16 subjects, collected with Dexcom sensors at 5-minute intervals. After preprocessing, it provides 3,017 monitoring hours, corresponding to an average duration of approximately 7.9 days per subject.

Colas. The Colas dataset [12] contains CGM recordings from 206 subjects after preprocessing, collected with iPro sensors at 5-minute intervals. It provides 9,544 monitoring hours, corresponding to an average duration of approximately 1.9 days per subject.

Stanford. The Stanford dataset [37] contains CGM recordings from 56 subjects, collected with Dexcom sensors at 5-minute intervals. Among them, 19 subjects lack the clinical metadata required for downstream label construction and are therefore used only for unlabeled pretraining. This pretraining

Table 6 | Subject-level label distributions for downstream clinical prediction tasks across four cohorts.

CGMacros (N=45)			Hall (N=56)		
Task	Class	Count	Task	Class	Count
Diabetes Risk	Normoglycemic	16	Diabetes	Normoglycemic	37
	Prediabetes	14		Abnormal	19
	Type 2 Diabetes	15	Glucotype	Normal	34
Insulin Resistance	Sensitive	13		Severe	22
	Resistant	32	Insulin Resistance	Sensitive	35
Obesity	Non-obese	22		Resistant	21
	Hyperlipidemia	Normal	33	Hyperlipidemia	Normal
Hyperlipidemia		12	Hyperlipidemia		8
Stanford (N=37)			ShanghaiT2DM (N=65)		
Task	Class	Count	Task	Class	Count
Diabetes	Normoglycemic	17	Hypoglycemia	No	56
	Abnormal	20		Yes	9
β -cell Dysfunction	Normal	17	Insulin Resistance	Sensitive	24
	Dysfunction	20		Resistant	41
Insulin Resistance	Sensitive	17	Hyperlipidemia	Normal	45
	Resistant	20		Hyperlipidemia	20

subset contains 8,761 monitoring hours, corresponding to an average duration of approximately 19.2 days per subject. The remaining 37 subjects have complete clinical profiles and are used for downstream evaluation.

ShanghaiT2DM. The ShanghaiT2DM dataset [60] contains CGM recordings from patients with type 2 diabetes, collected with FreeStyle Libre sensors at 15-minute intervals. Most participants have one recording session, while seven participants provide 2–3 separate sessions. Because clinical labels may vary across sessions separated by long intervals, we treat each session as a distinct subject-entry, following the baseline protocol. Among these subject-entries, 44 lack sufficient clinical metadata for downstream label construction and are used only for unlabeled pretraining. This pretraining subset contains 12,414 monitoring hours, corresponding to an average duration of approximately 11.8 days per subject-entry.

A.3. Downstream Datasets

The clinical thresholds below are used to define downstream prediction labels consistently across cohorts and are not intended as standalone diagnostic criteria. For all downstream datasets, CGM traces are divided into non-overlapping 1-day segments, which avoids duplicated temporal evidence across samples and reduces leakage or over-counting from highly correlated overlapping windows.

CGMacros. The CGMacros dataset [14] contains multimodal physiological data from 45 subjects, each wearing both Dexcom and FreeStyle Libre sensors for approximately 10 days. The Dexcom and Libre recordings provide 10,376 and 10,998 monitoring hours, respectively. To avoid subject leakage, recordings from both sensor brands for the same subject are always assigned to the same training or testing split. We define four downstream tasks: (1) diabetes risk, with three classes:

normoglycemic, prediabetes, and type 2 diabetes; (2) insulin resistance, where a subject is labeled positive if $\text{HOMA-IR} = (\text{Insulin}_{\mu\text{U}/\text{mL}} \times \text{Fasting Glucose}_{\text{mg}/\text{dL}}) / 405.0 > 2.9$; (3) obesity, defined as $\text{BMI} = \text{Weight}_{\text{kg}} / (\text{Height}_{\text{m}})^2 \geq 30$; and (4) hyperlipidemia, where a positive label is assigned if total cholesterol ≥ 240 , LDL ≥ 160 , or triglycerides ≥ 200 mg/dL.

Ha11. The Ha11 dataset [19] originally contains 57 subjects. We retain 56 subjects with sufficient clinical information for constructing diabetes risk, insulin resistance, hyperlipidemia, and glucotype labels. The processed CGM recordings are collected with Dexcom sensors at 5-minute intervals and contain 7,090 monitoring hours, with an average duration of approximately 5.3 days per subject. We define four binary downstream tasks: (1) diabetes risk, where prediabetes or diabetes is grouped as abnormal glucose regulation and compared against normoglycemic status; (2) glucotype, distinguishing severe glucose fluctuation from normal profiles, where low and moderate glucotype categories are grouped as non-severe; (3) insulin resistance, determined by steady-state plasma glucose (SSPG), where a subject is labeled positive if $\text{SSPG} > 120$, or, when SSPG is unavailable, by $\text{HOMA-IR} = (\text{Insulin}_{\mu\text{U}/\text{mL}} \times \text{FBG}_{\text{mg}/\text{dL}}) / 405.0 > 2.9$; and (4) hyperlipidemia, where a positive label is assigned if total cholesterol ≥ 240 , LDL ≥ 160 , or triglycerides ≥ 200 mg/dL.

Stanford. The downstream Stanford subset [37] contains 37 subjects with complete clinical profiles, providing 27,571 monitoring hours and an average duration of approximately 31 days per subject. We define three binary downstream tasks: (1) insulin resistance, mapping insulin-sensitive subjects to 0 and insulin-resistant subjects to 1 based on SSPG-derived classes; (2) β -cell dysfunction, where subjects are categorized as dysfunction versus normal based on the median disposition index (DI); and (3) diabetes risk, where subjects are labeled as abnormal glucose regulation if $\text{HbA1c} \geq 5.7\%$ and normoglycemic otherwise.

ShanghaiT2DM. The downstream ShanghaiT2DM subset [60] contains 65 labeled sessions, providing 15,634 monitoring hours and an average duration of approximately 10 days per session. We define three binary downstream tasks: (1) hypoglycemia, mapped directly from clinical records, where “yes” indicates the positive class and “no” indicates the negative class; (2) insulin resistance, computed using HOMA-IR after converting fasting insulin from pmol/L to $\mu\text{U}/\text{mL}$ by dividing by 6.945, where a session is labeled positive if $\text{HOMA-IR} = (\text{Insulin}_{\mu\text{U}/\text{mL}} \times \text{Glucose}_{\text{mg}/\text{dL}}) / 405.0 > 2.9$; and (3) hyperlipidemia, where lipid profiles are converted from mmol/L to mg/dL and a positive label is assigned if total cholesterol ≥ 240 ($\text{TC}_{\text{mmol}/\text{L}} \times 38.67$), LDL ≥ 160 ($\text{LDL}_{\text{mmol}/\text{L}} \times 38.67$), or triglycerides ≥ 200 ($\text{TG}_{\text{mmol}/\text{L}} \times 88.57$).

B. Baselines

We compare GlucoFM with three groups of baselines: general-purpose time-series foundation models, an open-weight CGM-specific foundation model pretrained on an external cohort, and CGM-specific foundation models retrained on our pretraining corpus. For all representation-based evaluations, encoders are frozen and the same downstream logistic regression classifier is trained unless otherwise stated.

B.1. General-purpose Time-series Foundation Models

Chronos-2. Chronos-2 [2] is a general-purpose time-series forecasting foundation model for zero-shot univariate, multivariate, and covariate-informed forecasting. It extends Chronos with group attention to share information across related series, variables, targets, and covariates. We evaluate both Chronos-2 and Chronos-2-small as general-purpose foundation model baselines for frozen representation extraction. To obtain sequence-level embeddings, we feed each CGM sequence into

the model and extract the output hidden states. We aggregate valid hidden states with mean pooling while excluding the EOS token, which performed best in our preliminary pooling comparison.

MOMENT. MOMENT [18] is an open time-series foundation model pretrained on the Time Series Pile with masked time-series modeling. Following the official pipeline, we remove null values, align each sequence to 288 points using linear interpolation, and extract frozen representations for downstream evaluation. We include MOMENT to assess whether large-scale general-purpose time-series pretraining transfers to CGM-based clinical prediction.

Mantis and MantisV2. Mantis [15] is a lightweight time-series foundation model for classification, using a Vision Transformer-style architecture and contrastive pretraining. MantisV2 [16] improves Mantis for zero-shot time-series classification through stronger synthetic-data pretraining, architectural refinements, and test-time representation strategies. Following the official preprocessing for both models, we linearly interpolate each input sequence to 512 points and extract frozen encoder representations for downstream evaluation.

B.2. Externally Pretrained CGM Foundation Model

CGMformer. CGMformer [30] is a CGM-specific Transformer pretrained with masked learning on daily CGM profiles. The released checkpoint is pretrained on an external cohort of 1,917 CGM-days from 964 participants and evaluated in the original work on tasks such as diabetes screening, metabolic subtyping, and dietary recommendation. We use it as an externally pretrained CGM-specific baseline. Following the official preprocessing scheme, each CGM window is represented on a 288-point 5-minute grid; missing bins are mapped to CGMformer’s <pad> token; glucose values are discretized using the released vocabulary; and a <cls> token is prepended to form a 289-token input. We keep the checkpoint frozen and use mean-pooled hidden states as window-level embeddings, following the official embedding extraction strategy; in our implementation, the mean is weighted by the attention mask to exclude <pad> positions.

B.3. CGM Foundation Models Retrained on Our Pretraining Corpus

CGM-JEPA. CGM-JEPA [38] is a CGM-specific predictive self-supervised model that predicts masked latent targets instead of reconstructing raw glucose values. We retrain it on the same unlabeled CGM corpus as GlucoFM using the official configuration: inputs are aligned to a 5-minute grid, linearly interpolated to 288-point daily sequences, normalized, and encoded by a 3-layer Transformer with hidden dimension 96 and 6 attention heads. It is trained with batch size 128, learning rate 10^{-4} , mask ratio 0.25, and 101 epochs. Downstream embeddings are extracted from the frozen encoder before the projection head and mean-pooled over sequence tokens.

X-CGM-JEPA. X-CGM-JEPA [38] uses the same encoder, preprocessing, and optimization configuration as CGM-JEPA, but adds an auxiliary Glucodensity-based cross-view objective. Following the official setting, Glucodensity views are constructed as KDE-based 2D joint density grids over three variable pairs: glucose–speed, glucose–acceleration, and speed–acceleration, where speed and acceleration denote first- and second-order glucose differences. Each density grid has size 32×32 , is divided into non-overlapping spatial patches, and is partially masked during pretraining. We retrain X-CGM-JEPA on the same corpus as GlucoFM and extract downstream embeddings from the frozen encoder using the same mean-pooling protocol as CGM-JEPA.

GluFormer. GluFormer [32] is a generative CGM foundation model trained with self-supervised autoregressive glucose-token prediction. We retrain two variants on the same pretraining corpus as GlucoFM. GluFormer (base) follows the original setting: 5-minute alignment, imputation, clipping

to [40, 500], discretization into shifted glucose tokens, and a 16-layer Transformer with hidden dimension 1024, 16 attention heads, and feed-forward dimension 2048, trained with Adam at learning rate 5×10^{-5} for 76 epochs. GluFormer (tiny) uses the same preprocessing and objective but a smaller 4-layer Transformer with hidden dimension 128, 4 attention heads, and feed-forward dimension 256, chosen to provide a parameter scale comparable to GlucoFM and CGM-JEPA. It is trained with Adam at learning rate 10^{-4} , batch size 128, for 100 epochs. Downstream embeddings are extracted from frozen hidden states over valid non-padding tokens using max pooling by default.

C. Additional Implementation Details

C.1. CGM Window Construction and Chronological Grid Alignment

All inputs to GlucoFM are pre-segmented 24-hour CGM windows. For datasets originally containing multi-day recordings, the segmentation strategy is described in Appendix A. Given a 24-hour segment with readings $X = \{x_i\}_{i=1}^N$ and timestamps $T = \{t_i\}_{i=1}^N$, we align it to a fixed 24-hour grid with 5-minute resolution, yielding $L = 288$ grid positions. The first timestamp t_1 defines the circadian start index

$$s = \left\lfloor \frac{60 \cdot \text{hour}(t_1) + \text{minute}(t_1)}{5} \right\rfloor, \quad (6)$$

and the absolute time-of-day index of grid position j is $a_j = (s + j) \bmod L$.

Each reading is assigned to a grid index based on its elapsed time from the window start:

$$u_i = \frac{t_i - t_1}{\Delta t}, \quad j_i = \mathcal{B}(u_i), \quad (7)$$

where $\Delta t = 5$ minutes and $\mathcal{B}(\cdot)$ denotes the binning rule used during preprocessing. We use floor-based assignment for most datasets and nearest-index rounding only when it better matches the dataset’s timestamp convention. Readings outside the valid range $[0, L - 1]$ are excluded, and multiple readings assigned to the same grid position are averaged.

The aligned glucose sequence is denoted as $\hat{X} \in \mathbb{R}^L$, and the physical observation mask $M \in \{0, 1\}^L$ indicates whether each grid position contains at least one real CGM reading. Missing positions are filled only for tensor construction; they are distinguished by the observation mask and are never treated as observed measurements. Thus, chronological grid alignment is separated from interpolation or imputation.

C.2. Mask-aware Physiological Statistics

All feature construction is mask-aware: unobserved grid positions do not contribute to statistics or loss terms. GlucoFM divides each 24-hour window into $P = 24$ non-overlapping one-hour patches, each containing $K = 12$ grid positions. For patch \mathcal{P}_i , the physical observation support is

$$d_i = \frac{1}{K} \sum_{j \in \mathcal{P}_i} M_j. \quad (8)$$

This patch density is reused in mask-aware loss weighting.

For the state stream, GlucoFM computes patch-level glucose statistics using only observed entries:

$$\mu_i = \frac{\sum_{j \in \mathcal{P}_i} M_j \hat{X}_j}{\sum_{j \in \mathcal{P}_i} M_j + \epsilon}, \quad \sigma_i = \left(\frac{\sum_{j \in \mathcal{P}_i} M_j (\hat{X}_j - \mu_i)^2}{\sum_{j \in \mathcal{P}_i} M_j + \epsilon} \right)^{1/2}. \quad (9)$$

Empty patches are zeroed by the validity mask.

For the event stream, rate-of-change features are computed only from valid observed positions. The implementation searches backward up to 9 grid steps and uses the closest previous observed value:

$$r_j = \frac{\hat{X}_j - \hat{X}_{j-b}}{b}, \quad (10)$$

where j and $j - b$ are both observed and no closer valid pair exists. If no valid previous observation is found, the rate-of-change entry is set to zero and marked invalid. Patch-level event mean and standard deviation are then computed from valid rate-of-change entries only.

C.3. Causal Gaussian State–Event Decoupling

GlucoFM separates each aligned CGM sequence into a low-frequency state component and a high-frequency event component using a causal, mask-aware Gaussian filter. The filter is applied after mask-aware normalization. Let \tilde{X} denote the normalized aligned glucose sequence and let M denote the corresponding observation mask used by the branch. For each grid position j , the state component is estimated from current and past observed values:

$$\tilde{X}_j^{\text{state}} = \frac{\sum_{r=0}^R K_\sigma(r) M_{j-r} \tilde{X}_{j-r}}{\sum_{r=0}^R K_\sigma(r) M_{j-r} + \epsilon}, \quad (11)$$

where invalid indices are ignored. The one-sided Gaussian kernel is

$$K_\sigma(r) = \frac{\exp(-r^2/(2\sigma^2))}{\sum_{u=0}^R \exp(-u^2/(2\sigma^2))}, \quad r = 0, \dots, R. \quad (12)$$

Using only $r \geq 0$ makes the filter causal, so future glucose values are not used to estimate the current state. In the implementation, the maximum lag is determined by the maximum allowed bandwidth and a truncation factor of 3, giving $R = \lceil 3\sigma_{\max} \rceil = 36$ grid steps.

The bandwidth σ is learnable and constrained as

$$\sigma = \sigma_{\min} + (\sigma_{\max} - \sigma_{\min}) \cdot \text{sigmoid}(\rho), \quad (13)$$

where ρ is an unconstrained learnable parameter, $\sigma_{\min} = 2$, and $\sigma_{\max} = 12$. On the 5-minute grid, this corresponds to a learnable Gaussian scale of approximately 10–60 minutes, initialized at $\sigma = 6$.

The event component is defined as the observed residual after removing the state trend:

$$\tilde{X}^{\text{event}} = (\tilde{X} - \tilde{X}^{\text{state}}) \odot M. \quad (14)$$

The state stream therefore receives smoothed baseline dynamics, while the event stream receives short-term deviations supported by real observations.

C.4. Architecture and Dimensionality

Following the above patching scheme, the state stream encodes each patch using a 64-dimensional waveform feature, a 16-dimensional intra-patch trend-difference feature, and a 48-dimensional projected statistics feature from patch mean and standard deviation. The event stream encodes each patch using a 48-dimensional residual waveform feature, a 48-dimensional rate-of-change feature, and a 32-dimensional projected statistics feature from valid rate-of-change mean and standard deviation. These components are projected into 64-dimensional state and event tokens, respectively.

The state and event tokens are fused into a unified physiological patch token of dimension $D = 128$. Circular time-of-day features from the absolute grid index are projected to the same dimension and combined with patch positional embeddings through a learnable gate. The context and EMA target encoders share a 3-layer Transformer architecture with 4 attention heads and feed-forward dimension 256. The masked-context predictor is a lightweight 1-layer Transformer, and the temporal dynamics objective uses two lightweight transition heads. During downstream evaluation, only the frozen online branch is retained. GlucoFM has 0.72M trainable parameters and 1.18M total parameters during pretraining, mainly due to the additional EMA target branch.

C.5. Pretraining Masking and Transition Loss

During masked contextual representation learning, GlucoFM applies random patch-level masking to the online branch, with the masking ratio sampled uniformly from $[0.5, 0.6]$. Selected patches are hidden from the visible signal used for mask-aware statistics and filtering, and their patch tokens are replaced by a learnable mask token before the context encoder. The EMA target branch uses the full physical observation mask and encodes the complete sequence to provide latent targets. The masked contextual loss is applied only at masked patch positions and is weighted by each patch’s physical observation density:

$$w_i = d_i = \frac{1}{K} \sum_{j \in \mathcal{P}_i} M_j. \quad (15)$$

For temporal dynamics modeling, GlucoFM predicts next-patch state and event targets from the current online state and event tokens before Transformer self-attention. Let $m_i^{\text{mask}} \in \{0, 1\}$ indicate whether patch i is masked, and let d_i denote its physical observation density. The transition weight is

$$q_i = (1 - m_i^{\text{mask}}) d_i d_{i+1}, \quad i = 1, \dots, P - 1. \quad (16)$$

This excludes transitions starting from masked context patches and down-weights transitions involving sparsely observed adjacent patches. The EMA next-patch targets are also taken before Transformer self-attention, preventing future contextual information from leaking into the transition objective. In the main experiments, GlucoFM optimizes the masked contextual representation loss and temporal dynamics loss with both loss weights set to 1.0.

C.6. Downstream Feature Extraction

For downstream evaluation, we freeze the pretrained online branch of GlucoFM and discard the EMA target branch and pretraining-only prediction heads. Each one-day CGM window is passed through the online state–event preprocessing modules, unified embedder, and context encoder to obtain patch representations $\{z_i\}_{i=1}^P$, where $P = 24$. We use global average pooling over patches to obtain a fixed-length window representation.

C.7. Data Augmentation Details

During pretraining, GlucoFM uses two augmentation families: *value perturbations* and *structural sparsification*. Value perturbations preserve the observation mask while modifying observed glucose values. Baseline wander is applied with probability 0.25 by adding a sinusoidal perturbation with amplitude sampled from $[5, 15]$ mg/dL and frequency from $[0.5, 2.0]$ cycles per window. Compression-like drops are applied with probability 0.10 by attenuating a contiguous 6–12-step segment using a V-shaped curve with minimum multiplier sampled from $[0.4, 0.7]$.

Table 7 | Full subject-disjoint linear-probe performance. All reported values represent the mean \pm std evaluated via 10 iterations of 5-fold subject-grouped cross-validation.

Method	Metrics	CGMacros				ShanghaiT2DM			Stanford		Hall				
		Diabetes	IR	Hyperlip.	Obesity	IR	Hyperlip.	Hypogly.	Diabetes	β -cell Dys.	IR	Diabetes	IR	Hyperlip.	Glucotype
<i>General Time-series Foundation Models with Large-scale Pretraining</i>															
Chronos-2 (small)	PR	51.6 \pm 4.5	82.7 \pm 6.5	30.5 \pm 6.5	56.0 \pm 4.8	65.0 \pm 5.4	34.8 \pm 6.0	16.0 \pm 4.3	69.2 \pm 6.6	58.6 \pm 5.1	62.5 \pm 5.0	51.7 \pm 10.3	44.9 \pm 7.0	24.2 \pm 6.8	54.2 \pm 8.2
	AUC	68.0 \pm 3.7	67.5 \pm 10.4	52.1 \pm 5.9	53.7 \pm 5.1	55.0 \pm 6.0	50.6 \pm 6.6	49.1 \pm 8.8	65.4 \pm 8.0	57.3 \pm 6.3	64.2 \pm 5.3	64.9 \pm 9.7	57.7 \pm 7.7	61.3 \pm 9.3	62.6 \pm 6.9
	F1	49.4 \pm 4.8	61.7 \pm 7.7	50.1 \pm 4.1	52.7 \pm 4.3	52.6 \pm 4.3	51.5 \pm 4.6	50.5 \pm 3.8	61.3 \pm 6.2	54.8 \pm 4.8	59.6 \pm 3.8	60.9 \pm 7.1	55.0 \pm 6.1	52.5 \pm 6.5	58.6 \pm 6.5
Chronos-2	PR	54.3 \pm 4.7	84.1 \pm 5.8	34.0 \pm 9.1	58.1 \pm 5.4	59.8 \pm 5.3	34.7 \pm 5.6	18.9 \pm 7.8	68.5 \pm 6.8	58.5 \pm 4.3	59.2 \pm 4.2	48.6 \pm 9.2	51.3 \pm 9.5	20.6 \pm 8.5	54.4 \pm 9.3
	AUC	69.7 \pm 3.9	69.9 \pm 9.9	55.8 \pm 7.9	56.6 \pm 6.9	49.5 \pm 7.2	49.7 \pm 7.8	53.0 \pm 10.8	65.6 \pm 7.8	57.8 \pm 5.5	60.2 \pm 5.3	60.4 \pm 9.2	62.7 \pm 8.2	50.3 \pm 10.7	63.0 \pm 8.6
	F1	50.2 \pm 4.4	63.3 \pm 7.5	53.7 \pm 4.6	54.2 \pm 5.9	49.0 \pm 5.6	50.4 \pm 5.4	52.8 \pm 5.6	61.9 \pm 5.6	55.5 \pm 4.2	56.6 \pm 4.2	58.4 \pm 7.9	58.2 \pm 6.3	50.9 \pm 4.9	56.2 \pm 7.8
MOMENT (small)	PR	54.0 \pm 4.8	83.8 \pm 5.8	30.3 \pm 8.5	60.9 \pm 6.3	58.3 \pm 5.3	38.3 \pm 7.4	16.3 \pm 5.3	70.4 \pm 7.4	57.2 \pm 5.2	63.0 \pm 5.6	59.2 \pm 9.7	53.1 \pm 8.2	19.4 \pm 6.7	55.6 \pm 10.0
	AUC	69.1 \pm 4.3	70.6 \pm 9.6	51.5 \pm 10.3	58.7 \pm 6.5	49.0 \pm 6.9	55.9 \pm 7.6	52.9 \pm 9.8	67.6 \pm 8.8	55.5 \pm 6.5	65.1 \pm 6.3	69.7 \pm 8.3	62.1 \pm 8.8	48.7 \pm 10.3	61.7 \pm 8.7
	F1	49.8 \pm 4.7	63.6 \pm 7.7	50.9 \pm 6.1	55.7 \pm 5.5	49.4 \pm 4.8	52.9 \pm 5.8	51.4 \pm 4.6	62.5 \pm 7.5	53.8 \pm 5.0	60.1 \pm 4.5	64.5 \pm 6.9	59.0 \pm 6.8	50.4 \pm 6.5	59.3 \pm 7.7
MOMENT (large)	PR	50.3 \pm 5.0	87.4 \pm 5.1	32.0 \pm 7.9	61.8 \pm 5.7	59.6 \pm 5.9	42.4 \pm 6.7	14.3 \pm 3.4	71.9 \pm 5.3	61.8 \pm 5.2	58.1 \pm 4.3	52.1 \pm 9.4	44.9 \pm 10.1	18.4 \pm 5.7	55.8 \pm 7.5
	AUC	66.1 \pm 4.6	75.2 \pm 9.7	53.2 \pm 8.3	59.9 \pm 6.8	47.8 \pm 7.5	60.8 \pm 6.3	49.6 \pm 8.1	69.1 \pm 6.4	58.9 \pm 5.4	59.4 \pm 4.5	65.0 \pm 8.0	56.6 \pm 8.8	51.4 \pm 12.2	63.2 \pm 7.6
	F1	46.8 \pm 5.4	67.2 \pm 8.2	52.5 \pm 4.9	56.3 \pm 4.8	48.6 \pm 5.5	57.2 \pm 5.3	49.7 \pm 3.5	63.7 \pm 5.0	55.7 \pm 4.1	56.1 \pm 3.0	60.5 \pm 6.5	53.3 \pm 7.5	47.7 \pm 5.9	57.8 \pm 6.4
Mantis	PR	61.8 \pm 5.9	90.9 \pm 5.5	30.1 \pm 10.0	63.4 \pm 8.1	59.2 \pm 5.5	30.6 \pm 4.5	22.9 \pm 12.4	75.1 \pm 5.4	63.5 \pm 9.0	67.1 \pm 7.3	54.2 \pm 11.5	55.7 \pm 12.4	24.8 \pm 9.7	77.5 \pm 7.6
	AUC	75.5 \pm 5.1	80.3 \pm 10.9	49.8 \pm 13.6	60.8 \pm 9.8	48.2 \pm 7.3	46.0 \pm 7.6	58.6 \pm 17.5	71.4 \pm 5.2	61.5 \pm 9.3	68.2 \pm 5.9	67.1 \pm 10.1	66.2 \pm 10.4	57.9 \pm 10.5	82.6 \pm 5.7
	F1	56.0 \pm 6.6	71.6 \pm 8.3	49.8 \pm 6.9	57.2 \pm 6.9	48.4 \pm 5.3	47.5 \pm 5.5	53.8 \pm 7.7	65.9 \pm 4.8	58.5 \pm 6.3	62.3 \pm 4.5	59.6 \pm 8.9	59.8 \pm 8.9	53.7 \pm 6.7	73.3 \pm 6.1
MantisV2	PR	63.6 \pm 6.2	91.2 \pm 4.2	30.3 \pm 10.0	62.8 \pm 7.1	64.1 \pm 5.9	33.3 \pm 6.6	22.0 \pm 12.8	75.2 \pm 6.7	65.7 \pm 7.2	64.6 \pm 9.1	57.7 \pm 14.4	59.3 \pm 13.6	25.0 \pm 9.9	81.5 \pm 7.8
	AUC	76.7 \pm 5.2	80.3 \pm 9.0	49.1 \pm 13.6	60.3 \pm 9.4	52.7 \pm 6.8	48.5 \pm 8.6	59.6 \pm 20.9	71.2 \pm 7.9	64.4 \pm 7.2	65.5 \pm 9.3	67.5 \pm 11.8	66.7 \pm 11.1	58.8 \pm 9.5	84.7 \pm 6.0
	F1	56.2 \pm 7.0	68.9 \pm 9.0	49.2 \pm 7.6	55.9 \pm 7.2	51.2 \pm 5.6	48.1 \pm 6.4	53.3 \pm 10.1	65.7 \pm 7.7	58.6 \pm 5.5	60.4 \pm 7.5	61.1 \pm 9.3	60.8 \pm 8.9	52.6 \pm 8.0	76.7 \pm 7.3
<i>Externally Pretrained CGM Foundation Model</i>															
CGMformer	PR	63.3 \pm 6.4	89.9 \pm 4.6	31.8 \pm 8.6	68.1 \pm 7.3	54.8 \pm 3.9	40.6 \pm 9.2	11.9 \pm 3.0	75.9 \pm 5.9	62.2 \pm 8.6	61.8 \pm 5.6	51.1 \pm 11.4	48.0 \pm 10.7	18.0 \pm 7.9	79.6 \pm 7.5
	AUC	77.1 \pm 4.7	78.0 \pm 9.5	54.2 \pm 10.8	66.0 \pm 8.2	43.6 \pm 6.3	58.4 \pm 10.3	42.1 \pm 10.4	71.4 \pm 7.2	59.2 \pm 8.5	63.2 \pm 4.3	66.6 \pm 10.1	58.2 \pm 10.2	46.5 \pm 20.7	84.3 \pm 5.3
	F1	57.2 \pm 5.4	67.6 \pm 7.6	52.1 \pm 6.4	60.5 \pm 6.4	45.5 \pm 5.1	55.1 \pm 6.3	45.3 \pm 4.0	66.2 \pm 5.8	55.7 \pm 6.6	59.0 \pm 3.0	59.3 \pm 8.8	56.3 \pm 7.9	48.4 \pm 8.1	77.1 \pm 5.6
<i>CGM Foundation Models Retrained on Our Pretraining Corpus</i>															
CGM-JEPA	PR	63.0 \pm 7.5	86.2 \pm 7.5	28.7 \pm 9.6	55.5 \pm 7.4	69.1 \pm 7.5	37.4 \pm 8.2	17.8 \pm 5.5	66.4 \pm 4.1	58.7 \pm 5.9	61.5 \pm 7.6	59.9 \pm 12.1	56.8 \pm 14.2	17.3 \pm 9.8	87.6 \pm 5.9
	AUC	75.9 \pm 6.0	73.8 \pm 12.2	47.6 \pm 13.4	53.8 \pm 10.0	60.8 \pm 8.9	53.6 \pm 10.0	56.8 \pm 11.6	61.2 \pm 6.9	55.4 \pm 6.7	61.6 \pm 7.5	73.5 \pm 9.4	68.1 \pm 12.5	40.5 \pm 10.5	90.7 \pm 4.5
	F1	55.4 \pm 7.5	66.3 \pm 8.1	48.2 \pm 7.9	53.2 \pm 6.9	57.2 \pm 6.9	51.3 \pm 6.4	50.4 \pm 6.2	58.7 \pm 5.4	53.9 \pm 5.5	58.1 \pm 5.4	65.0 \pm 7.9	59.4 \pm 10.8	42.8 \pm 5.9	82.2 \pm 5.9
X-CGM-JEPA	PR	63.6 \pm 7.2	86.6 \pm 6.9	29.8 \pm 10.3	55.3 \pm 7.4	66.9 \pm 7.4	35.5 \pm 8.1	16.9 \pm 6.2	67.4 \pm 3.8	60.0 \pm 6.5	61.9 \pm 7.7	59.3 \pm 11.9	56.2 \pm 14.2	17.5 \pm 9.4	87.7 \pm 5.9
	AUC	76.6 \pm 5.8	73.6 \pm 11.5	48.0 \pm 13.2	53.2 \pm 10.1	58.4 \pm 9.0	52.1 \pm 10.9	55.7 \pm 13.7	61.8 \pm 6.1	56.4 \pm 7.1	62.0 \pm 7.0	73.0 \pm 9.2	67.7 \pm 12.4	40.0 \pm 9.4	90.6 \pm 4.6
	F1	56.5 \pm 7.6	65.1 \pm 8.0	48.2 \pm 7.9	52.5 \pm 7.1	55.4 \pm 7.0	49.9 \pm 7.4	49.0 \pm 6.7	59.1 \pm 5.0	54.4 \pm 5.4	58.1 \pm 5.3	64.8 \pm 7.5	59.2 \pm 10.4	42.8 \pm 5.2	82.1 \pm 5.3
GluFormer (tiny)	PR	59.4 \pm 5.5	86.1 \pm 6.7	28.2 \pm 8.8	60.2 \pm 7.6	58.1 \pm 3.8	33.9 \pm 5.0	17.9 \pm 7.5	74.3 \pm 6.1	63.3 \pm 6.0	64.5 \pm 5.0	48.9 \pm 11.0	50.9 \pm 9.4	21.6 \pm 7.2	75.4 \pm 7.0
	AUC	73.9 \pm 4.6	72.5 \pm 11.8	47.9 \pm 11.4	57.9 \pm 8.3	47.6 \pm 4.7	51.1 \pm 7.7	53.3 \pm 13.3	68.9 \pm 6.3	61.9 \pm 7.2	65.4 \pm 5.0	63.3 \pm 9.4	63.6 \pm 8.2	58.0 \pm 12.4	81.7 \pm 4.8
	F1	51.7 \pm 5.7	65.4 \pm 8.1	48.0 \pm 6.2	55.4 \pm 6.1	47.8 \pm 4.2	50.3 \pm 5.9	49.1 \pm 6.0	63.0 \pm 5.4	58.5 \pm 5.9	61.7 \pm 3.8	57.9 \pm 7.6	59.4 \pm 7.3	53.1 \pm 6.6	72.7 \pm 5.1
GluFormer (base)	PR	62.9 \pm 4.6	87.2 \pm 6.2	31.4 \pm 8.4	61.4 \pm 6.5	56.5 \pm 4.1	31.5 \pm 5.4	11.5 \pm 1.9	69.8 \pm 6.1	61.1 \pm 5.1	56.1 \pm 4.4	51.9 \pm 12.2	51.6 \pm 10.5	16.4 \pm 6.0	82.7 \pm 7.8
	AUC	76.7 \pm 3.7	74.8 \pm 11.3	53.1 \pm 10.0	60.5 \pm 7.9	44.9 \pm 5.8	46.7 \pm 8.8	43.9 \pm 10.9	63.1 \pm 6.7	58.0 \pm 5.0	56.3 \pm 4.5	66.0 \pm 9.9	61.6 \pm 9.0	46.9 \pm 9.9	87.9 \pm 5.1
	F1	55.7 \pm 5.4	67.8 \pm 7.3	52.5 \pm 6.0	57.2 \pm 6.2	45.1 \pm 5.8	48.1 \pm 5.8	44.8 \pm 2.6	59.2 \pm 5.2	55.4 \pm 3.9	54.8 \pm 3.8	58.7 \pm 8.7	58.3 \pm 7.7	47.7 \pm 4.9	80.7 \pm 5.6
GlucoFM	PR	65.9 \pm 7.5	91.9 \pm 5.3	36.1 \pm 11.2	64.9 \pm 11.7	67.0 \pm 7.7	33.5 \pm 7.8	21.1 \pm 10.0	77.3 \pm 7.5	69.0 \pm 9.6	67.6 \pm 8.1	66.2 \pm 13.0	60.2 \pm 15.1	14.4 \pm 5.2	88.3 \pm 5.7
	AUC	78.7 \pm 6.1	81.2 \pm 12.7	54.7 \pm 15.9	62.6 \pm 13.2	57.8 \pm 8.2	50.5 \pm 13.4	59.2 \pm 15.9	72.8 \pm 7.4	68.7 \pm 8.9	69.1 \pm 6.6	75.9 \pm 10.2	70.7 \pm 12.2	41.6 \pm 11.6	90.7 \pm 4.3
	F1	58.3 \pm 8.5	69.6 \pm 11.0	50.2 \pm 9.7	59.4 \pm 9.9	55.4 \pm 6.4	49.1 \pm 9.1	50.7 \pm 6.9	66.2 \pm 6.6	63.3 \pm 6.9	64.0 \pm 5.8	64.5 \pm 9.2	62.0 \pm 10.4	43.1 \pm 4.9	82.4 \pm 5.6

Structural sparsification alters the observation mask itself. Decimation is applied with probability 0.40 to dense windows with more than 200 observed positions by keeping every third observation from a random 5-minute offset, producing a 15-minute-like sampling pattern. Disconnection blocks are applied with probability 0.05 by removing 1–3 contiguous blocks of 2–12 grid steps. Candidate augmentations are evaluated in random order; after one is applied, subsequent probabilities are multiplied by 0.25 to avoid excessive corruption.

D. Task Setup and Additional Results

D.1. Subject-Disjoint Linear Probing Details

We provide additional details for the subject-grouped linear probing protocol used in Table 3. For all methods, the pretrained encoder is frozen and only a linear classifier is trained on the extracted 24-hour window representations. We use the same scikit-learn logistic regression classifier with L2 regularization for all models, using the `lbfgs` solver, a maximum of 1000 iterations, and a fixed random seed. This ensures that performance differences mainly reflect the quality of the frozen representations rather than downstream classifier capacity or optimization choices.

For each dataset and task, we perform 5-fold subject-grouped cross-validation and repeat the procedure for 10 iterations with different fold assignments. All windows from the same subject are assigned to the same fold, ensuring that training and test subjects never overlap. The same subject splits are used for all methods within each task, enabling a paired comparison across representations. All preprocessing statistics and downstream classifiers are fit only on the training subjects in each fold, and evaluation metrics are computed over held-out test windows. We report mean performance in

the main paper for readability, and provide the full mean \pm standard deviation across repeated folds in Table 7.

The standard deviations are generally larger for smaller cohorts and more imbalanced tasks, reflecting sensitivity to which subjects appear in the training and test folds. This variability is expected in CGM-based clinical prediction, where glucose dynamics can differ substantially across subjects even under the same diagnostic label. Despite this fold-level variability, GlucoFM achieves the strongest task-averaged performance across PR-AUC, ROC-AUC, and Macro-F1, indicating that its gains are not limited to a single split or dataset. The appendix results also show that several challenging tasks, such as hypoglycemia and hyperlipidemia, exhibit high variance across methods, suggesting that these labels may be more sensitive to cohort composition, class imbalance, or limited subject counts.

D.2. Few-shot Adaptation Details

We provide additional details for the few-shot adaptation protocol used in Figure 3. For each pretrained model, we freeze the encoder and extract representations for all labeled 24-hour windows in each dataset. We perform 5-fold subject-grouped cross-validation with 10 repeated iterations, using the same subject splits across all methods. All windows from the same subject are assigned to the same fold, ensuring subject-disjoint train/test evaluation.

In the *limited-subject* setting, we sample exactly $K \in \{1, 2, 3, 4, 5\}$ labeled support subjects per class from the training fold. The same logistic regression classifier is then trained on all extracted window representations from the selected support subjects. In the *limited-observation* setting, we retain all training subjects but randomly subsample each subject’s 24-hour training windows at fractions $\{1\%, 5\%, 10\%, 20\%, 30\%, 40\%, 50\%\}$. For both settings, each fold and support configuration is evaluated with 5 random samplings, and metrics are computed over held-out test windows.

Few-shot adaptation with limited labeled subjects. Table 8 reports the full task-wise results when the number of labeled support subjects per class is restricted. The one-subject-per-class setting is highly challenging because a single support individual may not capture the clinical heterogeneity of a class, leading to substantial variability across tasks and datasets. GlucoFM remains competitive in this extreme regime and becomes more consistently strong as additional support subjects are added, especially for diabetes risk assessment, insulin resistance, and β -cell dysfunction. The relatively large standard deviations reflect the sensitivity of subject-grouped few-shot evaluation to support-subject selection, which is expected in CGM data with substantial inter-subject variability.

Few-shot adaptation with limited per-subject observations. Table 9 reports the full task-wise results when all training subjects are retained but only a fraction of each subject’s 24-hour windows is used for training. Compared with the limited-subject setting, performance changes more smoothly as the observation fraction increases, indicating that retaining subject diversity is more important than densely sampling a small number of individuals. GlucoFM maintains strong performance even at very low observation fractions and generally improves as more per-subject windows are included, showing robustness to sparse per-subject recordings. The gains are most consistent on tasks with clearer daily metabolic structure, such as diabetes risk assessment, insulin resistance, and β -cell dysfunction, while tasks with lower prevalence or weaker CGM signatures, such as hypoglycemia and hyperlipidemia, exhibit larger variance across folds. Overall, the two few-shot settings suggest that GlucoFM is label-efficient under scarce subject-disjoint supervision and robust when only sparse per-subject observations are available for downstream adaptation.

Table 8 | Few-shot adaptation with limited labeled subjects. All reported values represent the mean \pm std performance evaluated via 5-fold subject-level cross-validation with 10 repeated iterations and 5 random support samplings per split.

Method	# Sub.	Metrics	CGMacros				ShanghaiT2DM			Stanford			Hall			
			Diabetes	IR	Hyperlip.	Obesity	IR	Hyperlip.	Hypogly.	Diabetes	β -cell Dys.	IR	Diabetes	IR	Hyperlip.	Glucotype
CGM-JEPA	1	PR	52.6 \pm 7.9	81.7 \pm 9.9	31.2 \pm 12.6	56.2 \pm 12.6	61.3 \pm 10.5	39.3 \pm 12.7	17.3 \pm 11.0	60.6 \pm 10.6	55.4 \pm 9.7	55.2 \pm 9.3	48.6 \pm 17.5	47.1 \pm 16.5	20.3 \pm 12.1	76.0 \pm 15.7
		AUC	67.0 \pm 7.4	66.6 \pm 15.7	49.4 \pm 16.6	52.5 \pm 15.4	49.5 \pm 14.1	54.5 \pm 16.0	51.8 \pm 19.9	53.7 \pm 14.9	50.5 \pm 12.2	54.2 \pm 10.8	60.2 \pm 20.1	57.8 \pm 18.7	49.4 \pm 16.6	81.6 \pm 13.5
	2	PR	56.7 \pm 6.8	83.3 \pm 7.4	30.0 \pm 11.5	54.0 \pm 10.3	61.2 \pm 9.7	37.7 \pm 11.3	18.3 \pm 10.1	61.5 \pm 8.9	54.7 \pm 7.9	55.9 \pm 8.6	49.5 \pm 13.7	48.3 \pm 14.2	20.7 \pm 12.0	79.8 \pm 11.0
		AUC	70.9 \pm 5.8	69.5 \pm 11.1	48.8 \pm 14.3	50.6 \pm 13.1	49.6 \pm 12.5	52.5 \pm 14.0	53.8 \pm 17.8	55.6 \pm 12.1	50.1 \pm 10.3	55.5 \pm 9.1	63.8 \pm 14.7	60.6 \pm 14.7	49.5 \pm 14.8	85.0 \pm 8.1
	3	PR	57.8 \pm 7.2	83.5 \pm 6.8	30.4 \pm 10.9	54.5 \pm 9.8	61.9 \pm 9.4	36.4 \pm 10.7	17.7 \pm 8.2	61.2 \pm 8.1	55.6 \pm 7.3	55.6 \pm 7.8	50.2 \pm 12.4	48.5 \pm 13.4	20.1 \pm 10.6	81.5 \pm 9.1
		AUC	71.9 \pm 6.0	69.7 \pm 11.4	50.3 \pm 13.0	51.1 \pm 12.7	50.1 \pm 12.7	50.8 \pm 13.6	52.9 \pm 16.0	55.4 \pm 10.9	52.0 \pm 9.0	55.4 \pm 8.5	65.5 \pm 12.7	61.5 \pm 13.8	48.2 \pm 14.3	86.4 \pm 6.5
	4	PR	58.6 \pm 7.5	84.3 \pm 7.1	28.4 \pm 10.6	54.2 \pm 9.2	63.3 \pm 8.8	36.9 \pm 11.8	18.0 \pm 7.7	62.1 \pm 7.3	55.6 \pm 7.5	56.5 \pm 7.9	51.6 \pm 12.4	49.9 \pm 11.7	20.0 \pm 11.0	81.5 \pm 9.0
		AUC	72.5 \pm 6.2	71.0 \pm 11.3	47.4 \pm 13.7	51.0 \pm 12.3	52.2 \pm 11.2	51.5 \pm 14.1	53.4 \pm 15.4	56.4 \pm 10.3	51.7 \pm 9.2	56.4 \pm 8.6	66.8 \pm 11.2	63.5 \pm 10.9	47.3 \pm 13.2	86.6 \pm 6.2
	5	PR	59.5 \pm 7.1	84.5 \pm 7.0	30.3 \pm 11.1	54.9 \pm 9.6	63.7 \pm 8.5	37.6 \pm 11.0	18.4 \pm 8.4	63.5 \pm 6.7	55.9 \pm 7.4	58.2 \pm 8.0	51.5 \pm 12.2	50.7 \pm 11.7	18.3 \pm 8.9	83.0 \pm 8.8
		AUC	73.2 \pm 5.9	71.4 \pm 11.0	49.6 \pm 13.5	51.5 \pm 12.5	53.0 \pm 10.5	52.5 \pm 12.9	54.8 \pm 15.0	58.2 \pm 9.3	52.1 \pm 8.8	58.2 \pm 8.3	66.9 \pm 11.1	63.9 \pm 11.1	45.0 \pm 12.4	87.4 \pm 5.9
X-CGM-JEPA	1	PR	50.9 \pm 7.8	81.0 \pm 9.5	31.0 \pm 12.5	55.8 \pm 11.9	61.3 \pm 10.5	38.9 \pm 12.4	16.9 \pm 11.9	60.7 \pm 10.3	55.6 \pm 9.5	55.4 \pm 9.0	48.6 \pm 17.0	46.7 \pm 15.6	19.5 \pm 12.3	73.8 \pm 15.7
		AUC	65.5 \pm 7.7	65.2 \pm 14.8	49.4 \pm 16.7	52.1 \pm 14.7	48.8 \pm 14.1	54.3 \pm 15.6	50.7 \pm 19.9	54.0 \pm 14.5	50.7 \pm 11.7	54.5 \pm 10.5	60.5 \pm 18.8	57.7 \pm 17.5	47.9 \pm 17.1	80.0 \pm 13.4
	2	PR	55.2 \pm 6.7	82.8 \pm 7.0	29.4 \pm 11.1	54.0 \pm 9.9	61.6 \pm 9.5	36.9 \pm 10.8	17.1 \pm 10.4	61.7 \pm 8.6	54.8 \pm 7.9	56.5 \pm 9.0	48.8 \pm 13.4	48.1 \pm 13.7	20.6 \pm 12.2	77.8 \pm 11.7
		AUC	69.6 \pm 5.8	68.1 \pm 11.1	48.5 \pm 14.3	50.4 \pm 12.4	49.2 \pm 12.3	52.1 \pm 13.7	51.0 \pm 18.2	56.0 \pm 11.9	50.2 \pm 9.9	55.8 \pm 9.5	63.0 \pm 14.2	60.2 \pm 14.2	49.1 \pm 15.2	83.4 \pm 8.8
	3	PR	56.7 \pm 7.0	83.4 \pm 6.5	30.0 \pm 10.5	54.4 \pm 9.6	61.3 \pm 9.4	35.8 \pm 10.5	16.6 \pm 8.4	61.6 \pm 8.1	56.1 \pm 7.6	55.7 \pm 8.2	50.2 \pm 12.8	48.1 \pm 13.6	19.8 \pm 10.8	79.3 \pm 10.8
		AUC	70.8 \pm 6.0	68.8 \pm 10.9	49.9 \pm 12.9	50.9 \pm 12.2	49.1 \pm 12.9	50.5 \pm 13.8	50.9 \pm 16.1	55.8 \pm 11.1	52.3 \pm 9.2	55.2 \pm 9.0	65.0 \pm 12.9	60.7 \pm 14.1	47.3 \pm 14.5	84.8 \pm 7.3
	4	PR	58.3 \pm 7.4	84.1 \pm 7.0	28.6 \pm 10.3	54.4 \pm 9.2	62.5 \pm 8.8	36.0 \pm 11.5	16.6 \pm 7.8	62.8 \pm 7.5	56.1 \pm 7.6	56.7 \pm 8.2	51.1 \pm 12.0	49.1 \pm 11.6	20.1 \pm 11.3	79.8 \pm 9.9
		AUC	72.3 \pm 6.1	69.9 \pm 11.5	48.1 \pm 14.1	50.9 \pm 12.1	51.0 \pm 11.1	50.5 \pm 14.5	51.1 \pm 15.3	56.9 \pm 10.5	52.0 \pm 9.2	56.2 \pm 8.7	66.0 \pm 10.9	62.6 \pm 11.1	46.3 \pm 14.0	85.2 \pm 7.1
	5	PR	59.2 \pm 6.8	84.6 \pm 6.7	29.8 \pm 10.3	54.6 \pm 9.3	62.9 \pm 8.4	37.0 \pm 11.5	17.6 \pm 8.9	64.4 \pm 6.7	56.6 \pm 7.7	58.4 \pm 8.2	51.4 \pm 12.9	49.7 \pm 11.4	18.7 \pm 9.5	80.5 \pm 10.1
		AUC	73.0 \pm 5.7	70.7 \pm 10.9	49.4 \pm 13.6	51.0 \pm 11.9	51.8 \pm 10.5	51.6 \pm 13.7	53.3 \pm 15.5	59.0 \pm 9.2	52.4 \pm 9.2	58.1 \pm 8.4	66.6 \pm 11.3	63.1 \pm 10.9	44.0 \pm 13.4	85.7 \pm 7.0
GluFormer (tiny)	1	PR	58.4 \pm 8.9	84.4 \pm 12.9	32.0 \pm 16.5	58.5 \pm 15.4	59.9 \pm 9.2	38.5 \pm 12.1	17.2 \pm 10.7	63.9 \pm 12.7	60.7 \pm 11.1	59.0 \pm 9.5	49.4 \pm 17.1	49.7 \pm 17.0	18.8 \pm 11.6	72.0 \pm 14.3
		AUC	72.0 \pm 8.2	69.1 \pm 22.7	49.4 \pm 21.4	54.8 \pm 19.3	49.2 \pm 13.0	55.1 \pm 15.2	51.6 \pm 21.9	58.3 \pm 16.6	57.8 \pm 12.7	59.2 \pm 10.4	60.7 \pm 18.8	58.7 \pm 18.1	48.6 \pm 17.7	78.7 \pm 12.6
	2	PR	59.2 \pm 7.9	84.7 \pm 10.5	29.5 \pm 12.8	56.3 \pm 12.3	59.8 \pm 8.8	35.1 \pm 10.1	17.1 \pm 9.9	66.9 \pm 9.9	59.4 \pm 8.4	59.7 \pm 8.3	51.0 \pm 14.7	50.5 \pm 16.1	20.6 \pm 12.7	76.2 \pm 11.2
		AUC	73.4 \pm 6.8	70.1 \pm 17.9	48.1 \pm 16.5	52.7 \pm 16.0	48.9 \pm 12.0	51.5 \pm 13.3	51.8 \pm 19.9	61.9 \pm 11.8	56.8 \pm 9.6	59.8 \pm 8.8	63.9 \pm 14.8	60.1 \pm 16.3	51.1 \pm 16.5	82.2 \pm 9.0
	3	PR	59.1 \pm 7.3	83.0 \pm 10.0	30.8 \pm 12.5	56.4 \pm 10.6	59.0 \pm 8.0	35.4 \pm 9.3	16.7 \pm 8.8	67.0 \pm 8.2	60.5 \pm 8.5	59.4 \pm 7.5	50.9 \pm 14.0	50.9 \pm 15.2	19.9 \pm 9.9	77.7 \pm 10.6
		AUC	73.4 \pm 6.0	67.2 \pm 16.9	50.5 \pm 15.0	53.1 \pm 13.9	47.4 \pm 11.3	52.0 \pm 12.4	52.6 \pm 16.9	62.0 \pm 9.5	57.9 \pm 9.2	59.4 \pm 7.7	63.8 \pm 13.0	61.6 \pm 15.1	51.8 \pm 15.1	83.5 \pm 7.7
	4	PR	59.4 \pm 6.3	84.0 \pm 8.1	28.9 \pm 11.2	56.9 \pm 10.3	59.2 \pm 7.4	34.8 \pm 8.5	15.8 \pm 7.3	68.0 \pm 7.0	59.6 \pm 7.7	59.2 \pm 6.5	51.1 \pm 12.5	51.5 \pm 13.3	19.7 \pm 9.9	77.9 \pm 10.2
		AUC	73.8 \pm 5.1	68.7 \pm 14.3	49.2 \pm 14.1	53.8 \pm 12.5	48.1 \pm 9.6	51.6 \pm 10.8	52.3 \pm 15.6	62.8 \pm 8.2	57.0 \pm 8.6	59.6 \pm 6.9	64.5 \pm 11.9	62.8 \pm 12.7	52.4 \pm 14.6	83.6 \pm 7.3
	5	PR	58.3 \pm 6.2	84.0 \pm 7.7	29.6 \pm 10.8	56.2 \pm 9.4	59.8 \pm 6.8	35.1 \pm 9.1	16.0 \pm 7.0	68.3 \pm 6.4	60.3 \pm 7.0	60.2 \pm 6.0	50.8 \pm 12.9	51.2 \pm 12.9	20.6 \pm 9.4	77.8 \pm 9.8
		AUC	72.9 \pm 5.0	68.8 \pm 13.2	49.6 \pm 13.4	52.8 \pm 11.0	48.8 \pm 9.2	52.2 \pm 11.2	53.2 \pm 14.5	63.2 \pm 7.7	57.7 \pm 7.6	60.7 \pm 6.2	64.3 \pm 11.9	62.5 \pm 12.5	53.9 \pm 13.8	83.6 \pm 7.1
CGMformer	1	PR	53.6 \pm 9.2	83.6 \pm 10.5	29.7 \pm 12.7	59.5 \pm 13.1	60.5 \pm 9.5	37.6 \pm 11.4	16.1 \pm 9.8	62.4 \pm 11.5	58.6 \pm 10.6	57.2 \pm 9.7	48.5 \pm 17.0	45.7 \pm 15.2	17.7 \pm 9.8	74.4 \pm 15.5
		AUC	67.4 \pm 8.8	67.9 \pm 17.3	49.2 \pm 16.4	56.2 \pm 15.9	49.7 \pm 12.9	54.2 \pm 14.9	49.9 \pm 20.2	56.8 \pm 15.1	55.6 \pm 12.7	56.6 \pm 10.8	59.9 \pm 18.6	55.6 \pm 17.5	46.0 \pm 18.8	80.7 \pm 12.7
	2	PR	56.2 \pm 8.3	84.8 \pm 8.6	30.6 \pm 11.6	57.0 \pm 11.0	59.6 \pm 8.6	36.6 \pm 10.4	15.7 \pm 8.7	66.1 \pm 9.8	59.3 \pm 9.9	58.6 \pm 9.0	49.6 \pm 15.7	45.8 \pm 15.4	19.4 \pm 11.3	78.7 \pm 12.4
		AUC	70.5 \pm 7.5	70.1 \pm 14.3	51.2 \pm 14.4	54.1 \pm 13.9	48.6 \pm 11.9	52.8 \pm 13.4	50.0 \pm 18.4	61.4 \pm 12.0	56.1 \pm 11.1	58.4 \pm 9.6	61.9 \pm 15.5	55.7 \pm 16.4	48.7 \pm 18.1	83.8 \pm 9.6
	3	PR	57.1 \pm 7.1	84.4 \pm 8.5	31.8 \pm 11.5	57.9 \pm 10.4	59.3 \pm 8.4	37.7 \pm 10.9	14.9 \pm 7.7	66.8 \pm 9.3	60.1 \pm 9.4	58.3 \pm 8.2	50.8 \pm 14.6	45.7 \pm 14.6	18.5 \pm 9.9	81.3 \pm 9.9
		AUC	71.7 \pm 5.9	69.2 \pm 14.0	53.1 \pm 13.7	55.1 \pm 12.7	47.3 \pm 11.6	53.6 \pm 12.8	47.7 \pm 16.3	62.4 \pm 10.8	57.2 \pm 10.8	58.1 \pm 8.8	63.5 \pm 14.0	56.3 \pm 15.8	47.7 \pm 18.0	85.7 \pm 7.1
	4	PR	58.6 \pm 7.2	86.2 \pm 7.3	30.7 \pm 10.8	58.6 \pm 10.6	59.7 \pm 8.1	37.8 \pm 9.9	14.3 \pm 6.4	68.7 \pm 8.0	59.4 \pm 8.4	59.1 \pm 8.2	51.6 \pm 13.8	45.3 \pm 12.9	18.6 \pm 11.6	80.5 \pm 9.8
		AUC	73.2 \pm 5.9													

Table 9 | Few-shot adaptation with limited observations. All reported values represent the mean \pm std performance evaluated via 5-fold subject-grouped cross-validation with 10 repeated iterations and 5 random support samplings per split.

Method	Ratio	Metrics	CGMacros												ShanghaiT2DM			Stanford			Hall																	
			Diabetes				IR				Hyperlip.				Obesity				IR		Hyperlip.		Hypogly.		Diabetes		β -cell Dys.		IR		Diabetes		IR		Hyperlip.		Glucotype	
			Diabetes	IR	Hyperlip.	Obesity	IR	Hyperlip.	Hypogly.	Diabetes	β -cell Dys.	IR	Diabetes	IR	Hyperlip.	Glucotype																						
CGM-JEPA	1%	PR	52.8 \pm 6.2	81.0 \pm 5.4	27.9 \pm 7.3	54.5 \pm 6.0	63.6 \pm 6.6	37.3 \pm 8.1	18.4 \pm 7.5	53.4 \pm 3.8	53.3 \pm 4.7	49.9 \pm 9.0	49.7 \pm 10.3	20.9 \pm 9.6	80.6 \pm 8.7																							
		AUC	67.8 \pm 5.3	67.8 \pm 8.5	48.0 \pm 9.8	52.3 \pm 7.8	52.8 \pm 8.3	53.5 \pm 9.1	53.9 \pm 12.2	53.4 \pm 6.3	50.8 \pm 5.2	54.4 \pm 5.4	65.6 \pm 8.6	63.3 \pm 9.9	47.9 \pm 10.9	85.8 \pm 6.1																						
	5%	PR	53.1 \pm 6.7	81.1 \pm 5.3	27.5 \pm 7.3	55.6 \pm 6.3	63.4 \pm 7.3	37.0 \pm 8.6	18.1 \pm 7.9	59.8 \pm 5.0	53.7 \pm 4.5	54.0 \pm 4.8	50.0 \pm 9.1	48.2 \pm 10.0	19.3 \pm 8.8	80.1 \pm 8.5																						
		AUC	68.1 \pm 5.8	67.7 \pm 8.0	47.9 \pm 9.6	53.4 \pm 7.3	52.5 \pm 8.8	53.3 \pm 10.1	53.2 \pm 13.2	55.0 \pm 6.7	51.0 \pm 5.9	55.1 \pm 5.4	65.8 \pm 8.5	62.1 \pm 9.9	45.6 \pm 11.1	85.5 \pm 5.9																						
	10%	PR	55.8 \pm 6.5	81.9 \pm 5.3	28.2 \pm 7.7	55.3 \pm 7.1	63.3 \pm 7.5	36.8 \pm 8.6	18.6 \pm 7.8	62.9 \pm 5.4	54.8 \pm 4.3	55.8 \pm 5.5	50.8 \pm 9.0	48.5 \pm 10.3	20.2 \pm 9.5	80.8 \pm 8.5																						
		AUC	70.5 \pm 5.4	69.0 \pm 9.0	48.6 \pm 10.1	53.0 \pm 9.2	52.2 \pm 9.3	52.9 \pm 9.7	54.4 \pm 12.7	56.9 \pm 7.1	51.8 \pm 5.6	56.6 \pm 5.9	66.7 \pm 8.8	62.5 \pm 9.7	47.0 \pm 11.4	86.0 \pm 5.9																						
	20%	PR	58.7 \pm 6.8	83.7 \pm 5.3	27.9 \pm 8.1	55.6 \pm 6.8	65.9 \pm 8.2	38.4 \pm 8.8	17.7 \pm 6.3	63.3 \pm 4.5	55.9 \pm 4.9	58.0 \pm 6.0	49.7 \pm 9.1	48.9 \pm 10.1	20.1 \pm 9.4	81.8 \pm 8.6																						
		AUC	72.8 \pm 5.5	70.9 \pm 9.6	48.0 \pm 11.0	53.5 \pm 8.7	55.7 \pm 9.6	55.1 \pm 9.8	53.2 \pm 11.3	58.4 \pm 6.5	52.8 \pm 6.3	58.7 \pm 6.3	65.8 \pm 9.0	62.8 \pm 10.0	46.2 \pm 11.1	86.7 \pm 6.0																						
	30%	PR	60.4 \pm 7.2	84.1 \pm 6.4	27.6 \pm 8.1	55.0 \pm 6.8	66.6 \pm 7.7	38.0 \pm 8.4	18.1 \pm 7.7	64.1 \pm 4.8	56.5 \pm 5.0	59.4 \pm 6.4	55.1 \pm 10.4	52.5 \pm 11.6	18.5 \pm 8.4	84.3 \pm 7.2																						
		AUC	74.0 \pm 5.9	71.3 \pm 10.8	47.3 \pm 11.3	53.0 \pm 9.0	56.9 \pm 9.1	54.5 \pm 9.2	53.9 \pm 12.0	59.1 \pm 7.0	53.5 \pm 6.0	59.6 \pm 6.5	68.9 \pm 8.6	65.5 \pm 10.9	44.2 \pm 10.9	88.1 \pm 5.3																						
40%	PR	61.2 \pm 7.2	84.9 \pm 6.6	27.7 \pm 8.6	55.1 \pm 7.2	67.5 \pm 7.8	37.9 \pm 8.6	19.2 \pm 8.2	64.7 \pm 4.4	57.0 \pm 5.5	59.5 \pm 6.7	56.3 \pm 11.2	53.9 \pm 12.7	19.0 \pm 9.6	85.4 \pm 6.7																							
	AUC	74.7 \pm 5.7	72.2 \pm 11.0	47.1 \pm 11.8	53.2 \pm 9.8	57.9 \pm 9.0	54.0 \pm 9.7	55.2 \pm 12.4	59.6 \pm 6.7	53.5 \pm 6.5	59.9 \pm 6.9	70.6 \pm 9.2	66.3 \pm 11.3	43.8 \pm 11.0	89.1 \pm 4.8																							
50%	PR	61.9 \pm 7.0	85.4 \pm 6.9	28.1 \pm 8.8	55.7 \pm 7.3	68.0 \pm 7.8	38.2 \pm 8.6	18.6 \pm 7.5	65.1 \pm 3.9	57.3 \pm 5.2	60.2 \pm 6.8	57.8 \pm 12.0	55.3 \pm 12.8	18.1 \pm 8.8	86.1 \pm 6.6																							
	AUC	75.2 \pm 5.8	72.9 \pm 11.2	47.8 \pm 12.2	53.8 \pm 9.7	58.9 \pm 9.0	54.5 \pm 9.8	53.2 \pm 11.3	59.8 \pm 6.5	54.0 \pm 6.3	60.3 \pm 6.9	71.8 \pm 9.2	67.2 \pm 11.4	43.1 \pm 11.3	89.6 \pm 4.8																							
X-CGM-JEPA	1%	PR	50.8 \pm 6.3	81.1 \pm 5.5	27.7 \pm 7.5	54.6 \pm 6.1	62.2 \pm 6.4	36.2 \pm 7.7	17.2 \pm 7.2	58.7 \pm 5.2	53.6 \pm 3.9	54.0 \pm 5.3	49.9 \pm 9.5	49.6 \pm 10.8	20.8 \pm 9.6	78.9 \pm 9.1																						
		AUC	66.2 \pm 5.7	67.4 \pm 8.5	47.7 \pm 10.0	52.2 \pm 7.7	51.1 \pm 8.2	53.0 \pm 9.3	52.0 \pm 12.7	53.7 \pm 6.5	50.7 \pm 5.0	54.9 \pm 6.2	65.2 \pm 8.9	62.9 \pm 10.0	47.4 \pm 11.4	84.7 \pm 6.4																						
	5%	PR	51.8 \pm 6.4	80.9 \pm 5.5	27.6 \pm 7.5	55.6 \pm 6.3	62.0 \pm 7.3	36.2 \pm 8.3	17.0 \pm 7.3	60.2 \pm 5.1	54.0 \pm 4.5	54.5 \pm 5.5	49.6 \pm 8.6	48.0 \pm 10.1	19.4 \pm 9.0	78.8 \pm 9.1																						
		AUC	66.9 \pm 5.5	67.1 \pm 7.9	47.9 \pm 10.2	53.1 \pm 7.3	50.8 \pm 8.8	52.7 \pm 10.4	51.5 \pm 13.3	55.5 \pm 6.5	51.1 \pm 5.9	55.3 \pm 6.1	65.2 \pm 8.0	61.8 \pm 10.0	44.9 \pm 11.9	84.4 \pm 6.5																						
	10%	PR	54.5 \pm 6.1	82.2 \pm 5.4	28.0 \pm 7.8	55.3 \pm 7.2	61.8 \pm 7.2	35.9 \pm 8.9	17.3 \pm 7.5	62.5 \pm 5.3	55.1 \pm 4.5	56.3 \pm 5.9	50.7 \pm 9.5	47.8 \pm 10.1	20.0 \pm 9.2	79.4 \pm 8.7																						
		AUC	69.4 \pm 5.2	68.9 \pm 9.0	48.3 \pm 10.7	52.8 \pm 9.3	50.6 \pm 9.3	52.2 \pm 10.4	52.7 \pm 13.5	57.3 \pm 7.0	52.0 \pm 5.7	56.7 \pm 6.3	66.4 \pm 8.9	61.8 \pm 9.5	46.2 \pm 11.8	84.9 \pm 6.1																						
	20%	PR	58.2 \pm 6.7	84.3 \pm 5.1	28.5 \pm 8.8	55.1 \pm 6.6	64.1 \pm 7.9	37.4 \pm 8.5	16.2 \pm 5.9	64.2 \pm 4.5	56.5 \pm 5.2	58.4 \pm 6.1	49.7 \pm 9.2	48.8 \pm 10.4	19.8 \pm 8.8	80.9 \pm 8.8																						
		AUC	72.3 \pm 5.6	70.9 \pm 9.3	48.4 \pm 11.9	52.9 \pm 8.7	53.8 \pm 9.6	54.6 \pm 9.9	51.5 \pm 12.5	59.1 \pm 6.3	53.0 \pm 6.6	58.7 \pm 6.4	65.2 \pm 8.9	62.7 \pm 10.0	45.4 \pm 11.6	85.9 \pm 6.3																						
	30%	PR	60.3 \pm 7.0	84.8 \pm 5.9	28.2 \pm 8.5	54.9 \pm 6.8	64.9 \pm 7.5	36.4 \pm 7.8	17.3 \pm 8.5	65.2 \pm 4.8	57.3 \pm 5.4	59.8 \pm 6.6	54.7 \pm 10.3	51.9 \pm 11.6	18.3 \pm 8.3	83.8 \pm 7.4																						
		AUC	73.9 \pm 5.8	71.4 \pm 10.4	47.9 \pm 11.5	52.6 \pm 9.0	54.7 \pm 9.3	53.5 \pm 9.4	53.2 \pm 13.8	59.9 \pm 6.8	54.0 \pm 6.4	59.6 \pm 6.5	68.9 \pm 8.6	65.0 \pm 11.0	43.3 \pm 10.9	87.6 \pm 5.4																						
40%	PR	61.4 \pm 6.9	85.6 \pm 6.0	28.5 \pm 9.4	55.0 \pm 7.2	65.8 \pm 7.7	36.5 \pm 8.3	17.7 \pm 7.9	65.8 \pm 4.1	58.0 \pm 5.8	60.0 \pm 6.9	55.7 \pm 11.2	53.1 \pm 12.3	19.1 \pm 9.6	84.9 \pm 6.8																							
	AUC	74.8 \pm 5.6	72.2 \pm 10.5	47.7 \pm 12.0	52.7 \pm 9.7	56.0 \pm 9.2	53.0 \pm 10.2	54.0 \pm 13.8	60.4 \pm 6.2	54.2 \pm 6.9	60.1 \pm 6.8	70.1 \pm 9.1	65.8 \pm 11.0	43.3 \pm 11.0	88.6 \pm 5.0																							
50%	PR	62.2 \pm 6.9	86.0 \pm 6.3	29.2 \pm 9.5	55.4 \pm 7.2	65.9 \pm 7.5	36.3 \pm 8.3	17.4 \pm 7.8	66.2 \pm 3.8	58.3 \pm 5.7	60.7 \pm 7.1	57.7 \pm 11.9	54.4 \pm 12.6	18.3 \pm 8.8	85.8 \pm 6.7																							
	AUC	75.5 \pm 5.6	72.9 \pm 10.7	48.2 \pm 12.4	53.1 \pm 9.7	56.4 \pm 9.0	53.0 \pm 10.5	54.5 \pm 13.7	60.5 \pm 6.0	54.8 \pm 6.8	60.6 \pm 6.7	71.4 \pm 9.1	66.6 \pm 11.2	42.5 \pm 10.7	89.3 \pm 5.0																							
GluFormer (tiny)	1%	PR	61.4 \pm 6.8	86.7 \pm 7.0	28.5 \pm 9.0	60.2 \pm 9.5	58.8 \pm 5.7	35.5 \pm 7.5	16.4 \pm 7.1	68.5 \pm 7.6	62.0 \pm 8.0	61.1 \pm 7.6	50.3 \pm 11.4	52.8 \pm 11.8	19.5 \pm 8.9	79.3 \pm 8.7																						
		AUC	75.2 \pm 5.5	73.4 \pm 12.9	48.7 \pm 11.8	58.5 \pm 10.7	48.0 \pm 7.7	53.2 \pm 9.4	53.7 \pm 14.1	64.5 \pm 8.9	59.7 \pm 8.8	62.2 \pm 7.6	64.2 \pm 10.2	64.0 \pm 10.5	52.0 \pm 12.2	84.7 \pm 6.0																						
	5%	PR	60.9 \pm 6.5	86.4 \pm 6.7	28.9 \pm 10.1	58.6 \pm 9.4	59.3 \pm 5.4	34.7 \pm 7.1	16.3 \pm 6.5	68.9 \pm 6.8	61.2 \pm 7.1	61.0 \pm 6.1	49.9 \pm 10.9	51.9 \pm 10.5	19.3 \pm 8.7	78.7 \pm 9.4																						
		AUC	74.9 \pm 5.4	73.0 \pm 11.9	48.8 \pm 13.1	56.5 \pm 10.6	48.6 \pm 7.3	52.5 \pm 8.9	54.9 \pm 13.6	64.2 \pm 8.1	58.6 \pm 8.1	61.7 \pm 6.2	64.1 \pm 10.2	63.4 \pm 9.6	51.6 \pm 12.8	84.5 \pm 6.4																						
	10%	PR	60.4 \pm 6.5	85.8 \pm 6.6	28.1 \pm 9.2	59.1 \pm 8.3	59.1 \pm 6.2	35.4 \pm 7.5	16.4 \pm 7.4	69.1 \pm 6.2	61.1 \pm 6.1	60.0 \pm 5.6	51.4 \pm 11.6	52.5 \pm 11.3	20.1 \pm 9.5	79.3 \pm 9.1																						
		AUC	74.8 \pm 5.2	72.1 \pm 11.8	48.2 \pm 11.2	56.9 \pm 9.5	48.3 \pm 8.3	53.3 \pm 9.4	54.1 \pm 14.3	64.0 \pm 6.9	58.5 \pm 6.8	60.4 \pm 5.9	64.6 \pm 10.0	64.2 \pm 9.9	53.2 \pm 12.9	84.7 \pm 6.2																						
	20%	PR	59.7 \pm 6.0	84.9 \pm 6.3	27.8 \pm 8.3	58.5 \pm 7.4	58.6 \pm 4.5	35.1 \pm 6.1	16.1 \pm 6.5	68.8 \pm 5.5	60.2 \pm 5.9	60.0 \pm 5.0	49.8 \pm 11.6	51.3 \pm 12.1	19.9 \pm 9.0	79.6 \pm 8.7																						
		AUC	74.2 \pm 4.7	70.3 \pm 11.0	47.3 \pm 10.5	56.1 \pm 8.2	47.7 \pm 6.1	53.5 \pm 7.9	53.2 \pm 13.0	63.5 \pm 6.2	57.7 \pm 6.7	60.2 \pm 5.1	63.9 \pm 10.5	62.6 \pm 10.9	54.3 \pm 11.9	85.2 \pm 5.9																						
	30%	PR	58.9 \pm 5.8	84.4 \pm 5.7	28.0 \pm 8.7	58.3 \pm 6.9	58.6 \pm 4.7	34.6 \pm 6.4	16.1 \pm 6.3	69.3 \pm 5.6	60.3 \pm 5.5	60.0 \pm 5.0	49.0 \pm 10.4	52.1 \pm 9.9	20.3 \pm 8.8	79.2 \pm 8.0																						
		AUC	73.5 \pm 4.6	69.3 \pm 10.1	47.																																	

Table 10 | Subject label distributions for the multiday experiments. Counts are computed on the exact subject cohort used in each experiment.

Dataset	Task	Total	Label 0	Label 1	Label 2
CGMacros	Diabetes	42	15	12	15
CGMacros	IR	42	13	29	–
ShanghaiT2DM	IR	47	20	27	–
Stanford	Beta-cell	35	16	19	–
Stanford	Diabetes	35	16	19	–
Stanford	IR	35	17	18	–
Hall	Diabetes	37	23	14	–
Hall	Glucotype	37	22	15	–
Hall	IR	37	23	14	–

before transfer. For diabetes risk assessment, CGMacros originally includes normoglycemic, prediabetes, and type 2 diabetes categories; we convert it into a binary risk label by grouping prediabetes and type 2 diabetes as the positive class and normoglycemic status as the negative class, matching the binary diabetes-risk labels in Stanford and Hall. For insulin resistance, we use the dataset-provided binary labels while preserving the same positive/negative semantics across cohorts. This protocol evaluates whether frozen representations support transferable clinical decision boundaries across cohorts rather than relying only on dataset-specific label patterns.

D.4. Multiday Representation Observation Details

We provide additional details for the multiday representation observation analysis in Figure 4. The goal is to evaluate whether observing more days of CGM improves subject-level prediction using frozen GlucoFM representations. For each subject, CGM recordings are divided into non-overlapping 24-hour windows and aligned to the GlucoFM input format, a 288-point 5-minute chronological grid. A day is included only if it satisfies the preprocessing quality criteria, including a maximum consecutive missing interval of less than one hour. For each valid day, we extract one embedding using the frozen pretrained GlucoFM encoder. We then select one fixed eligible K_{\max} -day anchor episode for each subject. Stanford, CGMacros, and ShanghaiT2DM use $K_{\max} = 7$, while Hall uses $K_{\max} = 4$ due to the available near-continuous recordings. Table 10 shows the exact subject label distributions used in these experiments. Within each fixed anchor, we enumerate adjacent K -day subwindows for $K = 1, \dots, K_{\max}$.

For each K -day subwindow, we aggregate the frozen daily embeddings into one subject-level representation. We evaluate two aggregation variants. The first uses mean pooling:

$$\mathbf{z}_{i,K,s}^{\text{mean}} = \frac{1}{K} \sum_{d=s}^{s+K-1} \mathbf{h}_{i,d}, \quad (17)$$

where $\mathbf{h}_{i,d}$ is the frozen daily embedding for subject i on day d , and s is the subwindow start position. The second uses `concat(mean, max)` pooling:

$$\mathbf{z}_{i,K,s}^{\text{mean+max}} = \left[\text{mean}_{d=s}^{s+K-1}(\mathbf{h}_{i,d}); \text{max}_{d=s}^{s+K-1}(\mathbf{h}_{i,d}) \right], \quad (18)$$

which preserves both the average daily pattern and salient embedding dimensions across the observation window.

For each K and start position, every subject contributes exactly one representation, and each test subject receives exactly one prediction. Thus, adjacent subwindows from the same subject are not

Table 11 | Subject-level multiday PR-AUC across observation lengths. Values are mean PR-AUC (%) with 95% confidence intervals over repeated subject-level cross-validation. Mean+Max denotes concat(mean, max) pooling. The best value in each row is bolded. Hall is evaluated only for $K = 1-4$.

Dataset	Task	Pooling	K1	K2	K3	K4	K5	K6	K7
CGMacros-Dexcom	Diabetes	Mean	57.6 [57.0, 58.2]	58.5 [57.8, 59.4]	58.2 [57.4, 59.0]	58.5 [57.6, 59.4]	58.5 [57.5, 59.4]	58.6 [57.3, 59.7]	59.8 [58.5, 60.9]
CGMacros-Dexcom	Diabetes	Mean+Max	57.0 [56.3, 57.7]	57.9 [57.0, 58.7]	57.1 [55.7, 58.4]	58.0 [56.2, 59.8]	57.3 [54.9, 59.6]	57.3 [55.1, 59.3]	59.5 [57.5, 61.7]
CGMacros-Dexcom	IR	Mean	92.5 [91.7, 93.2]	93.3 [92.3, 94.0]	94.4 [93.3, 95.2]	94.9 [93.8, 95.7]	95.3 [94.2, 96.1]	95.6 [94.5, 96.5]	95.6 [94.7, 96.3]
CGMacros-Dexcom	IR	Mean+Max	92.3 [91.4, 92.9]	92.5 [91.5, 93.2]	93.3 [92.0, 94.3]	93.8 [92.3, 94.9]	94.6 [93.1, 95.7]	95.5 [94.1, 96.6]	97.8 [97.2, 98.3]
CGMacros-Libre	Diabetes	Mean	63.7 [62.1, 65.1]	65.5 [63.5, 67.2]	66.7 [64.5, 68.3]	67.0 [64.7, 68.8]	67.8 [65.5, 69.6]	67.5 [65.0, 69.5]	67.4 [64.9, 69.6]
CGMacros-Libre	Diabetes	Mean+Max	62.9 [61.1, 64.4]	63.9 [61.7, 65.6]	63.3 [61.1, 64.9]	63.3 [60.8, 65.0]	65.7 [62.9, 68.0]	63.3 [60.3, 65.9]	64.5 [61.2, 67.5]
CGMacros-Libre	IR	Mean	90.6 [90.1, 91.1]	91.8 [91.5, 92.2]	92.1 [91.8, 92.5]	92.1 [91.8, 92.5]	92.4 [92.0, 92.8]	92.5 [92.1, 92.9]	92.7 [92.3, 93.1]
CGMacros-Libre	IR	Mean+Max	89.7 [88.9, 90.3]	91.6 [91.2, 92.0]	91.5 [91.0, 91.9]	91.5 [91.1, 92.1]	92.5 [92.1, 93.0]	92.7 [92.3, 93.1]	92.2 [91.8, 92.7]
CGMacros-Fused	Diabetes	Mean	64.0 [63.0, 65.1]	65.6 [64.4, 66.7]	66.3 [65.0, 67.5]	67.0 [65.6, 68.3]	67.6 [66.1, 68.9]	67.4 [65.7, 69.1]	67.0 [65.0, 68.8]
CGMacros-Fused	Diabetes	Mean+Max	63.2 [62.2, 64.3]	64.0 [62.8, 65.3]	64.2 [62.6, 65.7]	65.7 [63.7, 67.6]	66.1 [63.9, 68.3]	63.9 [61.6, 66.1]	63.6 [61.6, 65.5]
CGMacros-Fused	IR	Mean	92.7 [92.4, 93.1]	93.2 [92.7, 93.8]	93.6 [92.9, 94.2]	93.8 [93.1, 94.6]	94.2 [93.5, 94.9]	94.4 [93.7, 95.1]	94.6 [93.9, 95.2]
CGMacros-Fused	IR	Mean+Max	92.3 [91.9, 92.7]	93.5 [92.9, 94.0]	93.5 [92.9, 94.0]	93.7 [93.1, 94.2]	93.9 [93.2, 94.6]	94.4 [93.7, 95.0]	95.0 [93.7, 95.8]
ShanghaiT2DM	IR	Mean	61.9 [60.7, 63.2]	61.9 [59.9, 63.7]	61.0 [58.4, 63.4]	61.7 [58.9, 64.4]	61.2 [58.3, 64.1]	61.4 [58.4, 64.4]	61.9 [59.5, 64.3]
ShanghaiT2DM	IR	Mean+Max	63.1 [61.8, 64.4]	62.5 [60.6, 64.3]	60.8 [58.4, 63.3]	62.1 [59.6, 64.6]	67.8 [65.3, 70.3]	75.2 [72.7, 77.6]	75.2 [73.6, 76.7]
Stanford	Beta-cell	Mean	60.3 [59.2, 61.3]	61.8 [60.5, 63.0]	64.0 [62.5, 65.4]	65.4 [63.8, 66.9]	66.8 [65.0, 68.5]	68.3 [65.7, 70.7]	69.9 [67.1, 72.4]
Stanford	Beta-cell	Mean+Max	59.7 [58.8, 60.5]	63.0 [62.2, 63.9]	63.7 [62.4, 65.0]	64.8 [63.7, 66.0]	63.6 [62.0, 65.1]	63.5 [61.5, 65.5]	65.8 [63.2, 68.3]
Stanford	Diabetes	Mean	67.6 [66.1, 69.1]	69.8 [68.3, 71.5]	70.6 [69.0, 72.3]	70.3 [68.2, 72.5]	70.5 [67.9, 73.4]	71.8 [68.7, 74.9]	73.6 [71.2, 75.9]
Stanford	Diabetes	Mean+Max	67.9 [66.3, 69.6]	67.7 [66.1, 69.4]	68.3 [66.5, 70.1]	66.9 [64.4, 69.6]	68.0 [65.1, 71.1]	69.5 [66.6, 72.5]	71.7 [69.5, 74.2]
Stanford	IR	Mean	60.3 [58.7, 61.9]	61.5 [59.4, 63.5]	62.4 [60.5, 64.2]	62.9 [60.9, 64.9]	64.1 [62.1, 66.1]	65.9 [64.0, 68.0]	66.6 [64.6, 68.9]
Stanford	IR	Mean+Max	60.1 [58.6, 61.4]	61.8 [60.0, 63.7]	63.3 [61.4, 65.0]	66.2 [64.3, 68.1]	63.9 [62.6, 65.3]	64.0 [62.9, 65.1]	65.3 [63.6, 66.8]
Hall	Diabetes	Mean	59.8 [58.7, 60.9]	62.8 [60.0, 65.5]	67.7 [64.9, 70.5]	73.8 [71.6, 75.9]	-	-	-
Hall	Diabetes	Mean+Max	57.8 [56.8, 58.7]	65.4 [62.7, 67.5]	63.6 [60.0, 67.1]	70.9 [67.8, 74.1]	-	-	-
Hall	Glucotype	Mean	85.9 [84.9, 86.8]	91.6 [90.9, 92.3]	96.0 [95.4, 96.5]	99.5 [98.9, 99.9]	-	-	-
Hall	Glucotype	Mean+Max	85.0 [83.9, 86.0]	90.9 [90.0, 91.9]	93.7 [92.5, 94.8]	98.8 [98.0, 99.4]	-	-	-
Hall	IR	Mean	46.3 [44.2, 48.4]	44.5 [42.3, 46.5]	46.3 [42.8, 49.5]	49.8 [46.0, 53.0]	-	-	-
Hall	IR	Mean+Max	45.0 [42.9, 47.2]	44.9 [42.8, 46.8]	41.5 [38.9, 44.2]	45.1 [42.1, 48.0]	-	-	-

treated as independent test samples. We train linear probes with 10 repeated iterations of 5-fold stratified subject-level cross-validation. Metrics are computed separately for each start position and averaged within each repeated evaluation. In CGMacros, Dexcom, Libre, and Fused are all evaluated on the same 42-subject fused-overlap 7-day anchor cohort. Dexcom and Libre are evaluated separately, while the matched fused setting averages same-subject same-day embeddings from both sensors before multiday aggregation. We report the paired PR-AUC change relative to the one-day representation: $\Delta_K = \text{PR-AUC}(K) - \text{PR-AUC}(1)$. Deltas are computed within the same repeated evaluation, and confidence intervals are estimated over repeat-level paired deltas.

Table 11 reports the full multiday PR-AUC results for both aggregation variants. Longer observation windows improve subject-level prediction in most settings, with consistent gains on Stanford and strong improvements on Hall from $K = 1$ to $K = 4$. CGMacros shows more moderate but mostly positive gains; because Dexcom, Libre, and Fused use the same 42-subject overlapping anchor cohort, these differences reflect sensor-specific and fusion effects rather than changes in subject composition. ShanghaiT2DM IR shows limited improvement under mean pooling, but concat(mean, max) aggregation yields strong gains at longer horizons, suggesting that retaining salient daily embedding dimensions can be important for this task. Overall, the results support the utility of multiday frozen representations while showing that the best aggregation strategy can be cohort- and label-dependent.

D.5. Pretraining Data Scalability Details

We provide additional details for the pretraining data scalability analysis in Figure 7. To assess how GlucoFM benefits from unlabeled CGM data, we construct reduced pretraining corpora by randomly sampling subjects from each pretraining cohort at ratios of 20%, 40%, 60%, and 80%. Subject-level sampling is performed within each cohort to preserve the overall cohort composition while varying the amount of available unlabeled data. For each ratio, we repeat the sampling with five random

Table 12 | Pretraining data scaling results. Each ratio is evaluated over 5 subject-subsampling runs; values report mean \pm std over 10-iteration 5-fold subject-grouped downstream evaluation.

Ratio	Run	Metrics	CGMacros				ShanghaiT2DM			Stanford			Hall			
			Diabetes	IR	Hyperlip.	Obesity	IR	Hyperlip.	Hypogly.	Diabetes	β -cell Dys.	IR	Diabetes	IR	Hyperlip.	Glucotype
20%	1	PR	64.1 \pm 6.7	90.3 \pm 7.3	31.8 \pm 11.8	63.3 \pm 9.4	61.3 \pm 6.5	33.4 \pm 6.6	19.2 \pm 8.4	76.8 \pm 6.8	64.6 \pm 9.2	64.8 \pm 9.1	59.3 \pm 13.2	56.3 \pm 11.3	22.3 \pm 9.7	86.5 \pm 5.3
		AUC	77.4 \pm 5.5	79.9 \pm 14.4	48.7 \pm 16.1	61.9 \pm 11.2	51.6 \pm 8.2	49.8 \pm 10.7	58.5 \pm 16.1	72.9 \pm 7.8	64.8 \pm 9.1	66.4 \pm 7.6	70.7 \pm 11.2	66.9 \pm 9.5	58.2 \pm 14.3	88.9 \pm 4.3
	2	PR	64.7 \pm 6.7	90.5 \pm 7.2	31.4 \pm 11.5	62.8 \pm 9.2	60.2 \pm 6.4	33.6 \pm 6.5	18.9 \pm 8.0	76.7 \pm 7.4	64.4 \pm 9.2	64.5 \pm 9.1	59.4 \pm 13.0	56.3 \pm 11.6	23.1 \pm 10.7	86.5 \pm 5.0
		AUC	77.8 \pm 5.5	80.2 \pm 14.2	48.1 \pm 16.1	61.3 \pm 11.2	50.4 \pm 8.2	50.1 \pm 10.3	58.1 \pm 14.7	72.8 \pm 8.1	64.4 \pm 8.9	66.0 \pm 7.5	71.0 \pm 11.2	66.4 \pm 9.7	58.9 \pm 14.2	88.9 \pm 4.1
	3	PR	64.1 \pm 6.9	90.3 \pm 7.2	30.5 \pm 11.0	62.7 \pm 9.3	61.8 \pm 6.6	34.2 \pm 6.3	18.7 \pm 7.3	76.9 \pm 7.2	64.1 \pm 9.1	64.3 \pm 9.1	59.2 \pm 12.9	56.9 \pm 11.4	22.8 \pm 9.3	86.7 \pm 5.1
		AUC	77.4 \pm 5.6	80.0 \pm 14.2	47.8 \pm 15.9	61.4 \pm 11.2	52.2 \pm 8.4	50.8 \pm 10.0	58.2 \pm 15.0	72.9 \pm 8.1	64.4 \pm 8.8	65.9 \pm 7.4	70.6 \pm 11.2	66.6 \pm 9.7	58.5 \pm 14.2	88.9 \pm 4.3
	4	PR	64.0 \pm 7.0	90.0 \pm 7.4	30.6 \pm 10.9	63.1 \pm 9.4	60.9 \pm 6.3	33.5 \pm 6.3	20.0 \pm 9.0	75.9 \pm 7.0	64.0 \pm 8.8	64.8 \pm 9.0	59.1 \pm 13.0	56.1 \pm 11.0	21.6 \pm 9.1	86.1 \pm 5.5
		AUC	77.2 \pm 5.6	79.5 \pm 14.5	47.9 \pm 15.7	61.5 \pm 11.2	51.0 \pm 8.2	49.9 \pm 10.2	59.1 \pm 16.3	72.2 \pm 8.0	64.1 \pm 8.5	66.3 \pm 7.6	70.7 \pm 11.3	66.3 \pm 9.6	57.5 \pm 15.3	88.6 \pm 4.4
	5	PR	64.1 \pm 7.0	90.2 \pm 7.3	31.4 \pm 11.7	62.5 \pm 9.4	60.7 \pm 6.7	33.5 \pm 6.7	20.2 \pm 8.8	76.7 \pm 6.9	64.1 \pm 9.0	64.6 \pm 9.3	59.1 \pm 13.2	56.6 \pm 11.1	21.8 \pm 9.2	88.9 \pm 4.1
		AUC	77.4 \pm 5.6	79.7 \pm 14.4	48.7 \pm 16.1	61.0 \pm 11.4	51.1 \pm 8.5	49.9 \pm 10.4	60.0 \pm 15.9	72.8 \pm 7.9	64.4 \pm 8.8	66.4 \pm 7.6	70.8 \pm 11.5	66.9 \pm 9.6	57.3 \pm 14.7	89.1 \pm 4.4
40%	1	PR	64.4 \pm 7.3	91.1 \pm 6.6	33.6 \pm 12.8	63.4 \pm 9.4	61.6 \pm 6.7	34.8 \pm 7.4	19.9 \pm 8.4	77.5 \pm 6.3	64.5 \pm 9.4	65.8 \pm 9.1	60.0 \pm 13.5	57.5 \pm 12.0	22.0 \pm 8.3	87.8 \pm 5.3
		AUC	77.5 \pm 5.9	80.5 \pm 13.7	50.9 \pm 16.8	62.6 \pm 11.6	51.1 \pm 8.4	51.4 \pm 11.1	60.7 \pm 14.6	72.8 \pm 8.1	64.8 \pm 9.1	68.1 \pm 7.1	71.1 \pm 11.5	68.6 \pm 10.3	58.2 \pm 14.3	88.9 \pm 4.3
	2	PR	64.4 \pm 7.3	91.0 \pm 6.7	34.1 \pm 13.0	63.9 \pm 9.4	60.7 \pm 6.6	34.1 \pm 7.2	19.4 \pm 8.1	77.1 \pm 6.3	64.7 \pm 9.3	65.7 \pm 9.2	59.3 \pm 13.2	57.0 \pm 11.7	22.0 \pm 8.6	87.5 \pm 5.4
		AUC	77.5 \pm 5.9	80.3 \pm 13.9	51.4 \pm 16.9	62.8 \pm 11.5	50.0 \pm 8.3	51.0 \pm 11.2	60.3 \pm 14.6	73.2 \pm 7.2	65.0 \pm 8.9	67.9 \pm 7.2	70.2 \pm 11.4	68.4 \pm 10.2	57.4 \pm 14.0	88.6 \pm 4.4
	3	PR	64.2 \pm 7.3	91.5 \pm 6.4	32.5 \pm 11.8	64.6 \pm 9.1	62.0 \pm 6.9	33.7 \pm 7.4	18.6 \pm 6.3	77.8 \pm 6.9	64.6 \pm 9.7	65.2 \pm 8.9	58.8 \pm 13.0	58.2 \pm 12.5	20.6 \pm 7.4	88.0 \pm 5.2
		AUC	77.5 \pm 6.0	81.3 \pm 13.3	50.3 \pm 16.4	63.1 \pm 11.0	52.2 \pm 8.0	49.1 \pm 11.0	60.1 \pm 12.3	73.6 \pm 8.0	64.5 \pm 9.5	67.4 \pm 7.0	70.0 \pm 11.6	69.1 \pm 10.2	56.2 \pm 12.5	90.0 \pm 4.1
	4	PR	64.2 \pm 7.2	91.0 \pm 6.8	33.5 \pm 12.7	64.3 \pm 9.4	61.9 \pm 6.8	34.4 \pm 7.6	19.1 \pm 6.9	77.5 \pm 6.4	64.4 \pm 9.7	65.3 \pm 9.0	59.3 \pm 13.3	57.5 \pm 12.2	21.3 \pm 7.7	87.9 \pm 5.4
		AUC	77.5 \pm 5.9	80.5 \pm 13.7	50.8 \pm 16.8	63.1 \pm 11.3	51.5 \pm 8.4	50.0 \pm 11.3	60.8 \pm 14.0	73.4 \pm 7.3	64.5 \pm 9.3	67.5 \pm 7.1	70.3 \pm 11.5	68.1 \pm 10.4	56.9 \pm 13.8	89.9 \pm 4.3
	5	PR	64.1 \pm 7.4	90.9 \pm 6.8	32.9 \pm 12.0	64.0 \pm 9.2	61.3 \pm 6.7	33.9 \pm 7.4	18.3 \pm 6.3	77.4 \pm 6.6	64.2 \pm 9.5	65.1 \pm 8.9	58.6 \pm 12.5	57.6 \pm 12.1	21.7 \pm 7.9	87.7 \pm 5.2
		AUC	77.4 \pm 5.9	80.4 \pm 13.7	50.5 \pm 16.6	62.2 \pm 11.2	50.9 \pm 8.1	49.3 \pm 11.4	59.6 \pm 13.6	73.2 \pm 7.7	64.1 \pm 9.2	67.2 \pm 7.0	69.7 \pm 11.1	68.4 \pm 10.3	57.5 \pm 13.1	89.8 \pm 4.2
60%	1	PR	65.9 \pm 7.2	91.8 \pm 5.9	31.8 \pm 11.6	63.9 \pm 9.7	61.6 \pm 7.1	34.8 \pm 7.6	19.5 \pm 6.6	78.5 \pm 7.3	66.4 \pm 10.2	65.8 \pm 8.4	61.1 \pm 12.6	57.3 \pm 12.8	20.7 \pm 7.9	88.5 \pm 5.5
		AUC	78.8 \pm 5.9	81.8 \pm 12.5	50.4 \pm 16.0	62.8 \pm 11.5	52.1 \pm 8.4	51.8 \pm 11.3	62.2 \pm 12.0	74.0 \pm 8.2	66.2 \pm 9.7	67.8 \pm 6.2	72.2 \pm 10.6	68.2 \pm 10.6	55.2 \pm 13.1	90.6 \pm 4.0
	2	PR	65.3 \pm 7.2	91.5 \pm 6.0	33.4 \pm 12.1	63.8 \pm 10.0	62.5 \pm 7.3	34.9 \pm 8.1	18.0 \pm 5.3	78.2 \pm 6.3	66.4 \pm 10.0	67.6 \pm 9.0	61.2 \pm 13.1	58.8 \pm 12.4	20.0 \pm 7.4	88.2 \pm 5.4
		AUC	78.3 \pm 5.8	80.7 \pm 13.3	51.8 \pm 16.8	62.9 \pm 11.6	51.6 \pm 8.4	51.3 \pm 11.8	60.5 \pm 11.2	74.0 \pm 7.0	66.3 \pm 9.5	69.7 \pm 6.8	71.0 \pm 11.2	69.5 \pm 10.3	53.7 \pm 13.8	90.4 \pm 4.0
	3	PR	65.0 \pm 7.3	91.5 \pm 6.1	33.4 \pm 12.1	63.7 \pm 10.0	62.3 \pm 6.9	34.7 \pm 7.9	18.0 \pm 5.5	78.2 \pm 6.4	66.3 \pm 10.0	67.0 \pm 9.1	60.2 \pm 13.1	58.9 \pm 12.4	20.2 \pm 7.9	88.0 \pm 5.5
		AUC	78.0 \pm 5.9	80.9 \pm 13.2	51.6 \pm 16.7	62.7 \pm 11.6	51.2 \pm 8.3	51.0 \pm 11.8	60.6 \pm 11.5	74.0 \pm 7.1	66.1 \pm 9.6	69.2 \pm 6.8	70.4 \pm 11.3	69.5 \pm 10.3	53.3 \pm 12.7	90.3 \pm 4.0
	4	PR	65.5 \pm 7.2	91.5 \pm 6.1	33.8 \pm 12.3	64.0 \pm 10.0	62.1 \pm 6.7	35.1 \pm 8.2	18.0 \pm 5.3	77.9 \pm 6.4	66.6 \pm 9.8	67.0 \pm 8.9	60.4 \pm 12.9	58.7 \pm 12.9	19.6 \pm 7.7	88.0 \pm 5.5
		AUC	78.5 \pm 5.8	81.0 \pm 13.4	52.0 \pm 17.2	62.7 \pm 11.5	51.1 \pm 7.8	51.3 \pm 11.6	60.0 \pm 11.2	73.8 \pm 7.2	66.4 \pm 9.3	69.1 \pm 6.7	70.5 \pm 11.0	69.5 \pm 10.5	52.4 \pm 13.7	90.3 \pm 4.1
	5	PR	65.4 \pm 7.2	91.6 \pm 6.2	33.5 \pm 12.1	64.6 \pm 9.9	63.0 \pm 7.0	34.5 \pm 8.0	17.7 \pm 5.7	78.3 \pm 6.5	66.6 \pm 10.1	66.8 \pm 8.8	60.8 \pm 13.1	59.1 \pm 12.8	19.9 \pm 7.9	88.1 \pm 5.6
		AUC	78.3 \pm 5.8	81.2 \pm 13.3	51.8 \pm 16.9	63.4 \pm 11.5	52.1 \pm 8.3	50.8 \pm 11.5	59.3 \pm 11.9	74.0 \pm 7.2	66.4 \pm 9.5	69.1 \pm 6.6	70.8 \pm 11.3	69.7 \pm 10.5	53.4 \pm 12.4	90.4 \pm 4.0
80%	1	PR	65.7 \pm 7.2	92.1 \pm 5.4	34.8 \pm 12.2	63.4 \pm 11.1	62.8 \pm 7.3	35.0 \pm 7.9	20.6 \pm 7.6	78.3 \pm 7.2	67.8 \pm 9.7	66.9 \pm 8.7	64.4 \pm 12.5	58.8 \pm 14.7	16.9 \pm 6.5	88.9 \pm 5.4
		AUC	78.8 \pm 6.0	81.8 \pm 12.6	53.3 \pm 17.1	62.2 \pm 12.7	52.8 \pm 8.3	52.5 \pm 12.0	61.6 \pm 12.6	74.1 \pm 7.5	67.7 \pm 9.1	68.9 \pm 6.6	74.6 \pm 10.3	69.3 \pm 11.9	46.6 \pm 16.0	91.0 \pm 4.1
	2	PR	66.1 \pm 7.1	92.1 \pm 5.3	33.4 \pm 10.9	63.8 \pm 11.0	63.9 \pm 7.4	35.3 \pm 8.5	20.0 \pm 6.8	78.2 \pm 7.0	68.3 \pm 9.5	67.4 \pm 8.9	63.2 \pm 12.9	58.4 \pm 14.2	19.3 \pm 7.4	88.3 \pm 5.9
		AUC	78.9 \pm 5.8	81.5 \pm 12.8	52.4 \pm 16.9	62.2 \pm 12.4	53.0 \pm 8.2	51.8 \pm 12.4	61.0 \pm 11.8	74.1 \pm 7.3	68.1 \pm 8.7	69.4 \pm 6.8	72.7 \pm 10.6	69.8 \pm 11.7	50.4 \pm 13.8	90.5 \pm 4.3
	3	PR	66.1 \pm 7.4	92.1 \pm 5.3	33.7 \pm 11.7	63.8 \pm 10.4	62.7 \pm 7.3	35.7 \pm 8.2	20.7 \pm 6.9	78.7 \pm 7.0	67.3 \pm 9.8	66.2 \pm 8.4	64.0 \pm 13.0	58.3 \pm 14.5	17.2 \pm 6.8	88.8 \pm 5.7
		AUC	78.9 \pm 6.1	81.8 \pm 12.1	52.8 \pm 16.4	62.4 \pm 12.2	52.7 \pm 8.1	52.6 \pm 12.0	62.6 \pm 11.4	74.4 \pm 7.6	67.3 \pm 9.4	68.3 \pm 6.4	74.7 \pm 10.4	68.8 \pm 11.9	47.6 \pm 16.2	90.9 \pm 4.2
	4	PR	66.4 \pm 7.3	92.0 \pm 5.5	32.8 \pm 11.1	63.7 \pm 10.4	63.4 \pm 7.3	35.5 \pm 8.5	20.7 \pm 6.9	78.6 \pm 7.3	67.9 \pm 9.9	66.5 \pm 8.6	65.2 \pm 13.4	58.4 \pm 14.5	16.7 \pm 5.8	88.9 \pm 5.4
		AUC	79.2 \pm 6.0	81.6 \pm 12.5	52.0 \pm 16.3	62.2 \pm 12.2	53.5 \pm 8.2	51.7 \pm 12.5	63.7 $\$							

Table 13 | Performance comparison of different encoder designs. All reported values represent the mean \pm std evaluated via a 10-iteration 5-fold cross-validation.

Encoder Design	Metrics	CGMacros				ShanghaiT2DM			Stanford			Hall			
		Diabetes	IR	Hyperlip.	Obesity	IR	Hyperlip.	Hypogly.	Diabetes	β -cell Dys.	IR	Diabetes	IR	Hyperlip.	Glucotype
Raw Input	PR	61.4 \pm 6.0	89.4 \pm 7.0	31.1 \pm 9.8	66.0 \pm 8.9	60.9 \pm 6.8	34.5 \pm 7.0	23.3 \pm 11.1	77.3 \pm 6.7	64.4 \pm 8.1	63.8 \pm 7.7	55.7 \pm 12.9	53.2 \pm 10.6	16.1 \pm 4.9	77.0 \pm 9.9
	AUC	75.4 \pm 4.9	79.0 \pm 13.8	49.9 \pm 14.6	64.5 \pm 9.4	50.8 \pm 8.4	50.1 \pm 10.3	63.2 \pm 16.0	73.0 \pm 7.4	64.0 \pm 8.4	65.0 \pm 6.7	68.1 \pm 10.4	63.1 \pm 10.6	43.3 \pm 11.6	82.1 \pm 7.0
	F1	55.3 \pm 5.9	70.6 \pm 10.3	48.8 \pm 7.6	60.5 \pm 7.1	50.5 \pm 6.4	49.7 \pm 6.5	56.3 \pm 8.7	66.4 \pm 6.6	59.7 \pm 6.8	60.1 \pm 4.5	60.1 \pm 7.9	58.0 \pm 7.3	46.6 \pm 5.8	73.4 \pm 6.4
State-stream Only	PR	62.8 \pm 6.7	91.0 \pm 5.6	34.5 \pm 12.9	62.6 \pm 9.1	59.2 \pm 6.1	33.2 \pm 8.4	18.2 \pm 7.1	74.5 \pm 4.7	62.7 \pm 7.9	62.2 \pm 6.9	54.1 \pm 11.3	58.9 \pm 12.0	18.5 \pm 5.1	86.2 \pm 6.4
	AUC	76.0 \pm 5.6	80.0 \pm 12.7	51.0 \pm 16.7	60.0 \pm 11.0	47.8 \pm 7.8	48.5 \pm 13.2	55.1 \pm 12.6	69.5 \pm 6.7	60.8 \pm 8.9	62.7 \pm 5.1	68.5 \pm 8.7	69.0 \pm 11.0	54.3 \pm 13.5	89.2 \pm 4.4
	F1	54.1 \pm 7.0	70.7 \pm 10.7	50.0 \pm 8.3	56.6 \pm 8.0	48.4 \pm 6.6	48.7 \pm 8.5	50.5 \pm 6.6	63.9 \pm 5.7	57.2 \pm 7.0	59.5 \pm 4.0	61.3 \pm 7.4	62.7 \pm 9.0	47.3 \pm 6.7	80.2 \pm 6.0
Event-stream Only	PR	60.1 \pm 4.8	84.7 \pm 9.7	28.6 \pm 8.2	60.5 \pm 7.4	62.2 \pm 6.5	34.7 \pm 5.9	13.9 \pm 5.8	76.9 \pm 5.9	62.0 \pm 8.1	57.2 \pm 6.5	53.1 \pm 13.2	52.0 \pm 11.5	19.4 \pm 7.7	59.4 \pm 9.7
	AUC	74.5 \pm 4.4	72.0 \pm 16.1	46.9 \pm 11.1	58.7 \pm 9.9	53.5 \pm 8.2	51.3 \pm 9.3	46.3 \pm 9.8	72.3 \pm 7.0	61.9 \pm 7.8	60.5 \pm 7.2	62.3 \pm 12.4	62.6 \pm 9.4	52.6 \pm 11.4	65.9 \pm 9.8
	F1	54.5 \pm 5.9	65.8 \pm 10.0	46.8 \pm 6.6	56.2 \pm 8.0	53.0 \pm 5.6	49.2 \pm 6.6	46.4 \pm 4.7	65.3 \pm 6.4	56.4 \pm 6.6	57.3 \pm 4.6	57.4 \pm 7.5	57.7 \pm 6.9	49.4 \pm 7.4	62.6 \pm 7.5
Dual-stream	PR	65.9 \pm 7.5	91.9 \pm 5.3	36.1 \pm 11.2	64.9 \pm 11.7	67.0 \pm 7.7	33.5 \pm 7.8	21.1 \pm 10.0	77.3 \pm 7.5	69.0 \pm 9.6	67.6 \pm 8.1	66.2 \pm 13.0	60.2 \pm 15.1	14.4 \pm 5.2	88.3 \pm 5.7
	AUC	78.7 \pm 6.1	81.2 \pm 12.7	54.7 \pm 15.9	62.6 \pm 13.2	57.8 \pm 8.2	50.5 \pm 13.4	59.2 \pm 15.9	72.8 \pm 7.4	68.7 \pm 8.9	69.1 \pm 6.6	75.9 \pm 10.2	70.7 \pm 12.2	41.6 \pm 11.6	90.7 \pm 4.3
	F1	58.3 \pm 8.5	69.6 \pm 11.0	50.2 \pm 9.7	59.4 \pm 9.9	55.4 \pm 6.4	49.1 \pm 9.1	50.7 \pm 6.9	66.2 \pm 6.6	63.3 \pm 6.9	64.0 \pm 5.8	64.5 \pm 9.2	62.0 \pm 10.4	43.1 \pm 4.9	82.4 \pm 5.6

E. Ablation Design Details

E.1. Encoder Design Ablation Details

Table 13 provides task-wise results for the encoder design ablation in Figure 8. All variants use the same pretraining data, optimization settings, masking strategy, and downstream evaluation protocol. To ensure a fair comparison, we do not remove auxiliary patch-level information from the ablated encoders. For each patch, we compute mask-aware physiological statistics consisting of state statistics, i.e., glucose mean and standard deviation, and event statistics, i.e., mean rate-of-change and rate-of-change standard deviation. The rate-of-change features are computed with a mask-aware dynamic backoff and normalized to the 5-minute grid.

For fairness, all variants are provided with the corresponding patch-level statistics and temporal-difference features. The variants differ only in how the waveform and auxiliary patch features are organized. The *Raw Input* variant directly tokenizes the aligned glucose sequence and receives both patch-internal differences and the full set of patch statistics, including glucose mean/std and rate-of-change mean/std. The *State-stream Only* variant uses the filtered low-frequency trend with trend differences and state statistics. The *Event-stream Only* variant uses the residual component with rate-of-change features and event statistics. The full *Dual-stream* model encodes the state and event streams separately before fusing them into a unified daily representation.

As shown in Table 13, the dual-stream encoder achieves the strongest overall performance, confirming that slow glycemic state and transient event dynamics provide complementary information. The event-only variant is generally the weakest, suggesting that residual fluctuations and short-term rates alone are too unstable for robust metabolic representation learning. In contrast, the raw-input and state-only variants remain competitive, indicating that generic glucose patterns and low-frequency baseline physiology both carry useful clinical signal. However, both fall short of the full dual-stream model, especially on CGMacros, Stanford, and Hall. These results support the core design of GlucoFM: its gains are not simply due to extra statistics or temporal-difference inputs, but to explicitly organizing slow and fast CGM dynamics into complementary streams before fusion.

E.2. Temporal Dynamics Weight Ablation Details

We provide additional task-wise results for the temporal dynamics weight ablation in Figure 9. In this experiment, we keep the architecture, pretraining data, masking strategy, augmentation pipeline, and downstream evaluation protocol fixed, and vary only the weight λ_{TD} of the temporal dynamics objective. The total pretraining loss is $\mathcal{L} = \mathcal{L}_{MCR} + \lambda_{TD}\mathcal{L}_{TD}$, where \mathcal{L}_{MCR} denotes masked contextual latent prediction and \mathcal{L}_{TD} denotes temporal dynamics modeling. We sweep λ_{TD} from 0 to 2.0, with $\lambda_{TD} = 0$ corresponding to masked contextual prediction alone.

Table 14 | Impact of temporal dynamics weight (λ_{TD}) variations. All reported PR-AUC values represent the mean \pm std evaluated via 10 iterations of 5-fold cross-validation.

Weight (λ)	CGMacros				ShanghaiT2DM			Stanford			Hall			
	Diabetes	IR	Hyperlip.	Obesity	IR	Hyperlip.	Hypogly.	Diabetes	β -cell Dys.	IR	Diabetes	IR	Hyperlip.	Glucotype
$\lambda = 0.0$	62.7 \pm 6.3	90.6 \pm 6.7	29.8 \pm 11.0	65.9 \pm 9.4	63.2 \pm 6.8	30.5 \pm 5.8	19.7 \pm 9.7	76.9 \pm 5.5	63.0 \pm 8.8	65.5 \pm 6.6	58.4 \pm 14.0	51.9 \pm 10.8	15.0 \pm 6.4	84.4 \pm 5.8
$\lambda = 0.2$	64.2 \pm 7.0	91.8 \pm 6.1	32.4 \pm 12.5	65.8 \pm 10.0	62.8 \pm 7.0	32.5 \pm 6.9	20.2 \pm 10.9	78.0 \pm 6.1	63.2 \pm 10.2	64.4 \pm 8.6	61.8 \pm 14.5	54.2 \pm 12.3	19.7 \pm 6.9	88.2 \pm 4.7
$\lambda = 0.4$	65.5 \pm 7.4	91.5 \pm 6.2	33.0 \pm 11.3	63.6 \pm 11.0	63.4 \pm 7.7	35.0 \pm 7.4	21.8 \pm 10.0	77.8 \pm 6.2	67.3 \pm 10.1	68.8 \pm 8.5	63.9 \pm 14.1	58.2 \pm 12.6	16.2 \pm 6.6	89.2 \pm 5.3
$\lambda = 0.6$	65.9 \pm 7.3	91.7 \pm 5.9	33.5 \pm 11.2	64.4 \pm 11.7	64.8 \pm 7.6	35.3 \pm 7.8	22.8 \pm 11.0	77.8 \pm 7.1	68.2 \pm 9.9	68.6 \pm 8.8	64.3 \pm 13.5	60.0 \pm 14.1	18.8 \pm 8.6	88.4 \pm 5.5
$\lambda = 0.8$	66.0 \pm 7.3	91.8 \pm 5.7	35.0 \pm 11.5	64.9 \pm 11.7	66.9 \pm 7.6	34.0 \pm 7.8	22.7 \pm 11.3	77.7 \pm 7.7	68.8 \pm 9.7	68.2 \pm 8.3	65.0 \pm 13.1	60.0 \pm 14.9	15.7 \pm 5.6	88.2 \pm 5.6
$\lambda = 1.0$	65.9 \pm 7.5	91.9 \pm 5.3	36.1 \pm 11.2	64.9 \pm 11.7	67.0 \pm 7.7	33.5 \pm 7.8	21.1 \pm 10.0	77.3 \pm 7.5	69.0 \pm 9.6	67.6 \pm 8.1	66.2 \pm 13.0	60.2 \pm 15.1	14.4 \pm 5.2	88.3 \pm 5.7
$\lambda = 1.2$	65.6 \pm 7.7	92.2 \pm 4.9	36.8 \pm 11.4	64.3 \pm 11.4	66.2 \pm 7.8	33.7 \pm 8.0	19.9 \pm 8.8	76.8 \pm 7.5	69.4 \pm 9.4	67.4 \pm 8.3	64.7 \pm 12.7	60.6 \pm 15.4	14.3 \pm 4.9	88.6 \pm 5.6
$\lambda = 1.4$	65.8 \pm 7.6	92.3 \pm 4.7	36.6 \pm 12.3	63.2 \pm 11.0	65.3 \pm 7.8	34.5 \pm 8.3	19.8 \pm 8.2	76.8 \pm 7.3	68.8 \pm 9.6	66.3 \pm 8.2	64.9 \pm 12.7	60.5 \pm 15.7	14.2 \pm 4.8	88.7 \pm 5.6
$\lambda = 1.6$	65.8 \pm 7.6	92.2 \pm 4.6	36.4 \pm 12.2	62.6 \pm 10.5	65.0 \pm 8.0	35.3 \pm 8.5	20.2 \pm 8.0	76.5 \pm 7.2	68.4 \pm 9.7	65.6 \pm 8.4	64.4 \pm 12.3	60.2 \pm 15.6	14.1 \pm 4.9	88.9 \pm 5.4
$\lambda = 1.8$	65.9 \pm 7.7	92.3 \pm 4.5	36.2 \pm 12.2	62.5 \pm 10.4	64.7 \pm 8.1	35.3 \pm 8.6	20.1 \pm 7.7	76.3 \pm 7.0	68.3 \pm 9.7	65.1 \pm 8.5	63.6 \pm 12.2	59.9 \pm 15.4	13.9 \pm 4.7	89.1 \pm 5.2
$\lambda = 2.0$	65.8 \pm 7.7	92.3 \pm 4.5	36.1 \pm 12.2	62.5 \pm 10.3	64.5 \pm 8.2	35.0 \pm 8.6	20.2 \pm 7.3	76.2 \pm 7.1	68.3 \pm 9.9	64.8 \pm 8.6	63.2 \pm 12.1	59.6 \pm 15.2	13.8 \pm 4.6	89.1 \pm 5.2

 Table 15 | Ablation Study on Data Augmentation Strategies. All reported values represent the mean \pm std evaluated via a 10-iteration 5-fold cross-validation.

Augmentation	Metrics	CGMacros				ShanghaiT2DM			Stanford			Hall			
		Diabetes	IR	Hyperlip.	Obesity	IR	Hyperlip.	Hypogly.	Diabetes	β -cell Dys.	IR	Diabetes	IR	Hyperlip.	Glucotype
No Aug.	PR	64.2 \pm 7.3	91.5 \pm 5.0	32.8 \pm 10.6	61.7 \pm 10.5	61.8 \pm 7.2	32.7 \pm 7.1	18.0 \pm 5.1	75.6 \pm 7.4	68.5 \pm 9.5	66.3 \pm 9.0	59.7 \pm 14.3	59.5 \pm 13.8	15.0 \pm 4.8	88.7 \pm 5.7
	AUC	77.2 \pm 6.0	79.9 \pm 12.2	50.1 \pm 15.7	60.3 \pm 12.6	51.4 \pm 8.7	49.6 \pm 12.6	58.8 \pm 10.7	71.3 \pm 8.1	67.6 \pm 8.8	68.0 \pm 7.4	71.8 \pm 11.6	69.8 \pm 12.3	42.8 \pm 10.8	90.9 \pm 4.2
	F1	55.6 \pm 8.0	68.0 \pm 10.6	47.6 \pm 9.0	57.4 \pm 9.1	52.0 \pm 6.6	48.6 \pm 8.5	50.6 \pm 6.1	64.6 \pm 7.7	62.5 \pm 6.6	63.4 \pm 6.3	63.7 \pm 9.9	62.2 \pm 10.2	42.2 \pm 5.1	82.3 \pm 5.7
Value Perturb.	PR	64.9 \pm 7.5	91.7 \pm 4.8	33.3 \pm 10.5	63.2 \pm 10.6	63.8 \pm 7.4	33.0 \pm 7.5	19.2 \pm 6.7	75.5 \pm 7.5	69.0 \pm 9.3	66.5 \pm 9.1	59.7 \pm 14.0	59.0 \pm 14.3	15.9 \pm 6.0	88.8 \pm 5.5
	AUC	77.8 \pm 6.1	80.4 \pm 11.9	51.4 \pm 15.6	61.7 \pm 12.7	53.5 \pm 8.5	49.8 \pm 12.7	59.0 \pm 12.5	71.0 \pm 8.3	67.8 \pm 8.6	67.6 \pm 7.3	71.8 \pm 11.4	69.6 \pm 12.4	45.6 \pm 11.0	90.9 \pm 4.0
	F1	56.5 \pm 8.2	68.1 \pm 10.7	48.4 \pm 9.3	58.8 \pm 9.1	53.1 \pm 6.5	49.0 \pm 9.0	50.5 \pm 6.2	64.3 \pm 7.8	62.7 \pm 6.7	63.4 \pm 5.7	63.0 \pm 9.7	61.6 \pm 10.2	44.0 \pm 5.5	82.5 \pm 5.3
Struct. Spars.	PR	66.6 \pm 7.3	91.8 \pm 5.3	34.6 \pm 11.2	62.8 \pm 11.6	64.2 \pm 7.9	34.5 \pm 8.3	19.7 \pm 7.6	77.4 \pm 7.6	69.0 \pm 9.6	67.4 \pm 8.1	65.0 \pm 13.0	60.2 \pm 15.1	15.8 \pm 5.8	88.7 \pm 5.4
	AUC	79.2 \pm 5.9	81.0 \pm 12.7	53.2 \pm 17.0	61.0 \pm 13.4	53.9 \pm 8.3	51.1 \pm 13.3	58.2 \pm 13.8	73.1 \pm 7.7	68.6 \pm 8.7	68.5 \pm 6.7	75.4 \pm 10.3	71.2 \pm 12.0	45.7 \pm 14.1	90.8 \pm 4.0
	F1	58.5 \pm 7.8	69.5 \pm 10.8	49.5 \pm 10.3	57.9 \pm 9.5	53.4 \pm 6.6	49.6 \pm 9.3	50.1 \pm 6.1	66.2 \pm 6.1	62.7 \pm 7.1	63.4 \pm 5.7	64.6 \pm 9.1	63.1 \pm 10.5	44.4 \pm 5.2	82.6 \pm 5.3
Full Aug. (ours)	PR	65.9 \pm 7.5	91.9 \pm 5.3	36.1 \pm 11.2	64.9 \pm 11.7	67.0 \pm 7.7	33.5 \pm 7.8	21.1 \pm 10.0	77.3 \pm 7.5	69.0 \pm 9.6	67.6 \pm 8.1	66.2 \pm 13.0	60.2 \pm 15.1	14.4 \pm 5.2	88.3 \pm 5.7
	AUC	78.7 \pm 6.1	81.2 \pm 12.7	54.7 \pm 15.9	62.6 \pm 13.2	57.8 \pm 8.2	50.5 \pm 13.4	59.2 \pm 15.9	72.8 \pm 7.4	68.7 \pm 8.9	69.1 \pm 6.6	75.9 \pm 10.2	70.7 \pm 12.2	41.6 \pm 11.6	90.7 \pm 4.3
	F1	58.3 \pm 8.5	69.6 \pm 11.0	50.2 \pm 9.7	59.4 \pm 9.9	55.4 \pm 6.4	49.1 \pm 9.1	50.7 \pm 6.9	66.2 \pm 6.6	63.3 \pm 6.9	64.0 \pm 5.8	64.5 \pm 9.2	62.0 \pm 10.4	43.1 \pm 4.9	82.4 \pm 5.6

As shown in Table 14, removing the temporal dynamics objective consistently weakens performance, indicating that masked contextual prediction alone does not fully capture clinically useful glucose evolution. Increasing λ_{TD} improves many tasks, especially diabetes risk assessment, insulin resistance, and β -cell dysfunction, where temporal transitions and state–event interactions are likely informative. The best overall performance occurs in a broad range around $\lambda_{TD} = 0.6$ – 1.0 , suggesting that GlucoFM is not overly sensitive to an exact weight choice. When λ_{TD} becomes too large, performance gradually saturates or declines on several tasks, indicating that over-emphasizing local transitions can weaken global contextual representation learning. These results support the use of a balanced JEPA-style objective: masked contextual prediction captures global daily metabolic context, while temporal dynamics modeling adds complementary transition information.

E.3. Data Augmentation Ablation Details

Table 15 provides task-wise results for the data augmentation ablation in Figure 10. We keep the architecture, pretraining objectives, masking strategy, and downstream evaluation protocol fixed, and vary only the training-time augmentation pipeline. The *No Aug.* setting removes all augmentations. The *Value Perturb.* setting includes value-level perturbations, such as low-frequency baseline wander and compression-like transient drops. The *Struct. Spars.* setting includes structural sparsification, such as decimation and sensor-disconnection blocks. The full setting combines both augmentation families.

The results show that augmentation improves GlucoFM most consistently as a robustness mechanism rather than as the sole source of performance. Value perturbation provides modest gains over no augmentation, indicating that robustness to amplitude shifts and transient artifacts is useful but not sufficient. Structural sparsification contributes larger improvements, especially on tasks and cohorts where sampling density, missingness, or sensor availability may vary, supporting its role in simulating

Table 16 | Ablation Study on Dense Interpolation Designs. All reported values represent the mean \pm std evaluated via a 10-iteration 5-fold cross-validation.

Preprocess	Metrics	CGMacros				ShanghaiT2DM			Stanford			Hall			
		Diabetes	IR	Hyperlip.	Obesity	IR	Hyperlip.	Hypogly.	Diabetes	β -cell Dys.	IR	Diabetes	IR	Hyperlip.	Glucotype
Dense Interp.	PR	66.3 \pm 5.9	89.9 \pm 6.6	30.7 \pm 10.9	61.8 \pm 10.4	55.6 \pm 6.7	31.8 \pm 7.2	17.8 \pm 5.4	77.3 \pm 7.9	69.6 \pm 10.8	67.2 \pm 9.5	63.6 \pm 15.4	56.3 \pm 14.1	16.8 \pm 6.5	88.7 \pm 5.4
	AUC	79.5 \pm 5.0	78.5 \pm 14.2	49.7 \pm 16.3	62.0 \pm 12.5	41.7 \pm 9.1	49.2 \pm 13.1	53.5 \pm 11.3	73.1 \pm 8.0	68.4 \pm 10.1	69.0 \pm 8.4	73.1 \pm 12.6	67.1 \pm 12.5	45.2 \pm 11.3	91.1 \pm 3.9
	F1	58.4 \pm 7.7	69.1 \pm 10.4	46.6 \pm 9.4	58.6 \pm 9.6	44.1 \pm 6.9	47.7 \pm 8.4	48.1 \pm 5.7	66.3 \pm 6.8	63.1 \pm 8.2	63.5 \pm 7.9	63.4 \pm 11.3	59.8 \pm 10.7	43.5 \pm 5.1	83.2 \pm 5.3
Dense Interp. + Spars.	PR	66.9 \pm 6.4	90.4 \pm 7.4	32.7 \pm 10.2	62.8 \pm 11.6	58.6 \pm 6.7	34.3 \pm 7.7	22.0 \pm 12.0	78.4 \pm 7.4	68.4 \pm 10.6	67.9 \pm 8.6	64.1 \pm 14.6	57.8 \pm 14.1	17.3 \pm 6.7	88.4 \pm 6.0
	AUC	79.9 \pm 5.3	79.4 \pm 15.8	52.6 \pm 16.1	62.5 \pm 13.5	45.9 \pm 8.1	52.4 \pm 13.1	58.6 \pm 16.0	74.3 \pm 7.3	67.6 \pm 10.0	69.1 \pm 7.7	74.0 \pm 12.0	69.4 \pm 12.1	49.6 \pm 14.6	91.0 \pm 4.2
	F1	59.3 \pm 8.1	69.3 \pm 11.5	48.2 \pm 9.4	58.7 \pm 10.0	46.6 \pm 6.5	51.3 \pm 8.7	51.3 \pm 6.7	67.6 \pm 6.6	61.4 \pm 7.6	64.4 \pm 6.0	63.6 \pm 10.6	60.4 \pm 10.7	44.6 \pm 7.3	82.3 \pm 5.4
Mask-aware (Ours)	PR	65.9 \pm 7.5	91.9 \pm 5.3	36.1 \pm 11.2	64.9 \pm 11.7	67.0 \pm 7.7	33.5 \pm 7.8	21.1 \pm 10.0	77.3 \pm 7.5	69.0 \pm 9.6	67.6 \pm 8.1	66.2 \pm 13.0	60.2 \pm 15.1	14.4 \pm 5.2	88.3 \pm 5.7
	AUC	78.7 \pm 6.1	81.2 \pm 12.7	54.7 \pm 15.9	62.6 \pm 13.2	57.8 \pm 8.2	50.5 \pm 13.4	59.2 \pm 15.9	72.8 \pm 7.4	68.7 \pm 8.9	69.1 \pm 6.6	75.9 \pm 10.2	70.7 \pm 12.2	41.6 \pm 11.6	90.7 \pm 4.3
	F1	58.3 \pm 8.5	69.6 \pm 11.0	50.2 \pm 9.7	59.4 \pm 9.9	55.4 \pm 6.4	49.1 \pm 9.1	50.7 \pm 6.9	66.2 \pm 6.6	63.3 \pm 6.9	64.0 \pm 5.8	64.5 \pm 9.2	62.0 \pm 10.4	43.1 \pm 4.9	82.4 \pm 5.6

realistic CGM acquisition conditions. The full augmentation setting achieves the best overall average performance, although not every task improves monotonically. This is expected because some labels, such as hyperlipidemia or hypoglycemia, may be weakly reflected in daily CGM patterns or sensitive to cohort composition. Overall, these results suggest that CGM-aware augmentation complements the physiology-aware representation design by improving robustness to realistic sensing variability.

E.4. Dense Interpolation Ablation Details

Table 16 provides task-wise results for the dense interpolation ablation in Figure 11. We compare three preprocessing designs while keeping the architecture, pretraining objectives, and downstream protocol fixed. The *Dense Interp.* variant linearly interpolates missing grid positions during both pretraining and downstream representation extraction, and treats the resulting sequence as densely observed. The *Dense Interp. + Aug.* variant uses the same dense interpolation protocol but further applies structural sparsification during pretraining to reintroduce missingness-like perturbations. The default *No Interp.* setting preserves the original observation mask and does not treat interpolated values as real measurements.

The results show that dense interpolation is not necessary for GlucoFM and can be less effective than the default mask-aware formulation. This gap is especially visible on ShanghaiT2DM and CGMacros, where sampling-rate heterogeneity is more prominent: ShanghaiT2DM is collected at a 15-minute sampling rate, while CGMacros contains a substantial portion of 15-minute recordings. In these settings, dense interpolation may create artificial high-frequency continuity and make imputed values indistinguishable from real observations. Adding structural sparsification improves the dense-interpolation variant, suggesting that exposure to structured missingness helps reduce interpolation-induced shortcuts. However, the default no-interpolation setting still achieves the strongest overall performance, especially on task-averaged PR-AUC and ROC-AUC. This supports the design choice of preserving observation masks and modeling irregular CGM recordings directly, rather than converting unobserved positions into fully observed values.